The Role of TOR Signaling in FRQ-Independent Rhythmicity in *Neurospora crassa*

ROJIN JALALJALALI

A THESIS SUBMITTED TO THE FACULTY OF GRADUATE STUDIES IN PARTIAL FULFILMENT OF THE REQUIRMENT FOR THE DEGREE OF MASTER OF SCIENCE

GRADUATE PROGRAM IN BIOLOGY

YORK UNIVERSITY

TORONTO, ONTARIO

SEPTEMBER 2026

© ROJIN JALALJALALI, 2026

Abstract

Circadian rhythms are near-24-hour biological oscillations that coordinate physiological and behavioral processes with environmental cycles. They are commonly regulated by transcription–translation feedback loops (TTFLs). In *Neurospora crassa*, the canonical TTFL involves *frq*, WC-1, and WC-2. However, rhythmicity in *frq*-deficient strains suggests additional mechanisms, including the FRQ-less oscillator (FLO).

The Target of Rapamycin (TOR) pathway is a conserved nutrient-sensing network and potential mediator of non-TTFL rhythmicity. Ribosomal protein S6 phosphorylation indicates TOR activity, which exhibits oscillations across metabolic conditions and genetic backgrounds. FLO-associated proteins VTA and GTR2 further link TOR signaling to circadian regulation.

My research investigates TOR as a potential oscillator in *Neurospora*. Under heat-pulse cycles, *frq10* strains show coordinated TOR activity and conidiation rhythms, while vta^{ko} *frq10* and $gtr2^{ko}$ *frq10* mutants show disrupted rhythmicity. These findings support TOR's involvement in FRQ-independent rhythmic regulation and its potential role as a metabolic oscillator alongside the canonical TTFL.

Dedication

To everyone whose dedication to *Neurospora* research continues to expand our understanding of biological time.

Acknowledgements

I would like to express my deepest gratitude to my supervisor, **Dr. Patricia Lakin-Thomas**, for giving me the opportunity to join her laboratory and complete my master's research under her guidance. Thank you for your patience, encouragement, and continuous support throughout this journey. Your scientific knowledge, thoughtful advice, and willingness to teach have not only shaped this project but have also helped me grow into a more confident researcher.

As this was my first research experience in Canada and my first graduate degree, everything from learning new laboratory techniques to developing scientific thinking, was a completely new experience for me. You always encouraged me to ask questions, think critically, and become more independent as a researcher. I truly appreciate the time you invested in teaching me and the confidence you placed in my abilities.

Beyond your role as a supervisor, I am grateful for your kindness, patience, and understanding. You created an environment where I always felt comfortable asking questions, discussing new ideas, and learning from my mistakes. Your support made what initially felt like an overwhelming experience both enjoyable and rewarding. This project has not only allowed me to complete my master's degree, but it has also shaped the way I approach scientific research. The knowledge, skills, and confidence I gained in your laboratory will remain with me throughout my future academic and professional career. I feel incredibly fortunate to have had the opportunity to learn from you, and I will always be grateful for everything you have done for me.

I would also like to sincerely thank my advisory committee member, **Dr. Mark Bayfield**, for his valuable feedback, insightful suggestions, and encouragement throughout my master's program. Your expertise and constructive comments helped strengthen both my research and my scientific thinking.

I would also like to thank everyone in the Lakin-Thomas Laboratory for making the lab a place where I always enjoyed coming to work. The friendly atmosphere, laughter, and sense of community made even the busiest days enjoyable. I am grateful for the friendships and memories that I will always carry with me beyond graduate school.

Finally, I would like to express my heartfelt gratitude to my family for their unconditional love, endless encouragement, and unwavering belief in me. Their support has been my greatest source of strength throughout my academic journey. Beginning a new life in a different country

while pursuing my first master's degree was both exciting and challenging, and I could not have reached this milestone without their love and encouragement. I am especially grateful to my parents for always believing in me, supporting my dreams, and inspiring me to keep moving forward. This achievement is as much theirs as it is mine.

I would also like to dedicate this thesis to the memory of my beloved grandmother, whose love, kindness, and unwavering belief in me have always been a source of strength. Although she is no longer here to see this milestone, I know she would have been proud of the person I have become. Her love, encouragement, and the values she instilled in me will remain with me throughout my life and continue to guide me in every step of my journey.

Additionally, ChatGPT (OpenAI) was used to assist with editing the language of this thesis, including improvements to grammar, sentence structure, clarity, and readability. All scientific ideas, experimental design, data collection, data analysis, interpretation of results, and conclusions are entirely my own.

Table of Contents

Abstract ..... *ii*

Dedication ..... *iii*

Acknowledgments ..... *iv*

Table of Contents ..... *vi*

List of Abbreviations ..... *viii*

List of Figures ..... *x*

1 Chapter 1: Introduction 1

1.1 Circadian Rhythms 1

1.1.1 General Definitions 1

1.1.2 Circadian Rhythms and Implications for Human Health 2

1.2 Molecular Basis of Circadian Rhythms 4

1.2.1 Transcription–Translation Feedback Loops (TTFLs) 5

1.2.2 Molecular Basis of Circadian Rhythms in *Drosophila melanogaster* 6

1.2.3 Molecular Organization of Circadian Rhythms in Mammalian Systems 8

1.2.4 Circadian Clocks in Plants 10

1.2.5 Circadian Clocks in Cyanobacteria 12

1.2.6 Circadian Clock Mechanisms in *Neurospora crassa* 15

1.3 Non-Canonical Circadian Behaviors in Multiple Species 19

1.3.1 FRQ-Less Oscillators (FLOs) in *Neurospora crassa* 21

1.4 TOR (target of rapamycin pathway) 23

1.4.1 Growth Factor Pathways Driving mTORC1 Activation 27

1.4.2 Amino Acid–Dependent Control of TORC1 Localization at the Lysosome 28

1.4.3 Mechanisms of Translational Control Downstream of TORC1 29

1.4.4 Control of TOR Signaling Networks in Plants 31

1.4.5 Regulation and Function of Ribosomal Protein S6 33

1.4.6 Feedback Regulation of TOR Signaling 34

1.4.7 TOR Signaling in *Neurospora crassa* 35

1.5 Temperature Entrainment of Circadian Rhythms in *Neurospora crassa* 37

1.6 Predictive Modeling of TOR Rhythmicity Using STELLA 40

2 Chapter 2: Methods 46

2.1 *Neurospora crassa* Strains 46

2.1.1 Genotyping of Progeny 47

2.1.2 Genomic DNA Isolation 47

2.1.3 S6-FLAG PCR and Agarose Gel Electrophoresis 47

2.2 Solid Agar Culture 49
2.2.1 Linear Growth Rate Measurement on Solid Agar Culture 49
2.2.2 Heat Pulse Treatment 51
2.3 Immunoblotting 52
2.3.1 Protein Extraction 52
2.3.2 Bio-Rad DC Protein Assay 52
2.3.3 Protein Separation by SDS-PAGE 52
2.3.4 Blotting 53
2.3.5 Immunodetection 54
3 Chapter 3: Results 56
3.1 Construction of *frq* knockout strains 56
3.1.1 PCR Validation of *frq* Genotypes and S6-FLAG Detection 56
3.1.2 Western Blot Analysis of S6-FLAG Expression in Selected Strains 57
3.2 Analysis of Conidiation Timing and TOR Activity Under T-Cycle Entrainment in *frq10*, *vta*, *gtr2* Strains 58
3.2.1 Analysis of Rhythmic Growth Patterns in *frq10 S6-FLAG* Under Heat Pulse Conditions 58
3.2.2 TOR Activity in *frq10* Strain Under Heat Pulse Entrainment 61
3.2.3 Role of VTA in Maintaining TOR Rhythmicity Under Heat Pulse Entrainment 68
3.2.4 Role of GTR2 in Maintaining TOR Rhythmicity Under Heat Pulse Entrainment 73
4 Chapter 4: Discussion 78
5 Future Work 82
6 References 83
7 Appendices 95
7.1 Appendix I. STELLA Model Equations and Simulation Parameters 95
7.2 Appendix II 99
7.3 Appendix III 100

List of Abbreviations

AD	Alzheimer's disease
BSA	Bovine Serum Albumin
ccgs	Clock Controlled Genes
CLK	Clock
CHK-2	Checkpoint kinase 2
CHX	Cycloheximide
CK1	Casein Kinase 1
CYC	Cycle
DAG	Sn-1,2-diacylglycerol
DBT	Double-Time
DD	Constant darkness
FFC	FRQ/FHR Complex
FGSC	Fungal Genetics Stock Centre
FHR	Frequency Interacting RNA Helicase
FLO	FRQ-less Oscillator
FRQ	Frequency
FWO	FRQ-WCC Oscillator
GTR2	GTP binding protein resemblance 2
GTR1	GTP binding protein resemblance 1
IDP	Inherently Disordered Protein
IP	Immuno-precipitation
LL	Constant light
MA	Maltose-Arginine Media
MAPKs	Mitogen-activated protein kinase
mTOR	Mammalian/Mechanistic TOR
Per	Period
PTO	Post translational Oscillator
RICTOR	Rapamycin-insensitive companion of mTOR
RPS6	Ribosomal Protein S6
S6K	S6 Kinase

SCN	Suprachiasmatic Nucleus
TOR	Target of Rapamycin
TORC1	TOR Complex 1
TORC2	TOR Complex 2
TTFL	Transcription/Translation Feedback Loop
VTA	Vacuolar TOR-associated
WC-1	White-Collar 1
WC-2	White-Collar 2
WCC	White Collar Complex
WT	Wildtype

List of Figures

Figure 1.1 The schematic diagram representing the circadian rhythms in the form of sinusoidal waves when tested under entrainment conditions LD: light-dark cycles) and free running conditions (LL: constant light). 2
Figure 1.2 General model for TTFL in organisms. 5
Figure 1.3 Schematic diagram representing the molecular components of transcriptional-translational feedback loops (TTFLs) in the circadian clockwork of *Drosophila* melanogaster. 8
Figure 1.4 Schematic diagram representing the molecular circuitry involved in the regulation of the mammalian circadian clock. 10
Figure 1.5 Schematic diagram representing the multiple interlocked transcriptional-translational feedback loops (TTFLs) involved in the circadian network of *Arabidopsis thaliana*. 12
Figure 1.6 Mechanism of the cyanobacterial circadian oscillator. 14
Figure 1.7 Neurospora life cycle. 16
Figure 1.8 Schematic diagram representing the molecular component of FWO (FRQ-WCC-Oscillator) as the core transcriptional-translational feedback loop (TTFL) involved in the circadian system of *Neurospora crassa*. 19
Figure 1.10 TORC domains in yeast. 25
Figure 1.11 TORC1 regulation in S. cerevisiae and mammals. 27
Figure 1.12 Schematic diagram representing the major regulators and downstream effectors of mTORC1 and mTORC2. 28
Figure 1.13 Schematic representation of the TOR signaling pathway in *Neurospora crassa*. 37
Figure 1.14 Entrainment of *Neurospora crassa* conidiation rhythms by repeated heat-pulse temperature cycles. 38
Figure 1.15 Conidiation density under T-cycle heat pulse conditions. 40
Figure 1.16 Conceptual STELLA model developed to simulate TOR signaling dynamics during heat-pulse entrainment. 41
Figure 1.17 Representative output generated by the STELLA simulation showing the predicted response of TOR activity (blue) to repeated heat-pulse T-cycle entrainment (red). 42
Figure 1.18 STELLA simulation predicting TOR activity in the frq knockout strain under different heat-pulse T-cycles (T19, T20, T22, and T22.5). 43
44
Figure 1.19 STELLA simulation predicting TOR activity in vta knockout and gtr2 knockout strains under different heat-pulse T-cycles. 44
Figure 2.1 Checking the genotypes of different strains for s6FLAG by PCR. 48
Figure 2.2 Representative plate image used for conidiation density analysis under a 16-h temperature cycle in constant darkness. 50
Figure 2.3 Measurement through ImageJ-based tracking of mycelial growth front over time in *frq10* under a 16 h T-cycle with temperature pulses from 22 °C to 37 °C in DD. Pulses are indicated by red bars. 51
Figure 2.4 Western blot of the 24h Tcycle with heat pulses from 22-37 degrees. 55
Figure 3.1 *S6-FLAG* genotyping of #259, #668 strains by PCR. 57
Figure 3.2 western blotting of *S6-FLAG* to see phosphorylation state (S6-P) of different strains. 58
Figure 3.4 Average conidiation density over time in *frq10 S6-FLAG* under a 16-h T-cycle with temperature shifts from 22°C to 32°C in constant darkness (DD), based on three experiments. 59

Figure 3.5 Average conidiation density over time in *frq10 S6-FLAG* under a 16-h T-cycle with temperature shifts from 22°C to 37°C in constant darkness (DD), based on three experiments. 60
Figure 3.6 Average conidiation density over time in *frq10 S6-FLAG* under a 24-h T-cycle with temperature shifts from 22°C to 32°C in constant darkness (DD), based on three experiments. 60
Figure 3.7 Average conidiation density over time in *frq10 S6-FLAG* under a 24-h T-cycle with temperature shifts from 22°C to 37°C in constant darkness (DD), based on three experiments. 61
Figure 3.8 S6 phosphorylation rhythm of the "wild-type" strain from 0 to 96 h in DD. 62
Figure 3.9 Time-course experiment for the *frq10* strain. 63
Figure 3.10 Western blot analysis of S6-FLAG expression following T16 heat-pulse entrainment in constant darkness (DD) using the *frq10 S6-FLAG* strain. 64
Figure 3.11 Average of S6 Phosphorylation of *frq10 S6 FLAG* strain in DD with T cycle 16 and heat pulses from 22 to 37 degrees. 65
Figure 3.12 Peak of TOR activity occurred before the conidiation peak of the strain in DD with T cycle 16 and heat pulses from 22 to 37 degrees. 65
Figure 3.13 Conidiation density compared to S6P timecourses. 66
Figure 3.14 Western blot analysis of S6-FLAG expression following T24 heat-pulse entrainment in constant darkness (DD) using the *frq10 S6-FLAG* strain. 67
Figure 3.15 Average of S6 Phosphorylation of *frq10 S6 FLAG* strain in DD with T cycle 24 and heat pulses from 22 to 37 degrees. 67
Figure 3.16 Peak of TOR activity occurred before the conidiation peak of the strain in DD with T cycle 24 and heat pulses from 22 to 37 degrees. 68
Figure 3.17 S6 phosphorylation rhythm of VTA mutant strain from 20 to 80 h in DD. 69
Figure 3.18 Western blot analysis of S6-FLAG expression following T16 heat-pulse entrainment in constant darkness (DD) using the *vta ^{ko} frq10 S6-FLAG* strain. 70
Figure 3.19 Average of S6 Phosphorylation of *vta frq10 S6 FLAG* strain in DD with T cycle 16 and heat pulses from 22 to 37 degrees. 70
Figure 3.20 TOR activity in *frq10 vtako S6 FLAG* strain and the conidiation peak of the strain in DD with T cycle 16 and heat pulses from 22 to 37 degrees. 71
Figure 3.21 Western blot analysis of S6-FLAG expression following T24 heat-pulse entrainment in constant darkness (DD) using the *vta ^{ko} frq10 S6-FLAG* strain. 71
Figure 3.22 Average of S6 Phosphorylation of *vta frq10 S6 FLAG* strain in DD with T cycle 24 and heat pulses from 22 to 37 degrees. 72
Figure 3.23 TOR activity in *frq10 vtako S6 FLAG* strain and the conidiation peak of the strain in DD with T cycle 24 and heat pulses from 22 to 37 degrees. 72
Figure 3.24 S6 phosphorylation rhythm of GTR2 mutant strain from 20 to 80 h in DD. 73
Figure 3.25 Western blot analysis of S6-FLAG expression following T16 heat-pulse entrainment in constant darkness (DD) using the *gtr2 ^{ko} frq10 S6-FLAG* strain. 74
Figure 3.26 Average of S6 Phosphorylation of *gtr2 frq10 S6 FLAG* strain in DD with T cycle 16 and heat pulses from 22 to 37 degrees. 74
Figure 3.27 TOR activity in *frq10 gtr2ko S6 FLAG* strain and the conidiation peak of the strain in DD with T cycle 16 and heat pulses from 22 to 37 degrees. 75
Figure 3.28 Western blot analysis of S6-FLAG expression following T24 heat-pulse entrainment in constant darkness (DD) using the *gtr2 ^{ko} frq10 S6-FLAG* strain. 75
Figure 3.29 Average of S6 Phosphorylation of *gtr2 frq10 S6 FLAG* strain in DD with T cycle 24 and heat pulses from 22 to 37 degrees. 76

Figure 3.30 TOR activity in *frq10 gtr2ko S6 FLAG* strain and the conidiation peak of the strain in DD with T cycle 24 and heat pulses from 22 to 37 degrees. 76
Figure 4.1 Conidiation density compared to s6P timecourses. 79

1 Chapter 1: Introduction

1.1 Circadian Rhythms

1.1.1 General Definitions

Circadian rhythms are endogenous biological oscillations with an approximately 24-hour period that regulate a wide range of physiological, metabolic, and behavioral processes across living organisms(Takahashi, 2017; Dunlap, 1999). These rhythms enable organisms to anticipate and adapt to predictable environmental cycles, primarily driven by the Earth's rotation (Panda et al., 2002). Rather than responding passively to environmental changes, circadian systems allow organisms to proactively coordinate internal processes with daily fluctuations in light, temperature, and nutrient availability (Roenneberg & Merrow, 2005). Circadian clocks are self-sustained timing systems that persist even in the absence of external cues, demonstrating their endogenous and autonomous nature (Dunlap, 1999).

These biological clocks are highly conserved across evolution, from cyanobacteria to fungi, plants, and mammals, underscoring their fundamental importance in maintaining cellular and organismal homeostasis (Bell-Pedersen et al., 2005). Although the molecular components of circadian systems differ among organisms, they are most commonly organized around transcription–translation feedback loops (TTFLs), in which rhythmic gene expression and protein turnover generate sustained oscillations (Takahashi, 2017). In addition to these canonical mechanisms, circadian rhythms can also be influenced by non-transcriptional processes, including metabolic and post-translational regulation (O-Neill & Reddy, 2011).

Circadian oscillations are commonly described using key parameters such as period, phase, and amplitude (Pittendrigh, 1993). The period represents the time required to complete one full cycle, the phase defines the timing of a specific point within the cycle relative to an external reference, and the amplitude reflects the magnitude of oscillation in a given biological output. These properties provide a quantitative framework for analyzing rhythmic behavior and are essential for understanding how circadian systems respond to environmental perturbations (Figure 1.1).

Despite being generated internally, circadian rhythms can be synchronized, or entrained, by environmental signals known as *zeitgebers*, including light, temperature, and nutrient availability

(Roenneberg & Merrow, 2016). This entrainment ensures that internal biological time remains aligned with the external environment. In the absence of such cues, circadian rhythms continue to oscillate under constant conditions, a phenomenon known as free-running, which further supports their endogenous nature (Roenneberg & Merrow, 2005).

A defining feature of circadian systems is temperature compensation, whereby the period of the rhythm remains relatively stable across a range of ambient temperatures (Pittendrigh, 1993). This property distinguishes circadian rhythms from most biochemical reactions, which typically accelerate with increasing temperature.

Circadian rhythms influence a broad range of biological functions, including metabolism, gene expression, cell division, and developmental processes (Bass & Takahashi, 2010). Disruption of these rhythms has been associated with numerous physiological and pathological conditions, emphasizing their critical role in maintaining biological stability(Takahashi, 2017). Together, the persistence, entrainment capability, and temperature compensation of circadian clocks establish them as fundamental and evolutionarily conserved regulatory systems in biology.

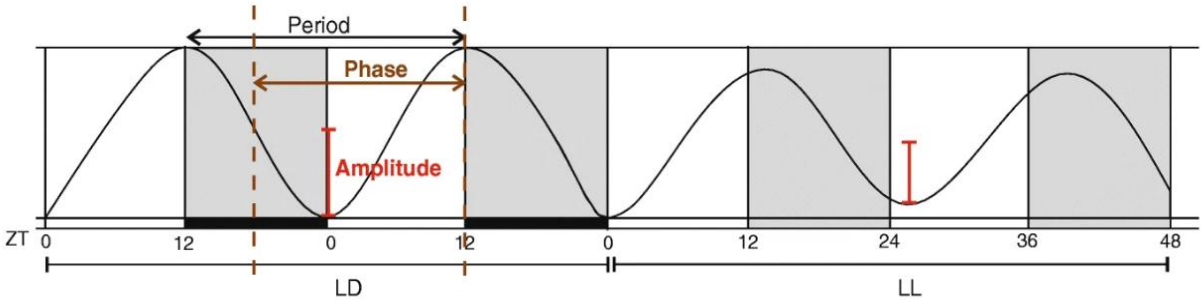


Figure 1.1 The schematic diagram representing the circadian rhythms in the form of sinusoidal waves when tested under entrainment conditions LD: light-dark cycles) and free running conditions (LL: constant light).

Biological oscillations can be described by mathematical terms such as period, phase, and amplitude. Period is the time required for completion of one cycle, which is the distance from one peak to another. Phase is a relative event, referring to any time point on a rhythmic cycle relative to an external time point. Amplitude represents the degree of change in a physiological parameter over the course of the cycle and is typically measured as the height of the wave. ZT: Zeitgeber Time.(Saini et al., 2019)

1.1.2 Circadian Rhythms and Implications for Human Health

Maintaining proper alignment between the endogenous circadian timing system and the external 24-hour environment is essential for human health. Circadian misalignment arises when internal biological rhythms become desynchronized from environmental cues such as the light–

dark cycle. Common contributors to this misalignment include irregular sleep schedules, transmeridian travel, exposure to artificial light at night, late-day consumption of stimulants such as caffeine, and occupational demands such as rotating or night-shift work (Walker et al., 2020).

Extensive evidence demonstrates that persistent circadian disruption is associated with elevated risk for a wide range of physiological disorders. Individuals engaged in shift work, for example, show increased incidence of hypertension, cardiovascular disease, and systemic inflammation compared with those maintaining regular diurnal schedules (Morris et al., 2016). Behavioral patterns that disturb circadian timing—including inconsistent meal timing and chronic sleep deprivation—can promote inflammatory pathways that contribute to metabolic and lifestyle-related diseases such as obesity, type 2 diabetes, endocrine dysregulation, and neurological disorders (Wright et al., 2015).

Neurodegenerative diseases are also closely linked to circadian dysfunction. Alzheimer's disease (AD) is characterized by pronounced disturbances in sleep–wake cycles and circadian rhythmicity alongside progressive cognitive decline. Growing evidence supports a bidirectional relationship between circadian disruption and AD pathology, whereby circadian misalignment exacerbates oxidative stress, alters neuronal metabolism, and impairs proteostasis, potentially accelerating disease progression (Musiek & Holtzman, 2016). Conversely, neurodegeneration itself may further destabilize circadian regulation, reinforcing pathological feedback loops.

Circadian misalignment has also been implicated in the development of metabolic disease at the population level. When internal biological rhythms are chronically out of phase with environmental signals—as occurs during jet lag, prolonged shift work, or socially imposed sleep restriction—individuals exhibit increased susceptibility to obesity, insulin resistance, and metabolic syndrome, conditions that represent major public health concerns in industrialized societies (Roenneberg & Merrow, 2016; Scheer et al., 2009).

Beyond metabolism and neurodegeneration, circadian regulation plays a critical role in cell-cycle control. The circadian clock temporally gates cell division, DNA replication, and repair processes, and disruption of this timing can promote genomic instability and tumorigenesis (Bhadra et al., 2017). Epidemiological studies have linked circadian disruption to elevated risk of several cancers, including breast, colorectal, and prostate cancers, particularly among individuals exposed to long-term night-shift work (Roenneberg & Merrow, 2016).

Collectively, these findings underscore the central role of circadian timing in coordinating physiological processes across multiple biological scales. A deeper understanding of circadian mechanisms and their integration with metabolic, neurological, and cellular regulatory networks is therefore essential, not only for advancing fundamental biological insight but also for informing strategies to improve human health and disease prevention.

1.2 Molecular Basis of Circadian Rhythms

Decades of research across multiple model organisms have revealed that circadian rhythms are governed by self-sustained molecular oscillators operating at the cellular level. In recognition of these discoveries, the 2017 Nobel Prize in Physiology or Medicine was awarded to Jeffrey C. Hall, Michael Rosbash, and Michael W. Young for identifying the molecular machinery underlying circadian timing in *Drosophila melanogaster*. Their pioneering work established the framework of the transcription–translation feedback loop (TTFL); a cycle in which clock genes and their protein products rhythmically regulate their own expression to generate approximately 24-hour oscillations. Since then, homologous molecular clocks have been identified in nearly all eukaryotes, from fungi to mammals, demonstrating the remarkable conservation of this mechanism throughout evolution (Dunlap, 1999; Lakin-Thomas & Brody, 2004).

Conceptually, circadian systems are organized around three functional components: input pathways, which perceive and relay environmental cues such as light, temperature, and nutrient availability to the clock; a core oscillator, which maintains rhythmicity even in constant conditions; and output pathways, which translate clock signals into rhythmic patterns of gene expression and physiology (Bell-Pedersen et al., 2005; Harmer et al., 2000). The core oscillator itself consists of interlocking feedback loops of gene expression that form the molecular basis of circadian timekeeping. In a typical TTFL, clock proteins produced during one phase of the cycle accumulate, translocate into the nucleus, and inhibit the transcription of their own genes, leading to oscillatory gene and protein expression over roughly 24 hours.

However, recent findings suggest that the classical TTFL model may represent only one layer of a more complex, interconnected system. Components of the circadian network can simultaneously participate in multiple roles. For example, light-sensitive photoreceptors not only mediate environmental entrainment but can also influence downstream clock outputs, while output factors can feed back to modify the oscillator itself (Harmer et al., 2000; Saini et al.,

2015). These observations indicate that circadian regulation is not strictly linear but rather consists of multiple coupled feedback loops that interact dynamically to maintain a robust and flexible rhythm (McClung et al., 2002; Saini et al., 2015). Despite this complexity, the TTFL remains a valuable conceptual model that continues to guide research into how molecular clocks sustain temporal order across diverse species and cellular contexts (Lakin-Thomas, 2006b) (Figure 1.2)

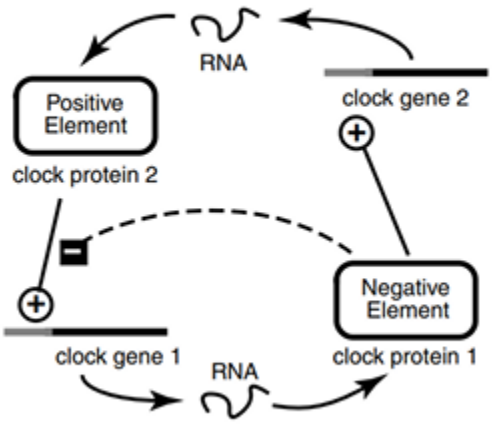


Figure 1.2 General model for TTFL in organisms.

TTFLs can contain one or more interlocked feedback loops. (Lakin-Thomas, 2006b)

1.2.1 Transcription–Translation Feedback Loops (TTFLs)

At the core of circadian regulation lies a molecular mechanism known as the transcription–translation feedback loop (TTFL) (Figure1.2), which serves as the fundamental oscillator driving rhythmic gene expression and protein accumulation within cells (Loros & Dunlap, 1991; Lakin-Thomas, 2019). This system forms the molecular foundation of nearly all characterized circadian clocks, providing a self-sustaining cycle of gene activation, protein synthesis, inhibition, and degradation that repeats roughly every 24 hours (Dunlap, 1999; Lakin-Thomas, 2006b). Although the specific clock genes and proteins differ among organisms, the overall logic of the feedback system remains remarkably conserved across the evolutionary spectrum, from fungi and plants to mammals (Bell-Pedersen et al., 2005; Young & Kay, 2001).

In the canonical TTFL model (Figure 1.2), positive elements (typically transcriptional activators that form heterodimeric complexes) bind to the promoters of negative element genes, initiating their transcription. The negative elements are translated in the cytoplasm and subsequently accumulate to sufficient levels before translocating into the nucleus, where they inhibit the transcriptional activity of the positive elements. This repression halts further transcription of their own genes, establishing a delayed negative feedback loop that sustains oscillations over approximately 24 hours (Loros & Dunlap, 1991; Mao et al., 2025).

Following inhibition, the negative-element proteins undergo post-translational modifications (Chi-Castañeda & Ortega, 2016; Lakin-Thomas et al., 2011). As these inhibitory proteins are degraded, repression on the transcriptional activators is lifted, allowing the cycle to restart. The combination of transcriptional repression, delayed protein turnover, and regulated degradation generates a robust rhythm of gene expression and protein abundance, which serves as the molecular basis for the organism's daily physiological and behavioral cycles.

The TTFL framework, while simplified, captures the essential logic of circadian timekeeping; a self-regulating molecular circuit capable of sustaining oscillations without external input yet flexible enough to synchronize with environmental cues. Multiple interlocked feedback loops and post-translational controls further stabilize this system, ensuring accurate 24-hour periodicity and resilience to environmental fluctuations. The conservation of this mechanism across eukaryotes emphasizes that, although the molecular players vary, the fundamental principles governing circadian timing are universal. Thus, understanding the TTFL in one organism provides powerful insights into how biological clocks function across all domains of life (Bell-Pedersen et al., 2005; Lakin-Thomas, 2006b).

1.2.2 Molecular Basis of Circadian Rhythms in *Drosophila melanogaster*

In the fruit fly *Drosophila melanogaster*, the circadian clock regulates a wide range of physiological and behavioral processes, including eclosion timing, locomotor activity, courtship behavior, learning, memory, and temperature preference rhythms (Ma et al., 2021; Tataroglu & Emery, 2015). In addition, circadian control extends to peripheral systems, influencing chemosensory functions such as olfaction and taste, as well as tissue homeostasis and regenerative processes in organs like the intestine (Chatterjee et al., 2010; Karpowicz et al., 2013;Allada & Chung, 2009) . Due to its powerful genetic tools and well-characterized molecular pathways, *Drosophila* has served as a key model organism in circadian biology. The

discovery of the *period (per)* gene and subsequent identification of mutants with altered rhythmicity established transcription–translation feedback loops (TTFLs) as the fundamental mechanism underlying circadian oscillations, a breakthrough recognized by the 2017 Nobel Prize in Physiology or Medicine (Huang, 2018).

At the core of the *Drosophila* circadian clock is a transcriptional activation system driven by the basic helix–loop–helix PAS-domain transcription factors CLOCK (CLK) and CYCLE (CYC). (Figure 1.3) These proteins form heterodimers that bind to E-box regulatory sequences (5′-CACGTG-3′) in the promoters of *period (per)* and *timeless (tim)*, promoting their rhythmic transcription (Dunlap, 1999; Hardin, 2005; Tataroglu & Emery, 2015). As PER and TIM proteins accumulate in the cytoplasm, PER undergoes phosphorylation by DOUBLETIME (DBT), targeting it for degradation via the proteasome. However, association with TIM stabilizes PER and allows formation of a PER–TIM complex that delays nuclear entry (Allada & Chung, 2009; Huang, 2018).

During the night, additional phosphorylation events mediated by Casein kinase 2 (CK2) and Shaggy (SGG) facilitate the nuclear translocation of the PER–TIM complex. Once inside the nucleus, this complex inhibits CLK–CYC activity, thereby repressing its own transcription and completing the negative feedback loop (Menet et al., 2012). Light entrainment is mediated by the blue-light photoreceptor CRYPTOCHROME (CRY), which responds to light at dawn by binding to TIM and promoting its degradation. This process destabilizes the PER–TIM complex and relieves repression on CLK–CYC, allowing the next cycle of transcription to begin (Allada & Chung, 2009; Tataroglu & Emery, 2015).

In addition to this primary feedback loop, a secondary regulatory network fine-tunes circadian oscillations. CLK–CYC also activates transcription of *vrille (vri)*, *PAR domain protein 1 (pdp1)*, and *clockwork orange (cwo)*. VRI acts as a repressor of *clk* expression by binding to V/P-box elements, while PDP1 functions antagonistically to promote *clk* transcription. CWO further reinforces repression by competing with CLK–CYC for E-box binding, thereby strengthening the overall negative feedback architecture (Hardin, 2005; Patke et al., 2020).

Although the molecular architecture of circadian clocks in *Drosophila* provides a well-established model for TTFL-driven rhythmicity, emerging evidence from other organisms suggests that transcriptional feedback alone may not fully account for circadian regulation. In fungi such as *Neurospora crassa*, rhythmic behavior persists even in the absence of core TTFL

components, indicating the presence of additional oscillatory mechanisms, including the FRQ-less oscillator (FLO). These observations highlight the potential contribution of non-transcriptional and metabolic pathways to circadian timing. In this context, the Target of Rapamycin (TOR) signaling pathway has gained attention as a candidate regulator of circadian rhythmicity, linking cellular metabolism with timekeeping processes. Investigating the role of TOR in *Neurospora crassa* therefore provides an opportunity to expand current models of circadian regulation beyond classical TTFL frameworks and to explore the integration of metabolic and oscillatory networks. (Figure 1.3)

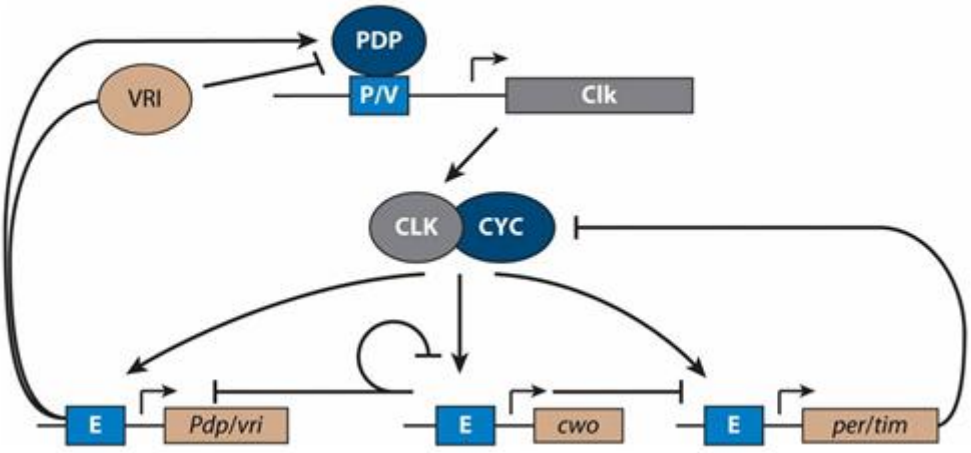


Figure 1.3 Schematic diagram representing the molecular components of transcriptional-translational feedback loops (TTFLs) in the circadian clockwork of *Drosophila* melanogaster.

In the core TTFL, the heterodimeric transcription complex CLK-CYC binds to E-box element (E) in the promoter region of per and tim and drives their transcription. PER and TIM undergo various modifications, which lead to their nuclear localization where they repress CLK-CYC activity. The CLOCK-CYCLE complex also promotes the expression of pdp, vri, and cwo. In a secondary loop, PDP1 activates the transcription of clk, while VRI inhibits it. CWO feeds back to negatively regulate the activity of the positive elements CLK-CYC Adapted from (Allada & Chung, 2009).

1.2.3 Molecular Organization of Circadian Rhythms in Mammalian Systems

In mammals, circadian rhythms are generated as intrinsic ~24-hour oscillations that operate at molecular, cellular, and behavioral levels. These rhythms regulate a broad spectrum of physiological processes, including body temperature regulation, immune function, metabolism, gene expression, cell cycle progression, and neural plasticity (Ko & Takahashi, 2006; Ma et al., 2021). Unlike simpler systems, mammalian circadian organization is highly hierarchical, with a

central pacemaker located in the suprachiasmatic nucleus (SCN) of the hypothalamus. This structure consists of a network of coupled neurons that coordinate rhythmic activity across the organism by synchronizing peripheral clocks present in nearly all tissues (Buhr & Takahashi, 2013; Partch et al., 2014).

Light serves as the primary environmental cue for entrainment in mammals. Photoreception is mediated by melanopsin-containing intrinsically photosensitive retinal ganglion cells (ipRGCs), which transmit light information to the SCN via the retinohypothalamic tract (RHT). This photic input allows the central clock to adjust its phase in response to the external light–dark cycle. Once synchronized, the SCN communicates timing information to peripheral oscillators through endocrine signals, neural pathways, and behavioral cues, thereby maintaining systemic circadian alignment (Reinke & Asher, 2019; Honma, 2018).

At the molecular level, circadian rhythms in mammals are driven by interconnected transcription–translation feedback loops (TTFLs). In the primary loop, the transcription factors CLOCK and BMAL1 form heterodimers that activate expression of the *period (Per1–3)* and *cryptochrome (Cry1–2)* genes. As PER and CRY proteins accumulate in the cytoplasm, they undergo phosphorylation by *casein kinase 1* (CK1), which regulates their stability and degradation. During the night, PER and CRY form complexes that translocate into the nucleus, where they inhibit CLOCK–BMAL1 activity, thereby suppressing their own transcription and completing the negative feedback cycle (Partch et al., 2014; Takahashi, 2017).

This core loop is reinforced by additional regulatory circuits. CLOCK–BMAL1 also drives expression of nuclear receptors such as REV-ERBα and RORα, which compete for binding to regulatory elements in the *Bmal1* promoter. While RORα promotes *Bmal1* transcription, REV-ERBα represses it, generating a secondary feedback loop that stabilizes oscillatory dynamics. Additional factors, including DEC1 and DEC2, further contribute to transcriptional repression, enhancing the robustness and precision of the circadian system;(Honma, 2018) (Figure 1.4).

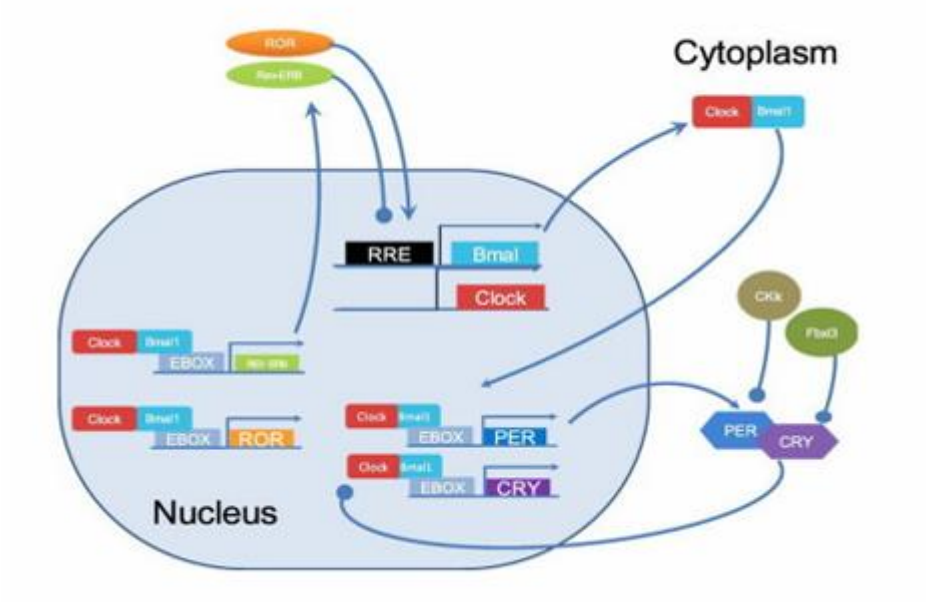


Figure 1.4 Schematic diagram representing the molecular circuitry involved in the regulation of the mammalian circadian clock.

In the core TTFL, CLOCK-BMAL1 heterodimers act as positive elements and drive the transcription of negative components *period (per)* and *cryptochrome (cry*). As PER and CRY accumulate in the cytoplasm, they form a dimer and translocate to the nucleus to repress the activity of positive regulators (CLOCK BMAL1). PER and CRY are subsequently degraded, through the activity of auxiliary enzymes such as CK1 and Fbx13, respectively; then, the next cycle starts. In a secondary loop, the transcriptional activator RORa and the inhibitor REV-ERBa antagonistically modulate Bmal1 transcription Adapted from (Robinson & Reddy, 2014).

1.2.4 Circadian Clocks in Plants

As immobile organisms, plants must adapt in place to constantly changing environmental conditions such as fluctuations in light, temperature, and humidity. Because of their reliance on photosynthesis, they require a precisely regulated internal timing system that aligns energy production, growth, and resource allocation with the daily light–dark cycle (Panter et al., 2019; McClung, 2019; McClung et al., 2002). The plant circadian clock fulfills this role by maintaining endogenous rhythmicity that is synchronized with environmental cues, thereby optimizing metabolism, development, and stress responses (Harmer, 2009).

Environmental information is primarily perceived through specialized photoreceptors, which serve as the main input pathways to the plant circadian system. Photoreceptors such as phytochromes (PHYs) and cryptochromes (CRYs) detect changes in light quality, intensity, and duration, transmitting these signals to the core oscillator to entrain internal rhythms with the external environment. In addition to light, temperature fluctuations can also act as entraining

cues, further refining circadian timing and ensuring robust synchronization under varying environmental conditions.

The plant circadian system regulates a wide range of physiological and metabolic outputs, including photosynthesis, chlorophyll biosynthesis, CO_2 fixation, hormone signaling, flowering time, and defense responses (Creux & Harmer, 2019; Dodd et al., 2005). These outputs are achieved through rhythmic control of gene expression, where clock-regulated transcription factors coordinate the timing of downstream target genes, often referred to as clock-controlled genes (CCGs). Through this mechanism, the circadian clock translates temporal information into coordinated cellular and organismal responses.

The model plant *Arabidopsis thaliana* has been instrumental in uncovering the molecular architecture of the plant circadian oscillator (Figure1.5), which consists of multiple interlocking transcriptional feedback loops (Barros Dantas et al., 2023; Hsu & Harmer, 2014). At the core of this system are the morning-expressed MYB transcription factors CIRCADIAN CLOCK ASSOCIATED 1 (CCA1) and LATE ELONGATED HYPOCOTYL (LHY), which repress expression of the evening gene TIMING OF CAB EXPRESSION 1 (TOC1). As CCA1 and LHY levels decline during the day, TOC1 accumulates and subsequently represses their transcription, forming a central negative feedback loop (Hsu & Harmer, 2014).

During the night, the Evening Complex (EC), composed of LUX ARRHYTHMO (LUX), EARLY FLOWERING 3 (ELF3), and EARLY FLOWERING 4 (ELF4), suppresses TOC1 expression, resetting the oscillator for the next cycle (Adams et al., 2015; Sanchez & Kay, 2016). Additional regulation is provided by the Pseudo-Response Regulator (PRR) family, including PRR9, PRR7, and PRR5, which act as transcriptional repressors to fine-tune the timing of morning gene expression (McClung, 2019; Adams et al., 2015).

Complementing this regulatory network, REVEILLE (RVE) transcription factors promote the expression of afternoon and evening genes, while themselves being rhythmically repressed by PRRs, creating a dynamic balance between activation and repression (Sanchez & Kay, 2016). Together, these interconnected feedback loops, coupled with photoreceptor-mediated input and transcriptional output pathways, enable plants to maintain robust circadian rhythms that support growth, survival, and adaptation to a changing environment.

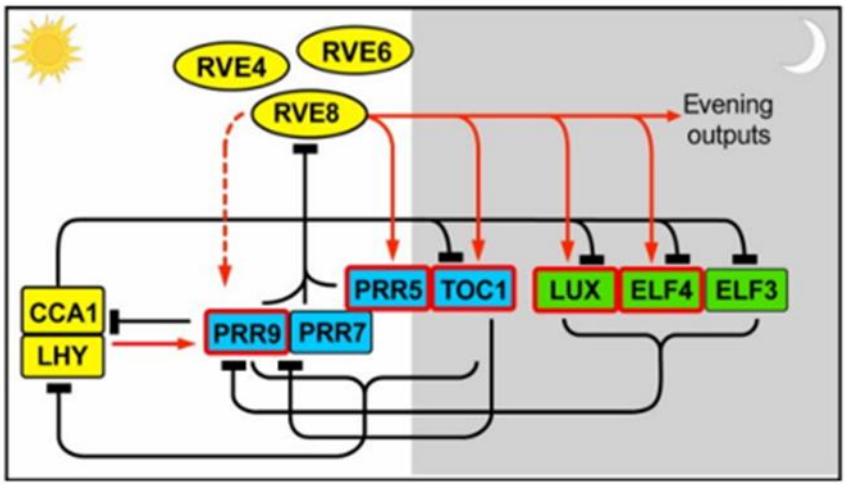


Figure 1.5 Schematic diagram representing the multiple interlocked transcriptional-translational feedback loops (TTFLs) involved in the circadian network of *Arabidopsis thaliana*.

The clock components are depicted from left to right according to the time of their peak expression. The white and gray backgrounds represent the subjective day and night respectively. Solid red arrows indicate activation, and the black perpendicular bars indicate repression. At dawn, the morning-phased elements CCA1 and LHY repress the expression of the majority of clock genes including TOC1, PRR genes and the EC complex (LUX, ELF3 and ELF4). The sequential expression of PRR9, PRR7, PRR5, and TOC1 downregulates the transcription of CCA1 and LHY. In the afternoon, RVE complex (RVE4, RVE6, and RVE8) promotes the transcription of PRR9, PRR5, TOC1, and the EC complex. In the evening, TOC1 further represses the expression of the morning elements such as CCA1 and LHY. Adapted from (Hsu & Harmer, 2014).

1.2.5 Circadian Clocks in Cyanobacteria

For many years, circadian rhythmicity was thought to be a defining feature of eukaryotic life, as it was believed that complex subcellular organization, such as the separation between the nucleus and cytoplasm, was required for proper clock regulation (Cohen & Golden, 2015; Young & Kay, 2001). However, subsequent discoveries revealed that circadian clocks are also present in prokaryotic organisms, particularly in cyanobacteria, the photosynthetic microbes that played a central role in oxygenating Earth's early atmosphere billions of years ago (Foster & Kreitzman, 2009). These organisms demonstrate that robust circadian rhythms can operate in relatively simple, single-celled systems, regulating essential processes such as photosynthesis, respiration, nitrogen fixation, cell division, and global gene expression (Y. I. Kim et al., 2008; Markson et al., 2013).

Among cyanobacteria, the freshwater species *Synechococcus elongatus* has become the primary model for studying prokaryotic circadian mechanisms. Its clock is composed of three core proteins, KaiA, KaiB, and KaiC, which together form a self-sustained and temperature-compensated oscillator (Y. I. Kim et al., 2008; Tomita et al., 2005). These proteins are encoded

within a single operon, and disruption of any one component abolishes rhythmicity, while mutations can alter the period of oscillation (Tomita et al., 2005) (Figure 1.6).

The KaiABC system functions as a post-translational oscillator (PTO), in which rhythmicity is generated through cycles of protein phosphorylation and dephosphorylation, independent of transcription and translation (Fagiani et al., 2022); (Swan et al., 2018). This was demonstrated in vitro, where the three purified Kai proteins and ATP were sufficient to produce sustained, temperature-compensated oscillations in KaiC phosphorylation over approximately 24 hours (Cohen & Golden, 2015). These findings established that circadian rhythms can arise purely from biochemical interactions, without requiring gene expression.

At the molecular level, KaiC forms a hexameric complex with two domains (CI and CII) and exhibits autokinase, autophosphatase, and ATPase activities (Tseng et al., 2017). During the subjective day, KaiA promotes phosphorylation of KaiC at specific residues, leading to conformational changes that enable KaiB binding during the subjective night. This interaction shifts KaiC toward dephosphorylation, completing a cyclical 24-hour rhythm (Cohen & Golden, 2015).

Importantly, the Kai oscillator is not isolated but is integrated into a broader regulatory network that includes input and output pathways. Environmental signals, particularly light and cellular redox state, are sensed through input factors such as CikA (circadian input kinase), which modulates the phase of the oscillator in response to external conditions. This allows the clock to become entrained to daily environmental cycles. On the output side, the histidine kinase SasA interacts with phosphorylated KaiC and transfers temporal information to the response regulator RpaA, which functions as a global transcription factor controlling rhythmic gene expression across the genome (Johnson et al., 2011; Hidalgo & Chiu, 2024; Taton et al., 2020). Through this coupling of input, oscillator, and output pathways, cyanobacterial clocks achieve precise coordination between environmental signals and cellular processes.

The discovery of the KaiABC system fundamentally reshaped our understanding of circadian biology by demonstrating that circadian timing can emerge from purely biochemical processes. These findings highlight that circadian oscillators are ancient and evolutionarily conserved systems that predate the emergence of eukaryotic cellular complexity. Moreover, the existence of rhythmic behavior in organisms lacking Kai homologs, such as *Bacillus subtilis*, suggests that

diverse prokaryotic systems may have evolved distinct mechanisms to maintain temporal organization in response to environmental cycles (Hidalgo & Chiu, 2024).

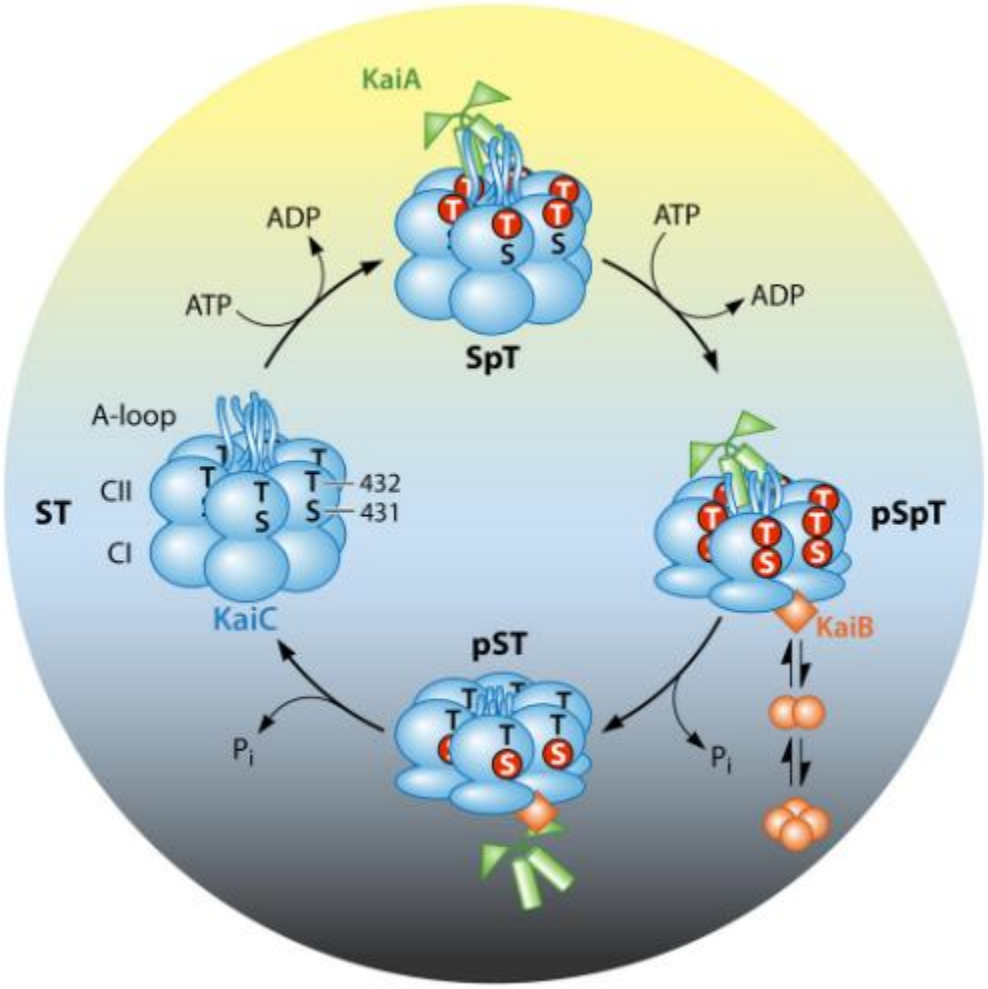


Figure 1.6 Mechanism of the cyanobacterial circadian oscillator.

KaiC is a hexameric protein that comes together to form a "double doughnut" shape comprised of CI and CII rings with A-loop segments extending from the C terminus in the CII ring. KaiC in the nonphosphorylated state (ST) (far left) can interact with KaiA. KaiA, a dimer, binds to and stabilizes the A-loop segment in the exposed state, promoting KaiC autophosphorylation during the day. Red circles enclosing "S" and "T" represent phosphorylation of S431 and T432residues, respectively, located in the CII ring. T432 becomes phosphorylated first (SpT), followed by S431, resulting in the doubly phosphorylated species(pSpT). Phosphorylation of S431 induces the stacking of the CII ring onto the CI ring. Ring-ring stacking exposes a binding site for KaiB (B-loop) on the CI ring. In order to for KaiB to interact with KaiC, both the B-loop must be exposed and KaiB must rearrange its tertiary fold from a ground-state fold found in tetramer and dimer species (orange circles) to a monomeric fold-switched form, fs-KaiB (orange diamond). Once both are achieved, fold-switched KaiB can bind to KaiC. fs-KaiB also interacts with KaiA, sequestering KaiA away from the A-loops on the CII domain. This action promotes burial of the A-loops into the hexamer and KaiC's autophosphatase activity during the nighttime portion of the cycle. Dephosphorylation occurs first on T432, resulting in pST species, followed by S431, resulting in a nonphosphorylated species (ST). Adapted from (Cohen & Golden, 2015).

1.2.6 Circadian Clock Mechanisms in *Neurospora crassa*

The filamentous ascomycete fungus *Neurospora crassa* is a eukaryotic organism widely distributed in natural environments, particularly in warm and humid regions rich in organic material (Baker et al., 2012). As a saprophytic fungus, *N. crassa* thrives on carbohydrate-rich substrates and is well adapted to colonizing recently burned vegetation, as its sexual spores require heat activation for germination (Davis & Perkins, 2002). These ecological traits, together with its rapid growth and genetic accessibility, have contributed to its long-standing use as a model organism in fungal biology and circadian research.

Vegetative growth in *N. crassa* occurs through elongated hyphae that form a branching mycelial network. These hyphae are separated by incomplete septa, allowing cytoplasmic continuity and efficient transport of nutrients and organelles toward the growing tips (Davis & de Serres, 1970; Galagan et al., 2003). Frequent fusion between genetically distinct hyphae results in the formation of heterokaryons—multinucleated networks that enhance physiological flexibility and adaptive potential (Hickey et al., 2002; Baker et al., 2012).

The life cycle of *N. crassa* (Figure 1.7), alternates between asexual and sexual reproduction depending on environmental conditions such as nutrient availability, temperature, and light (Giebultowicz, 2004). During the asexual phase, vegetative mycelia differentiate into aerial hyphae that generate chains of asexual spores, or conidia. Two types of conidia are produced: macroconidia, which are multinucleated, robust, and highly dispersible, and microconidia, which are uninucleate and generally less viable (Davis & Perkins, 2002). These spores are bright orange due to carotenoid pigmentation and are readily dispersed by air currents, allowing rapid colonization of new substrates (Baker et al., 2012).

When conditions become unfavorable for vegetative growth, *N. crassa* enters its sexual reproductive phase. Specialized female structures known as protoperithecia are formed and attract compatible male cells through pheromone-mediated chemotropic growth (Borkovich et al., 2004; Aramayo & Selker, 2013). Fertilization initiates meiotic and mitotic divisions that ultimately produce haploid ascospores enclosed within asci inside mature perithecia. Upon maturation, these ascospores are forcibly discharged and may remain dormant until appropriate environmental stimuli, such as heat shock, trigger germination and restart the life cycle (Davis & Perkins, 2002).

Beyond its well-characterized developmental biology, *Neurospora crassa* has played a foundational role in uncovering the molecular basis of circadian rhythms(Baker et al., 2012).

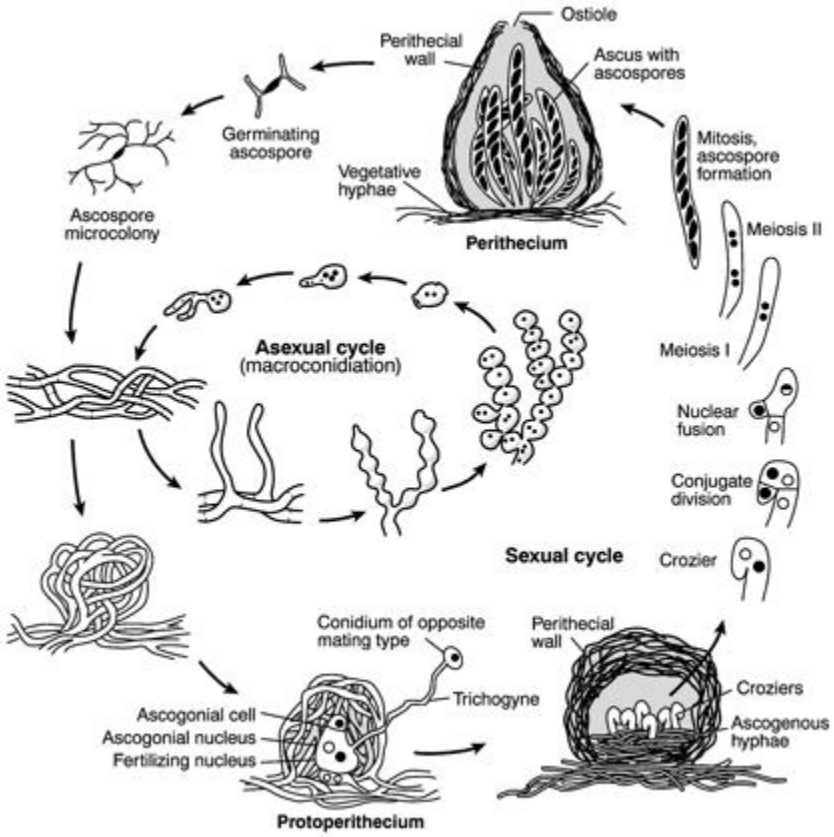


Figure 1.7 Neurospora life cycle.

Both Sexual and asexual phases are depicted in the figure. Adapted from (Davis & Perkins, 2002).

The organism displays robust daily rhythms in growth, morphology, and gene expression, reflecting the activity of an endogenous circadian clock (Giebultowicz, 2004). One of the most visible outputs of this clock is rhythmic conidiation, which appears as alternating bands of spores and vegetative growth when cultures are grown in race tubes under constant conditions (Lakin-Thomas et al., 2011; Baker et al., 2012). This clear and quantifiable phenotype, combined with fast growth, haploid genetics, and experimental tractability, has positioned *Neurospora* as a premier model for circadian biology (Baker et al., 2012; Roche et al., 2014).

At the molecular level, the circadian clock of *N. crassa* is organized around an interlocked transcription–translation feedback loop (TTFL) composed of core clock genes and their protein products (Lakin-Thomas, 2006b; Baker et al., 2012). Central to this oscillator is the White-Collar

Complex (WCC), a heterodimeric transcription factor formed by WHITE COLLAR-1 (WC-1) and WHITE COLLAR-2 (WC-2). Acting as the positive arm of the clock, WCC rhythmically binds to regulatory elements within the promoter of the *frequency (frq)* gene, thereby activating its transcription (Liu & Bell-Pedersen, 2006) (Figure 1.8).

The *frq* gene encodes the protein FREQUENCY (FRQ), which functions as the core negative regulator of the oscillator. Following translation, FRQ rapidly associates with its binding partner, the FRQ-interacting RNA helicase (FRH), forming a stable complex essential for clock function (Liu & Bell-Pedersen, 2006;Dunlap & Loros, 2017) . The FRQ–FRH complex accumulates and subsequently enters the nucleus, where it inhibits WCC activity through phosphorylation-dependent mechanisms involving casein kinases CKI and CKII (Cha et al., 2015).

Progressive phosphorylation of FRQ over the circadian cycle ultimately targets the protein for ubiquitination by the F-box protein FWD-1 and degradation by the proteasome, leading to a decline in FRQ levels during the late subjective night(Baker et al., 2012; Lakin-Thomas, 2019). As FRQ-mediated repression is relieved, newly synthesized or dephosphorylated WCC reactivates *frq* transcription, initiating the next cycle (Brunner & Káldi, 2008). This delayed negative feedback generates oscillations with a period of approximately 24 hours.

In addition to the negative feedback loop, FRQ participates in a positive regulatory circuit by stabilizing WC-1 and promoting *wc-2* expression, thereby enhancing the robustness of the oscillator (Baker et al., 2012; Cha et al., 2015). WC-1 also functions as a blue-light photoreceptor through its LOV (Light, Oxygen, Voltage) domain, enabling the circadian clock to synchronize with environmental light cues and rapidly reset in response to changes in illumination (Schafmeier et al., 2005; Lakin-Thomas et al., 2011).

Beyond its core oscillatory function, the *Neurospora* circadian clock transmits temporal information through well-defined output pathways. The White Collar Complex (WCC), composed of WC-1 and WC-2, acts as a central transcriptional regulator that drives rhythmic expression of numerous downstream targets, commonly referred to as clock-controlled genes (CCGs). These genes regulate a wide range of physiological and developmental processes, including conidiation, metabolic activity, and stress responses, thereby linking the internal oscillator to observable phenotypic rhythms.

Together, these interconnected feedback and output mechanisms enable the *Neurospora crassa* circadian clock to integrate environmental signals, maintain temporal precision, and coordinate rhythmic outputs essential for fungal growth, development, and survival.

While the circadian clock in *Neurospora crassa* shares the conserved transcription–translation feedback loop (TTFL) architecture found in mammals and *Drosophila*, important differences distinguish its regulatory organization. In all three systems, rhythmicity arises from delayed negative feedback; however, mammalian and *Drosophila* clocks operate within more complex, multi-layered networks involving numerous regulatory components and, in mammals, hierarchical organization through the suprachiasmatic nucleus (SCN).

In contrast, the *Neurospora* clock is comparatively simpler and relies primarily on the White Collar Complex (WCC) and the FRQ–FRH complex, making it highly experimentally tractable. Additionally, while transcriptional regulation dominates in mammals and *Drosophila*, *Neurospora* places greater emphasis on post-translational mechanisms, particularly FRQ phosphorylation and degradation. Differences are also evident in input and output pathways. In mammals and *Drosophila*, light entrainment is mediated through specialized photoreceptors and complex signaling pathways, whereas in *Neurospora*, WC-1 directly functions as a blue-light photoreceptor. Furthermore, although all systems regulate clock-controlled genes, *Neurospora* provides a more direct link between the molecular oscillator and observable outputs such as conidiation rhythms.

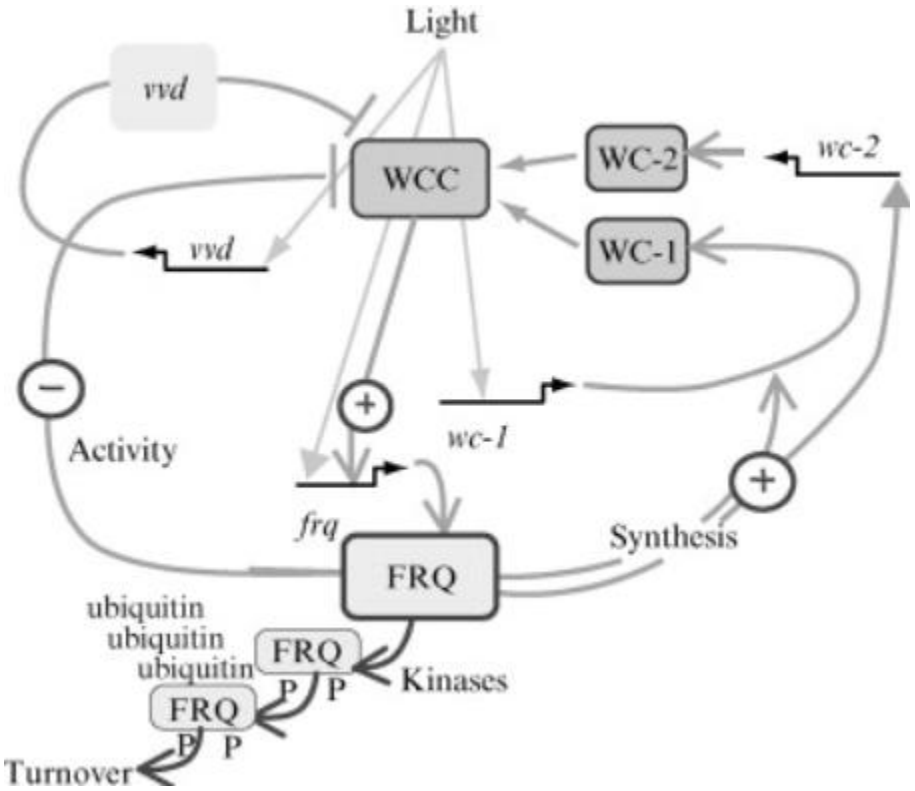


Figure 1.8 Known molecular components in the *Neurospora* circadian clock.

Genes and proteins with known roles in the clock are shown. Lines ending in bars connote negative regulation or repression, and arrows connote positive regulation (activation). P on FRQ denotes phosphorylation. Adapted from (Dunlap & Loros, 2005)

1.3 Non-Canonical Circadian Behaviors in Multiple Species

Several influential observations from diverse model systems have demonstrated that circadian rhythmicity does not always depend strictly on transcription–translation feedback loops, challenging classical views of clock architecture. One of the earliest organisms to suggest this possibility was the marine unicellular green alga *Acetabularia*, which inhabits shallow coastal waters near coral reefs. Although once central to circadian research, it has received less attention in recent decades. *Acetabularia* possesses a distinctive morphology consisting of a basal rhizoid that anchors the cell to the substrate and a long stalk that can reach several centimeters in length during the vegetative phase. Remarkably, the organism contains a single nucleus located within the rhizoid for most of its life cycle. Experimental removal of the nucleus-bearing rhizoid revealed that enucleated cells remain metabolically active and are capable of

sustaining circadian rhythms in photosynthesis for several weeks. In addition, rhythmic chloroplast movements persist in the absence of the nucleus. Studies further demonstrated that inhibiting both nuclear and organellar RNA synthesis does not abolish these rhythms, although blocking protein synthesis alters phase and disrupts phosphorylation cycles, indicating that post-translational processes play a dominant role in timekeeping in this system (Lakin-Thomas, 2006b; Pifer et al., 2024).

As discussed previously, studies in the cyanobacterium *Synechococcus* have provided strong evidence that circadian rhythms can persist independently of transcriptional regulation. Although the *kaiA*, *kaiB*, and *kaiC* genes form a canonical transcriptional feedback system, rhythmicity has been shown to depend primarily on the phosphorylation state of KaiC rather than gene expression itself (Ditty et al., 2003). These phosphorylation cycles continue under conditions where transcription and translation are minimized, such as constant darkness, and remain self-sustained and temperature-compensated (Tomita et al., 2005). Furthermore, in vitro reconstitution experiments demonstrated that the three Kai proteins, together with ATP, are sufficient to generate robust ~24-hour oscillations in phosphorylation, providing clear evidence that post-translational mechanisms alone can sustain circadian rhythmicity (Tomita et al., 2005).

Evidence questioning the absolute requirement of transcriptional cycling has also been obtained from animal systems. In *Drosophila*, which provided the first experimental evidence for transcription–translation feedback loops (TTFLs) as the molecular basis of circadian rhythms, the clock is traditionally described as two interlocked transcriptional feedback loops involving the CLK–CYC activator complex and the PER–TIM repressor complex, with additional regulation mediated by transcriptional repressors such as VRI. However, experimental manipulation of clock gene expression challenged this framework. When *clk* expression was driven by the *per* or *tim* promoter—thereby eliminating its normal antiphase relationship—flies maintained rhythmic molecular and behavioral outputs. Similarly, constitutive expression of *per* and *tim* restored rhythmicity in mutant flies lacking normal gene cycling, indicating that oscillations in RNA abundance enhance robustness but are not strictly required for rhythmic behavior (Hardin, 2004; Kim et al., 2007).

In mammals, the complexity of the circadian system has made it more difficult to dissect the contribution of individual clock components. Studies using combinations of clock gene knockouts have revealed that rhythmicity depends on multiple factors, including age, genetic

background, lighting conditions, and duration of constant darkness. Single knockouts of negative clock elements such as *Cry1* or *Cry2* often retain rhythmicity, whereas double knockouts typically result in immediate arrhythmicity. Similar patterns have been observed for *Per* gene mutants, with partial rhythmicity in single knockouts and complete loss of rhythms in double mutants. Intriguingly, some combinations of mutations restore rhythmic behavior, suggesting compensatory interactions among clock components. In contrast, disruption of positive clock elements such as *Bmal1* leads to immediate arrhythmicity, while mutations in *Clock* produce rhythms that can be temporarily rescued by light exposure. Collectively, these findings suggest that although transcriptional regulation contributes significantly to clock stability and amplitude, it may not be strictly essential for the generation of circadian rhythmicity in mammals (Lakin-Thomas, 2006b)

Together, observations from algae, bacteria, insects, and mammals converge on the conclusion that circadian timekeeping can arise from diverse molecular architectures. These systems highlight the importance of post-translational regulation, protein modification cycles, and metabolic processes in sustaining biological rhythms, providing strong support for the existence of non-canonical oscillators that operate alongside or independently of classical transcription–translation feedback loops.

1.3.1 FRQ-Less Oscillators (FLOs) in *Neurospora crassa*

Although the FRQ/WCC transcription–translation feedback loop is considered the canonical circadian oscillator in *Neurospora crassa*, multiple studies have demonstrated that rhythmicity can persist even when this core loop is disrupted (Aronson et al., 1994; Baker et al., 2012). These observations led to the identification of FRQ-less oscillators (FLOs)—alternative timing mechanisms that can generate circadian rhythms independently of the *frequency (frq)* gene and, in some cases, the White-Collar Complex (Lakin-Thomas & Brody, 2000; Montenegro-Montero et al., 2015). The existence of FLOs challenges the long-held assumption that the FRQ/WCC TTFL is the sole driver of circadian timing in *Neurospora* and instead suggests a more distributed architecture of circadian regulation.

Early evidence for FRQ-independent rhythmicity emerged from experiments showing that *frq*-null and *wc*-null strains retain rhythmic conidiation under specific environmental or genetic conditions (Aronson et al., 1994; Lakin-Thomas & Brody, 2000). These rhythms are most clearly observed when cultures are subjected to nutritional stress or temperature-based entrainment

paradigms, indicating that environmental inputs can reveal oscillatory mechanisms distinct from the canonical clock (Lakin-Thomas, 1998). Compared with FRQ-dependent rhythms, FLO-driven oscillations tend to be more conditional and variable in amplitude, suggesting that they arise from different molecular frameworks.

One of the best-characterized experimental systems for studying FLO activity involves choline-deficient *chol-1* mutant strains, in which robust rhythmic conidiation persists even in the absence of FRQ (Lakin-Thomas & Brody, 2000). In parallel, heat-pulse entrainment experiments conducted in constant darkness have demonstrated sustained rhythmic responses in *frq*-null backgrounds, further supporting the existence of an endogenous oscillator capable of entrainment without the FRQ/WCC loop (Ratnayake et al., 2018). These two approaches—choline starvation and cyclic temperature entrainment—have become standard assays for probing FRQ-less rhythmicity in *Neurospora*.

Genetic dissection of FLO function has identified several key molecular components that affect FRQ-less rhythms. Notably, deletion of *vta* (vacuolar TOR-associated protein) abolishes FLO-driven conidiation rhythms and simultaneously weakens circadian output in FRQ-positive strains (Ratnayake et al., 2018). The *vta* gene encodes a vacuolar membrane–associated protein homologous to components of the TOR signaling pathway in other eukaryotes, linking nutrient signaling to circadian regulation. Subsequent studies identified GTR2, a small GTP-binding protein, as a functional and physical partner of VTA (Eskandari et al., 2021). Loss of *gtr2* disrupts FRQ-less rhythms, compromises heat-pulse entrainment and alters circadian properties even in the presence of FRQ, indicating that FLOs and the canonical clock share overlapping regulatory pathways.

The discovery of FRQ-less oscillators in *Neurospora crassa* has significant implications for circadian biology more broadly. Rather than operating as a single, centralized clock, the circadian system may consist of multiple coupled oscillators, including transcription-based loops and post-translational or metabolic oscillators (Baker et al., 2012; Dunlap & Loros, 2017). This layered organization could provide resilience under fluctuating environmental conditions and may reflect ancestral timing mechanisms that predate the evolution of complex TTFLs. In this context, FLOs are thought to represent either parallel oscillatory systems or foundational metabolic clocks that interact with the FRQ/WCC oscillator.

Collectively, these findings demonstrate that circadian regulation in *Neurospora crassa* extends beyond the classical TTFL framework. The persistence of rhythmicity in FRQ-deficient strains, the sensitivity of FLOs to metabolic and environmental cues, and the requirement for TOR-associated components strongly suggest that cellular metabolism plays a direct role in circadian timekeeping (Ratnayake et al., 2018; Eskandari et al., 2021). These observations have led to the hypothesis that the Target of Rapamycin (TOR) pathway may function as, or contribute to, the FRQ-less oscillator—a hypothesis that forms the central focus of this thesis.

1.4 TOR (target of rapamycin pathway)

The growth, proliferation, and survival of eukaryotic cells depend on their ability to continuously assess and respond to internal metabolic status and external environmental conditions, particularly nutrient availability and stress signals. Central to this regulatory capacity is the Target of Rapamycin (TOR) signaling pathway, an evolutionarily conserved system that functions as a master coordinator of cellular metabolism and growth across eukaryotic lineages (Roelants et al., 2017; Shukla et al., 2025). TOR—known as mTOR in mammals—acts as a signaling hub that promotes anabolic processes, including protein synthesis, ribosome biogenesis, nucleotide and lipid production, while simultaneously suppressing catabolic pathways such as autophagy. Through this coordinated control, TOR signaling maintains metabolic balance and ensures that cell growth occurs only under favorable conditions (Liu et al., 2025).

The TOR pathway was first identified in the budding yeast *Saccharomyces cerevisiae* through genetic screens for mutants resistant to the immunosuppressive compound rapamycin, which inhibits cell growth. Subsequent studies revealed conserved TOR homologs in mammals and other eukaryotes, highlighting the ancient and universal nature of this pathway (Loewith & Hall, 2011). Dysregulation of TOR signaling has profound physiological consequences: excessive TOR activity is associated with pathological cell growth observed in cancer, tumorigenesis, and neurological disorders, whereas reduced TOR signaling has been linked to delayed aging and increased lifespan in multiple organisms (Condon & Sabatini, 2019; Shukla et al., 2025).

At the molecular level, TOR proteins belong to the phosphoinositide 3-kinase–related kinase (PIKK) family and are atypical serine/threonine kinases characterized by a conserved modular

architecture (Saxton & Sabatini, 2017). From the N-terminus to the C-terminus, TOR proteins contain extensive HEAT repeat regions that mediate protein–protein interactions, followed by the FAT domain, the FKBP–rapamycin binding (FRB) domain, the catalytic kinase domain, and a short FATC domain essential for enzymatic activity (Loewith & Hall, 2011; Tatebe & Shiozaki, 2017). This conserved domain organization allows TOR to assemble into multiprotein complexes and interact with numerous regulatory partners.

TOR functions within two structurally and functionally distinct complexes: TOR complex 1 (TORC1) and TOR complex 2 (TORC2). While mammals encode a single TOR protein that participates in both complexes, several fungi possess two TOR paralogs that differentially contribute to TORC1 and TORC2 assembly (Saxton & Sabatini, 2017; González & Hall, 2017). TORC1 is uniquely sensitive to rapamycin, whereas TORC2 is resistant due to structural differences that prevent drug binding. In yeast, TORC2 is essential for viability, while TORC1 can be supported by either TOR paralog, underscoring functional specialization between the two complexes (Eltschinger & Loewith, 2016) (Figure 1.10).

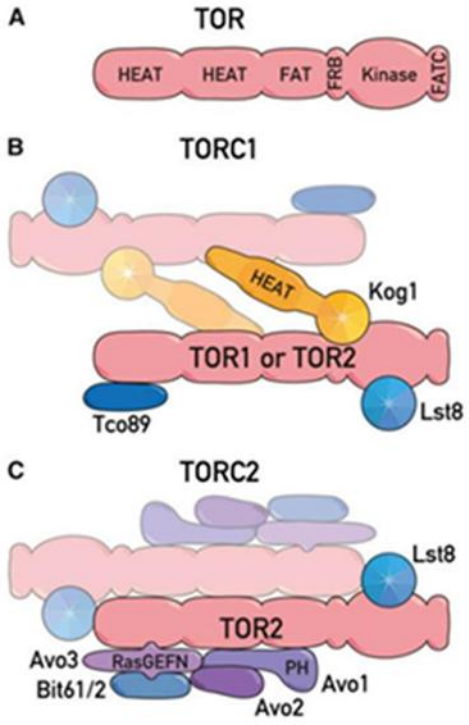


Figure 1.10 TORC domains in yeast.

A) Conserved domain of TOR, B) composition of TOR Complex1 which is approximately 2 MDa in size, C) composition of TOR Complex2 which is approximately 2 MDa in size. (Adapted from Loewith & Hall, 2011).

The biochemical identity of each TOR complex is determined by its associated regulatory subunits. TORC1 includes the scaffold protein RAPTOR (or Kog1 in yeast), which mediates substrate recruitment, and mLST8, which stabilizes the kinase domain. Additional inhibitory components, such as PRAS40 and DEPTOR, fine-tune TORC1 activity (Laplante & Sabatini, 2012; Saxton & Sabatini, 2017). In contrast, TORC2 is defined by the presence of RICTOR, SIN1, and additional accessory proteins that regulate cytoskeletal organization, cell survival, and kinase activation within the AGC family (Shimobayashi & Hall, 2014). Although the overall architecture of TOR complexes is conserved between fungi and mammals, species-specific subunits introduce regulatory flexibility that reflects distinct cellular demands (González & Hall, 2017).

Functionally, TORC1 serves as a primary sensor of nutrient and energy status. In unicellular organisms, nutrient availability alone, particularly amino acids and carbon sources, is sufficient

to activate TORC1 signaling, whereas in multicellular organisms, growth factors such as insulin act in concert with nutrients to regulate TOR activity (González & Hall, 2017; Lakin-Thomas, 2019). TORC1 integrates signals from amino acids, cellular energy levels, oxygen availability, and stress pathways through a coincidence-detection mechanism that ensures activation only when growth conditions are optimal (Laplante & Sabatini, 2012; Condon & Sabatini, 2019). This process requires both recruitment of TORC1 to the lysosomal membrane via Rag GTPases and activation by the small GTPase Rheb, effectively functioning as an AND gate for growth-promoting signals (Rabanal-Ruiz & Korolchuk, 2018) (Figure 1.11).

Once activated, TORC1 stimulates biosynthetic pathways that drive cell growth and division while suppressing autophagy and other catabolic processes. In contrast, TORC2 primarily responds to growth factor signaling and regulates cell polarity, cytoskeletal remodeling, and metabolic homeostasis (Saxton & Sabatini, 2017; González & Hall, 2017). Together, these two complexes allow the TOR pathway to coordinate cellular physiology across diverse environmental and developmental contexts. Owing to its central role in metabolism, growth, and stress adaptation, TOR signaling has become one of the most intensively studied pathways in yeast and mammalian systems and represents a key interface between nutrient sensing and broader regulatory networks.

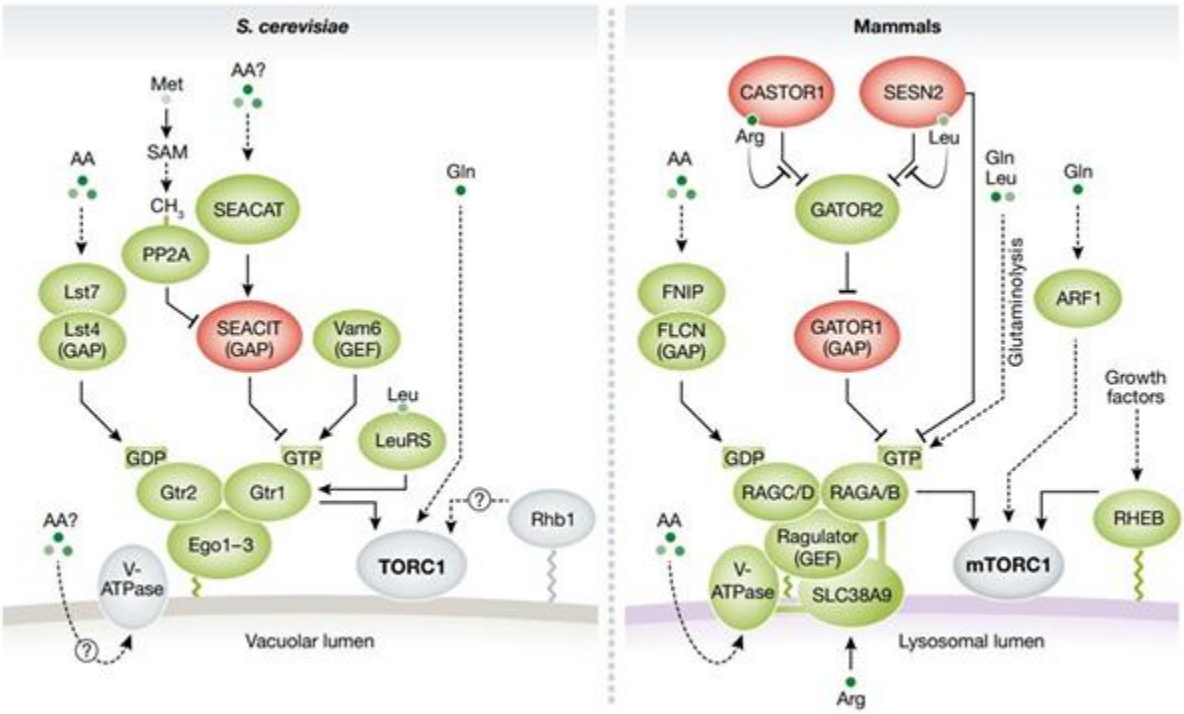


Figure 1.11 TORC1 regulation in S. cerevisiae and mammals.

Green proteins activate TORC1 and red proteins inhibit TORC1. Dashed lines show indirect interaction. Adapted from González & Hall (2017).

1.4.1 Growth Factor Pathways Driving mTORC1 Activation

Growth factor signaling activates mTORC1 through intracellular kinase networks that converge upstream of the complex. A principal route involves PI3K-dependent activation of PDK1 and AKT, which subsequently targets the tuberous sclerosis complex (TSC1/2), a key suppressor of mTORC1 signaling. Phosphorylation of TSC1/2 by AKT diminishes its inhibitory control over the small GTPase Rheb, allowing Rheb to accumulate in its active, GTP-bound state and promote mTORC1 activation (Shimobayashi & Hall, 2014). In parallel, AKT enhances mTORC1 signaling through a TSC-independent mechanism by phosphorylating PRAS40, an inhibitory subunit of the complex, leading to its dissociation and further relief of repression (Condon & Sabatini, 2019). Growth factor inputs are also transmitted through MAPK signaling pathways; in particular, ERK-dependent phosphorylation of TSC2 has been shown to weaken its inhibitory function and reinforce Rheb-mediated activation of mTORC1 (Ma et al., 2005).

Collectively, these signaling events culminate at the lysosomal membrane, where GTP-bound Rheb directly engages mTORC1 and stimulates its kinase activity (Condon & Sabatini, 2019)(Figure 1.12)

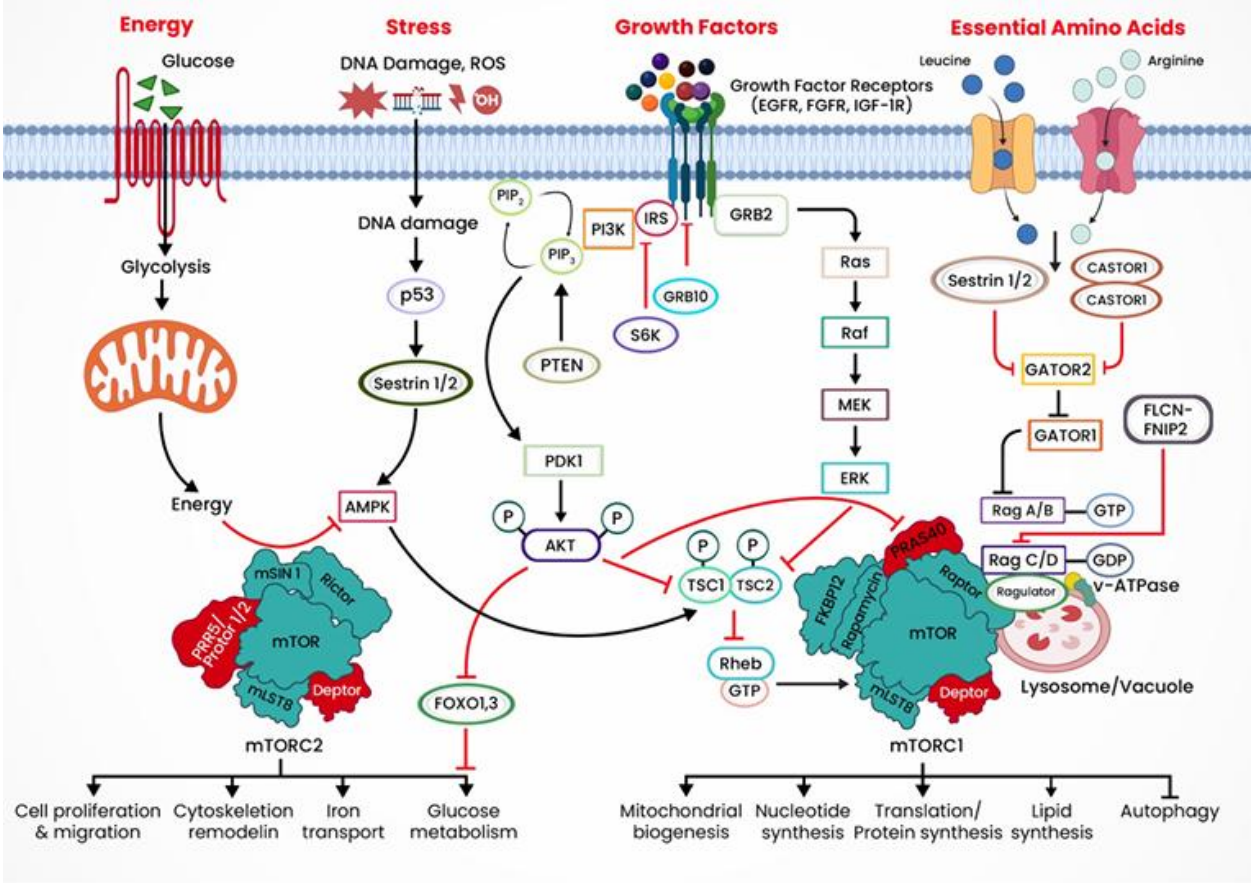


Figure 1.12 Schematic diagram representing the major regulators and downstream effectors of mTORC1 and mTORC2.

mTORC1 is primarily composed of mTOR, Raptor, and mLST8, while the main subunits of mTORC2 are mTOR, Rictor, mLST8, and mSin1. Multiple stimuli such as growth factors, amino acids like arginine and leucine, energy sources such as glucose, and cellular stresses including DNA damage, and ROS stimulate mTORC1 activity through the GATOR2-GATOR1-Rag GTPases axis and the TSC2-Rheb GTPase route. mTORC1 activates anabolic processes such as mitochondrial biogenesis, nucleotide, protein, and lipid synthesis while blocking catabolic events such as autophagy. mTORC2 mainly responds to growth factors or insulin and regulates cell proliferation, migration, cytoskeleton remodeling, ion transport and glucose metabolism. The negative regulatory elements of mTORC1 (PRAS40 and Deptor) and mTORC2 (PRR5/Protor1/2 and Deptor) are depicted in red, Adapted from (Panwar et al., 2023).

1.4.2 Amino Acid–Dependent Control of TORC1 Localization at the Lysosome

Amino acid availability regulates mTORC1 signaling through a conserved module composed of small GTPases of the Ras superfamily, known as Rag GTPases, which function primarily as spatial regulators rather than direct enzymatic activators of the kinase. In mammalian cells, Rag

GTPases control the recruitment of mTORC1 from the cytosol to the lysosomal membrane, a subcellular location required for its activation by the small GTPase Rheb (Sancak et al., 2010; González & Hall, 2017). This nutrient-dependent relocalization is mediated through interactions between the Rag heterodimer and the mTORC1 scaffolding subunit Raptor, thereby coupling intracellular amino acid levels to mTORC1 signaling output.

Mammalian cells express four Rag proteins—RagA, RagB, RagC, and RagD—which assemble into obligate heterodimers consisting of one RagA or RagB subunit paired with one RagC or RagD subunit (Laplante & Sabatini, 2012). The activity of these heterodimers is determined by their nucleotide-loading state. Amino acid sufficiency, particularly the presence of leucine and arginine, promotes a configuration in which RagA/B is GTP-bound, and RagC/D is GDP-bound. This active conformation enables binding to Raptor and facilitates mTORC1 recruitment to the lysosomal surface, positioning the complex for activation by Rheb (González & Hall, 2017). Importantly, Rag GTPases remain associated with lysosomes independently of nutrient status through their interaction with the Ragulator complex, which acts as a stable lysosomal scaffold rather than a nutrient sensor itself (Sancak et al., 2010; Laplante & Sabatini, 2012).

In budding yeast, a related but distinct regulatory scheme operates. The Rag homologs Gtr1 and Gtr2 form a heterodimer that associates with the vacuolar membrane—the functional equivalent of the mammalian lysosome—via the EGO complex (Hughes Hallett et al., 2014; González & Hall, 2017). Unlike mammalian mTORC1, yeast TORC1 is constitutively localized to the vacuolar membrane regardless of nutrient availability. In this system, amino acids and nitrogen sources regulate TORC1 activity primarily by modulating the nucleotide state of Gtr1 and Gtr2 rather than by controlling TORC1 localization (Dokládal et al., 2021). When nutrients are abundant, the GTP-loaded Gtr1–GDP-bound Gtr2 configuration promotes interaction with Kog1, the yeast homolog of Raptor, thereby stimulating TORC1 activity. Thus, while the core components of amino acid signaling to TORC1 are evolutionarily conserved, the relative contributions of spatial regulation versus activity modulation differ between yeast and mammalian systems.

1.4.3 Mechanisms of Translational Control Downstream of TORC1

The stimulation of protein production is one of the most extensively studied anabolic outputs governed by mTORC1 signaling (Laplante & Sabatini, 2012). mTORC1 exerts its influence over

translation primarily by modulating key regulators of initiation and ribosome function, most notably the translational repressor 4E-binding protein 1 (4E-BP1) and the serine/threonine kinase S6K1 (Albert & Hall, 2015; Saxton & Sabatini, 2017). When mTORC1 is active, it phosphorylates 4E-BP1, reducing its affinity for eIF4E and thereby permitting assembly of the eIF4F initiation complex at the 5′ cap of mRNAs. This event facilitates cap-dependent translation initiation and promotes increased protein synthesis across the cell (Ben-Sahra & Manning, 2017).

S6K1, a member of the AGC kinase family, also functions as a major downstream effector of mTORC1. Full activation of S6K1 requires coordinated phosphorylation at multiple residues: mTORC1 targets a conserved threonine residue within the hydrophobic motif, while PDK1—acting downstream of PI3K signaling—provides an additional activating phosphorylation (Finger & Kramer, 2021; Wullschleger et al., 2006). Once activated, S6K1 phosphorylates the ribosomal protein S6 on several serine residues, an event that enhances translation of mRNAs containing 5′ terminal oligopyrimidine (TOP) motifs. These transcripts encode components of the translational apparatus, including ribosomal proteins and elongation factors, thereby expanding the overall translational capacity of the cell (Shimobayashi & Hall, 2014; Wullschleger et al., 2006). Genetic studies further underscore the importance of this pathway: loss of S6K activity or mutation of S6 phosphorylation sites markedly disrupts ribosome biogenesis and reduces expression of genes involved in protein synthesis (Shimobayashi & Hall, 2014).

Beyond its effects on ribosomal protein production, S6K1 also fine-tunes translation by targeting additional factors involved in mRNA processing and initiation. For example, S6K1 promotes the activity of the RNA helicase eIF4A by phosphorylating and recruiting its cofactor eIF4B, while simultaneously inhibiting the translation suppressor PDCD4. Through these combined actions, S6K1 facilitates efficient unwinding of structured mRNAs during early stages of translation (Albert & Hall, 2015; Ben-Sahra & Manning, 2017).

Many of these regulatory principles are conserved in yeast. In *Saccharomyces cerevisiae*, the AGC kinase Sch9—an ortholog of mammalian S6K—is directly phosphorylated by TORC1 at multiple sites within its C-terminal region, a modification that is essential for Sch9 activity (Loewith & Hall, 2011; Yan et al., 2006). Because Sch9 phosphorylation rapidly responds to nutrient availability and is abolished upon rapamycin treatment, it serves as a widely used biochemical readout of TORC1 activity in fungal systems (Loewith & Hall, 2011). Activated

Sch9 influences diverse growth-related processes, including ribosome production, translational initiation, stress resistance, and transitions into quiescence (Urban et al., 2007).

TORC1 also regulates ribosomal biogenesis through transcriptional control. Phosphorylation of the zinc-finger transcription factor Sfp1 by TORC1 enhances expression of ribosomal protein genes and other growth-associated transcripts (Loewith & Hall, 2011). Interestingly, Sfp1 regulation appears to be mechanistically distinct from Sch9, as its activity is less sensitive to certain stress conditions, suggesting that TORC1 employs multiple parallel strategies to coordinate protein synthesis (Loewith & Hall, 2011).

Despite its central role in promoting translation, TORC1 activity is itself influenced by protein synthesis rates. Experimental inhibition of translation—either pharmacologically or through reduced ribosomal gene expression—can paradoxically lead to elevated TORC1 signaling, potentially as a consequence of increased intracellular amino acid availability (Albert & Hall, 2015; Eltschinger & Loewith, 2016). Although the precise molecular basis of this feedback remains unresolved, it highlights the close coupling between nutrient sensing, translational output, and TORC1 regulation.

In addition to kinases and transcription factors, TORC1 signaling interfaces with serine/threonine phosphatases in a nutrient-dependent manner. When TORC1 is active, phosphorylation of the regulatory protein Tap42 promotes its association with phosphatase catalytic subunits, including Sit4 and PP2A-like complexes, thereby restraining their activity (Di Como & Arndt, 1996; Finger & Kramer, 2021; Loewith & Hall, 2011). Upon TORC1 inhibition, Tap42 is dephosphorylated, leading to phosphatase release and activation of downstream pathways involved in nitrogen metabolism, mitochondrial function, and stress adaptation (Yan et al., 2006). Mutations in Tap42 that disrupt this regulatory axis confer resistance to rapamycin, underscoring its importance as a key effector of TORC1 signaling (Finger & Kramer, 2021; Loewith & Hall, 2011).

1.4.4 Control of TOR Signaling Networks in Plants

Although the TOR signaling pathway has been extensively characterized in yeast and mammals, its functional organization in plants remains comparatively less well defined. While core features of TOR signaling are evolutionarily conserved, plants are missing several canonical components that mediate TOR regulation in other eukaryotes, indicating the presence of plant-specific regulatory adaptations (Burkart & Brandizzi, 2021). Notably, the TOR kinase itself is

highly conserved across kingdoms; the kinase domains of *Arabidopsis thaliana* TOR and human mTOR share approximately 73% amino acid sequence similarity, underscoring the preservation of catalytic function despite divergence in regulatory architecture (Wu et al., 2019).

In plants, TOR assembles into a TORC1-like complex that includes the conserved regulatory proteins RAPTOR (Regulatory-Associated Protein of mTOR) and LST8 (Lethal with SEC13 Protein 8), both of which are required for proper TOR signaling output (Shi et al., 2018). Unlike their yeast and mammalian counterparts, however, plant TOR signaling is uniquely shaped by the sessile and autotrophic nature of plant life. In addition to responding to universal metabolic cues such as glucose availability, amino acids, and cellular energy status, plant TOR integrates signals derived from light, phytohormones, and inorganic nutrients including nitrate, ammonium, phosphate, and sulfate (Fu et al., 2020). This expanded input repertoire positions TOR as a central signaling nexus that coordinates environmental and endogenous information to regulate growth-associated processes such as cell cycle progression, nutrient uptake and transport, metabolic reprogramming, and global protein synthesis.

In *Arabidopsis thaliana*, glucose and cellular energy availability play a pivotal role in TOR activation, acting in concert with light and hormonal signals to modulate developmental outcomes. While glucose alone can stimulate TOR-dependent proliferation in root meristems, TOR-mediated growth of leaf primordia requires the combined presence of both glucose and light, highlighting tissue-specific differences in signal integration (Shi et al., 2018). Light signals are perceived through photoreceptors including phytochromes and cryptochromes, which converge on the COP1–auxin–RPS6 signaling axis to promote TOR activation and translational control (Chen et al., 2018). Auxin signaling further enhances TOR activity through the small Rho-like GTPase ROP2, as constitutive activation of ROP2 leads to sustained TOR signaling and enhanced growth responses (Shi et al., 2018).

Unlike yeast and mammals, plants lack the Rag GTPases and Ragulator complex that mediate amino acid sensing upstream of TORC1, suggesting that plants rely on alternative mechanisms to couple amino acid availability to TOR activation. Emerging evidence indicates that elevated levels of certain amino acids, including proline and alanine, are sufficient to stimulate TOR signaling and promote protein synthesis in plant cells (Burkart & Brandizzi, 2021). In addition, mutations in isopropylmalate synthase 1 (IPMS1), a key enzyme in leucine biosynthesis, result in the accumulation of branched-chain amino acids—particularly valine—

which in turn leads to heightened TOR activity (Cao et al., 2019). Intriguingly, increased TOR signaling under these conditions is associated with enhanced actin filament bundling. Given that actin cytoskeleton dynamics are regulated by TORC2 in yeast and mammals, these findings suggest that plant TOR may influence cytoskeletal organization through a noncanonical mechanism, despite the apparent absence of a classical TORC2 complex (Burkart & Brandizzi, 2021; Cao et al., 2019).

1.4.5 Regulation and Function of Ribosomal Protein S6

Ribosomal protein S6 (RPS6) is a component of the 40S small ribosomal subunit and represents one of the best-characterized downstream targets of ribosomal protein S6 kinase (S6K). RPS6 can exist in several phosphorylation states within the cell, reflecting different levels of signaling activity. The highly phosphorylated form of the protein is typically associated with increased translational activity and is therefore considered the functionally active state. Phosphorylation of RPS6 occurs predominantly downstream of the mTORC1 signaling pathway, where activation of S6 kinase leads to the modification of multiple residues on RPS6, linking cellular nutrient and growth signals to the regulation of protein synthesis (Roux & Topisirovic, 2012).

In mammalian systems, the regulatory phosphorylation sites of RPS6 are clustered in the C-terminal region of the protein. Five serine residues: Ser235, Ser236, Ser240, Ser244, and Ser247, have been identified as the principal phosphorylation sites that regulate RPS6 activity (Roux & Topisirovic, 2012; Ruvinsky & Meyuhas, 2006). These residues can be phosphorylated by members of the S6 kinase family as well as by certain mitogen-activated protein kinases (MAPKs). The number and combination of phosphorylated residues vary depending on cellular conditions and signaling inputs. However, phosphorylation at multiple sites within this cluster is generally associated with maximal activation of RPS6 and enhanced translational capacity. Evidence suggests that phosphorylation of these residues may occur in a defined sequence, with Ser236 proposed as one of the initial sites targeted due to its compatibility with the recognition motif of S6K (Ruvinsky & Meyuhas, 2006).

Comparative analyses across eukaryotes reveal differences in the number of regulatory phosphorylation sites present in RPS6. In budding yeast, the S6 protein contains only two phosphorylation sites, whereas the mammalian protein contains five. Functional studies in mice in which these serine residues were replaced with non-phosphorylatable alanine residues

demonstrated that loss of RPS6 phosphorylation affects several physiological processes, including cell growth, proliferation, and glucose homeostasis (Ruvinsky & Meyuhas, 2006).

Structural investigations have also provided insight into the architecture of RPS6 in filamentous fungi. Cryo-electron microscopy analysis of ribosomes from *Neurospora crassa*, stabilized with the translation inhibitor cycloheximide, revealed the structure of the 40S ribosomal subunit and its associated proteins (Shen et al., 2021). The *Neurospora* RPS6 protein consists of 239 amino acids and contains a combination of α-helical and β-sheet structural elements. Two putative phosphorylation sites are located in the C-terminal α-helical tail of the protein, within the sequence VQKADARKRRASSMRK239 (PDB: 7R81)(Shen et al., 2021) .

Because RPS6 phosphorylation reflects the activity of the TOR–S6K signaling axis, monitoring the phosphorylation state of this protein provides a useful biochemical indicator of TOR pathway activation. In this study, the phosphorylation status of RPS6 is therefore used as a molecular readout of TOR signaling activity in *Neurospora crassa*.

1.4.6 Feedback Regulation of TOR Signaling

The TOR signaling pathway is regulated through a network of positive and negative feedback mechanisms that enable cells to respond dynamically to changes in nutrient availability, energy status, growth factors, and environmental stress. When TORC1 is activated, it promotes anabolic processes such as protein synthesis, ribosome biogenesis, and lipid and nucleotide synthesis. These processes consume large amounts of amino acids and ATP, gradually reducing the intracellular resources required to sustain TOR activity. As nutrient and energy levels decline, energy-sensing pathways, including AMPK, inhibit TORC1 activity. At the same time, reduced TORC1 activity relieves the inhibition of autophagy, allowing intracellular components to be degraded and recycled to replenish amino acid pools and restore cellular energy. Once nutrients become available again, TORC1 is reactivated, initiating another round of anabolic activity. This sequence of TOR activation, nutrient depletion, TOR inhibition, nutrient recycling, and TOR reactivation forms a delayed negative feedback loop. Since delayed negative feedback is a fundamental characteristic of biological oscillators, this regulatory architecture has led to the proposal that TOR signaling could function as a metabolic oscillator independently of the canonical transcription–translation feedback loop (TTFL). Such a mechanism may provide an explanation for rhythmic cellular processes that persist even when the TTFL is disrupted. (Lakin-Thomas, 2023)

1.4.7 TOR Signaling in *Neurospora crassa*

The high degree of conservation of the Target of Rapamycin (TOR) signaling pathway across the fungal kingdom highlights its evolutionary importance as a central nutrient- and growth-sensing system that enables eukaryotic organisms to adapt to fluctuating environmental conditions (Shertz et al., 2010). Within fungi, TOR signaling has been studied most extensively in the budding yeast *Saccharomyces cerevisiae*, the fission yeast *Schizosaccharomyces pombe*, and the human pathogen *Candida albicans*. In contrast, comparatively little is known about the molecular organization and regulation of the TOR pathway in the filamentous fungus *Neurospora crassa*. (Figure 1.13)

Several components of the TOR pathway have nevertheless been identified in *N. crassa*. Multiple FK506-binding proteins (FKBPs), which mediate rapamycin sensitivity, have been characterized in this organism (Ratnayake et al., 2018). A large-scale serine/threonine kinase deletion screen further revealed the presence of TOR kinase homologs based on sequence similarity to yeast TOR1 and TOR2. The apparent absence of a viable homokaryotic TOR deletion strain in the Fungal Genetics Stock Center suggests that TOR is an essential gene in *Neurospora* (Ratnayake et al., 2018). The same screening effort identified STK-10 as the *Neurospora* homolog of the yeast AGC kinase Sch9 and mammalian S6 kinase. Deletion of *stk-10* results in severe growth defects and impaired osmoregulation, consistent with its role as a downstream effector of TOR signaling (Ratnayake et al., 2018).

In parallel, our laboratory's efforts to identify components of the FRQ-less oscillator within the circadian system of *N. crassa* led to the discovery of two TOR pathway–associated proteins, VTA and GTR2 (Eskandari et al., 2021; Ratnayake et al., 2018). These proteins, beyond their canonical roles in nutrient sensing and growth regulation, also contribute to circadian rhythmicity. Deletion of *vta* or *gtr2* results in dampened conidiation rhythms and compromised FRQ protein oscillations in both FRQ-sufficient and FRQ-deficient genetic backgrounds (Eskandari et al., 2021; Ratnayake et al., 2018). VTA, a homolog of yeast Ego1 and mammalian LAMTOR1, localizes to the vacuolar membrane and participates in the transmission of nutritional signals to the TOR kinase, while GTR2 functions as the *Neurospora* counterpart of the yeast Rag GTPase Gtr2 (Eskandari et al., 2021; Lakin-Thomas, 2019).

Additional evidence linking TOR signaling to circadian regulation in *Neurospora* comes from studies of *prd-4*, the fungal ortholog of mammalian checkpoint kinase 2 (CHK2). PRD-4 is

activated by TOR kinase in response to translational stress and subsequently phosphorylates the core clock protein FRQ, leading to phase advancement of the conidiation rhythm (Dong et al., 2008). Together with comparative observations across species, these findings suggest that TOR signaling may play an integral role in the generation or modulation of FRQ-less oscillations in *Neurospora crassa*, providing a strong rationale for investigating TOR as a candidate metabolic oscillator within the circadian network.

Our laboratory recently developed an assay to monitor TOR pathway activity in *N. crassa* by measuring the phosphorylation state of the ribosomal protein S6. Ribosomal protein S6 is highly conserved across eukaryotes, particularly within its functional domains, underscoring its essential role in ribosome structure and translational control (González & Hall, 2017). Similar to yeast Rps6, which contains two TOR-dependent phosphorylation sites at its C-terminus, the *Neurospora* S6 protein also harbors two conserved phosphorylation sites. Western blot analysis resolves three distinct S6 species corresponding to unphosphorylated, mono-phosphorylated, and di-phosphorylated forms, which collapse into a single band following phosphatase treatment, confirming their phosphorylation-dependent mobility shifts (Akhtari et al., 2026). Using this approach, robust circadian oscillations in S6 phosphorylation were observed in solid agar cultures grown under constant darkness and temperature, indicating rhythmic TOR kinase activity (Akhtari et al., 2026; Lakin-Thomas, 2023).

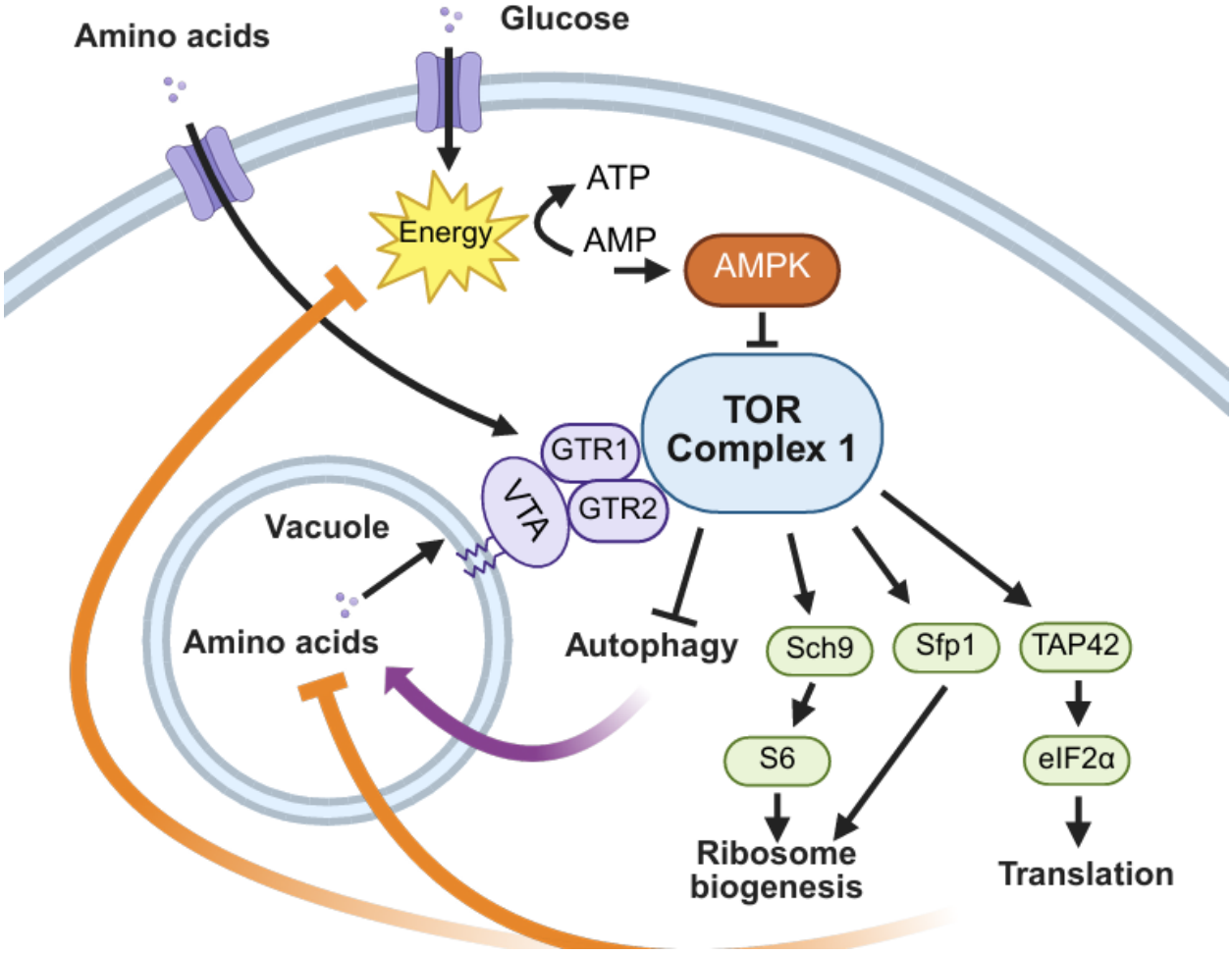


Figure 1.13 Schematic representation of the TOR signaling pathway in *Neurospora crassa*.

Illustration of the integration of nutrient and energy signals, including amino acids, glucose, and cellular energy status (ATP/AMP), through upstream regulators such as GTR1, GTR2, and VTA. TOR Complex 1 (TORC1) coordinates multiple downstream processes, including ribosome biogenesis, protein translation, and autophagy, through key effectors such as Sch9, S6, Sfp1, TAP42, and eIF2α. In addition, AMPK acts as an energy sensor that negatively regulates TOR activity under low-energy conditions, highlighting the balance between growth and stress responses. Together, this pathway links environmental and metabolic inputs to cellular growth, protein synthesis, and homeostasis. (Adapted from Lakin-Thomas 2023).

1.5 Temperature Entrainment of Circadian Rhythms in *Neurospora crassa*

Environmental temperature fluctuations represent an important class of zeitgebers that can synchronize endogenous circadian clocks with external environmental cycles. In the filamentous fungus *Neurospora crassa*, periodic changes in temperature are capable of entraining circadian rhythms even when organisms are maintained in constant darkness, demonstrating that thermal cues alone can act as potent synchronizing signals. Under laboratory conditions, rhythmic

conidiation has been widely used as a measurable output of the fungal circadian clock, and studies have shown that alternating temperature regimes can establish stable phase relationships between the internal oscillator and the imposed environmental cycle. These responses display key properties of circadian entrainment rather than simple environmental forcing. For example, when the period of the temperature cycle differs from the organism's endogenous free-running period, the phase of the rhythm shifts systematically relative to the external cycle, indicating that the environmental signal is interacting with the underlying circadian oscillator rather than directly driving the rhythmic output (Merrow et al., 1999) (Figure 1.14).

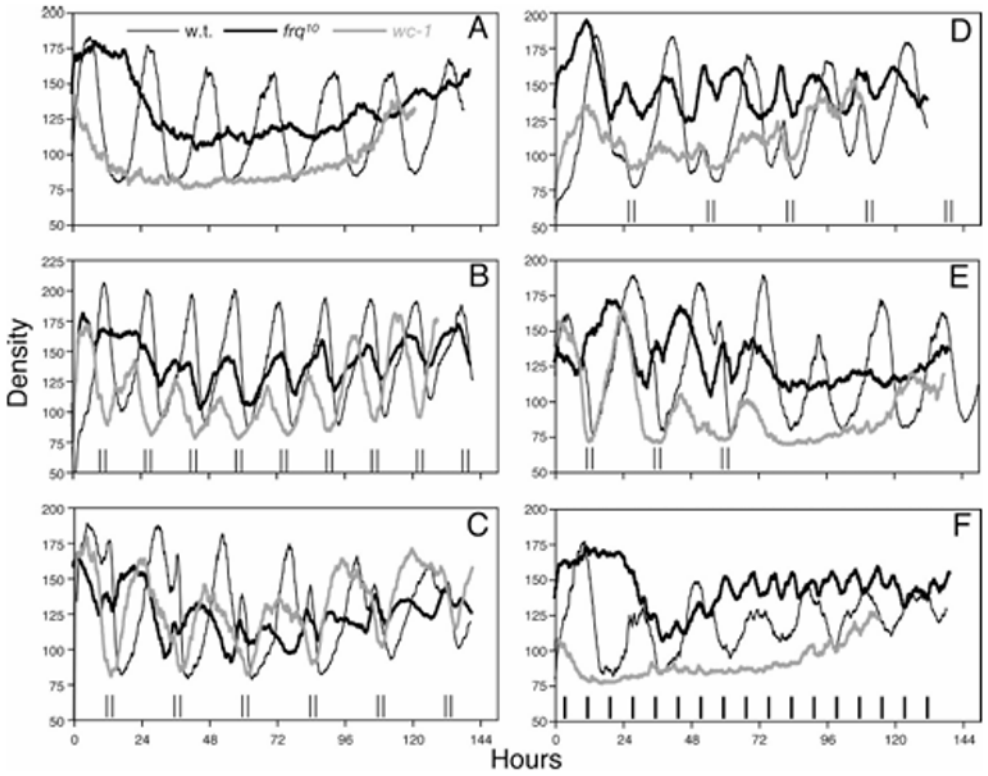


Figure 1.14 Entrainment of *Neurospora crassa* conidiation rhythms by repeated heat-pulse temperature cycles.

Density traces show rhythmic banding patterns under different T-cycles applied in constant darkness. Density traces from six replicate race tubes were averaged, and the mean trace was plotted against total culture time in constant darkness (DD). The experiments shown are representative examples. Thin lines represent wild-type (w.t.) strains, thick black lines represent *frq10* strains, and thick gray lines represent *wc-1* strains. Short vertical marks along the x-axis indicate the onset and termination of heat pulses. Experimental conditions were as follows: (A) control cultures with no heat pulses; (B) a 16-h temperature cycle (T16) consisting of 2-h heat pulses at 30°C; (C) a 24-h temperature cycle (T24) consisting of 2-h heat pulses at 37°C; (D) a 28-h temperature cycle (T28) consisting of 2-h heat pulses at 30°C; (E) a 24-h temperature cycle (T24) consisting of 2-h heat pulses at 37°C, with heat treatment discontinued after the third pulse; and (F) an 8-h temperature cycle (T8) consisting of 0.5-h heat pulses at 30°C. (Adapted from Lakin-Thomas, 2006a).

Further experimental work has demonstrated that temperature cycles can generate additional characteristic circadian behaviors, such as frequency demultiplication when organisms are exposed to short temperature cycles. In these conditions, rhythmic outputs may occur every second environmental cycle, reflecting the intrinsic periodicity of the circadian clock rather than the imposed environmental period. These findings highlight that thermal entrainment mechanisms reveal fundamental properties of the circadian oscillator and provide insights into how environmental signals interact with internal timekeeping systems. (Lakin-Thomas, 2006a)

Together, these studies demonstrate that temperature signals are capable of synchronizing the circadian clock independently of light and can reveal oscillator properties that may otherwise remain masked under constant conditions. Therefore, applying controlled thermal regimes, such as T-cycles of repeated heat pulses in constant darkness, provides an effective experimental framework for investigating the mechanisms underlying circadian oscillations and their interaction with metabolic and signaling pathways in *Neurospora crassa*.

Published results have characterized conidiation density patterns under different T-cycle heat pulse conditions, providing insight into the presence or absence of entrained oscillatory behavior. In the frq10 strain, peaks of conidiation were observed to occur at different time points depending on the imposed T-cycle, indicating that the timing of conidiation is responsive to external entrainment cues. This phase shifting across T-cycles is consistent with the presence of an entrained oscillator, often referred to as a FRQ-less oscillator (FLO). In contrast, in both vta and gtr2 mutant strains, conidiation peaks occurred at the same time regardless of the T-cycle applied. This lack of phase adjustment across different entrainment conditions suggests an absence of functional rhythmicity in these mutants. (Figure1.15)

These findings highlight a fundamental difference in the ability of these strains to respond to environmental timing cues and suggest that while frq10 retains an entrainable rhythmic mechanism, disruption of key TOR pathway components such as VTA and GTR2 abolishes this capacity.

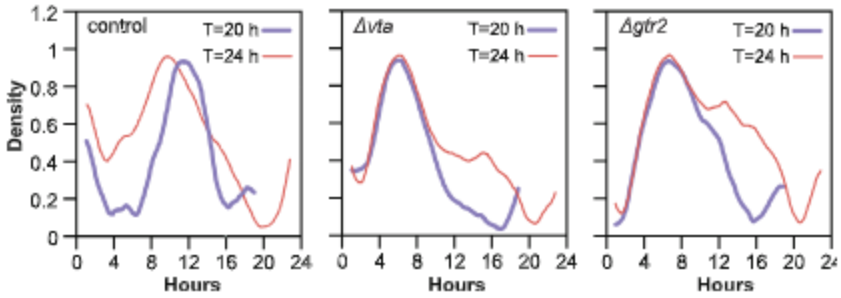


Figure 1.15 Conidiation density under T-cycle heat pulse conditions.

In the *frq10* strain, conidiation peaks shift with T-cycle length, indicating an entrained oscillator (FLO). In contrast, *vtafrq10* and *gtr2frq10* mutants show consistent peak timing across T-cycles, suggesting loss of rhythmicity.(Eskandari et al., 2021)

1.6 Predictive Modeling of TOR Rhythmicity Using STELLA

A computational model was developed, using the dynamic simulation software STELLA (ISEE Systems) to predict the expected behavior of TOR signaling during heat-pulse entrainment. The purpose of this model was to establish a theoretical framework for understanding how rhythmic TOR activity might respond to repeated thermal stimuli and to guide the interpretation of the experimental observations. By simulating the proposed interactions among heat pulses, TOR activity, protein synthesis, amino acid availability, the VTA/GTR signaling module, and conidiation, the model enabled different T-cycle lengths and pulse parameters to be evaluated *in silico*. **(**Figure 1.16**)** illustrates the conceptual STELLA model used in this study. The model did not include any input from the FRQ-based TTFL, because it is a simulation of FRQ-less strains. In this model, heat pulses serve as the primary environmental input regulating TOR activity. TOR signaling is linked to downstream processes including ribosomal protein S6 phosphorylation, protein synthesis, amino acid availability, and ultimately conidiation. The proposed VTA/GTR regulatory module is also incorporated into the signaling network. Furthermore, experimental parameters such as T-cycle duration, pulse length, pulse size, and the timing of the first heat pulse can be adjusted to predict their effects on TOR rhythmicity. (Appendix I)

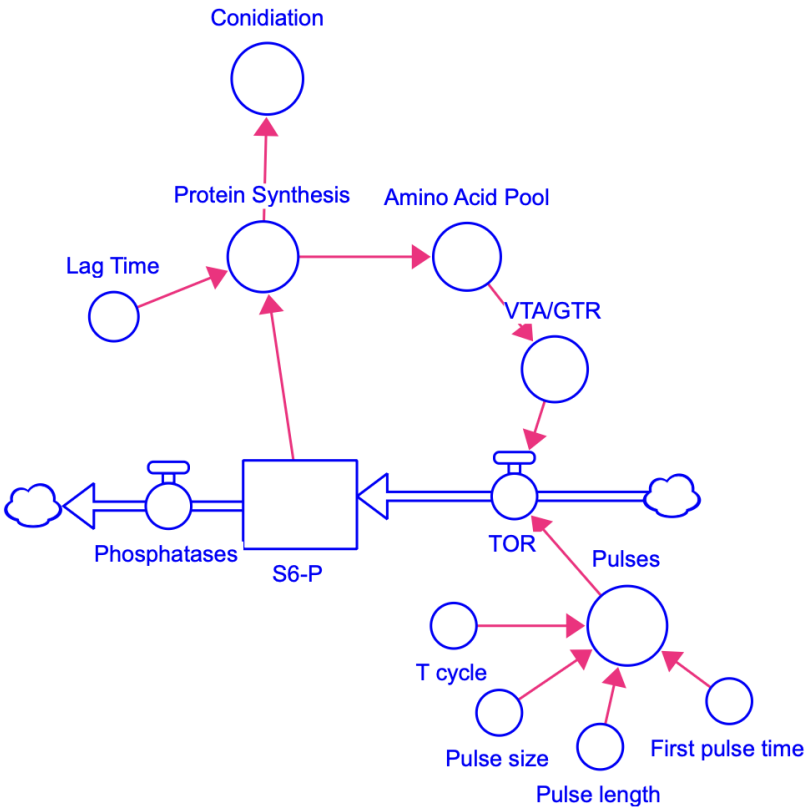


Figure 1.16 Conceptual STELLA model developed to simulate TOR signaling dynamics during heat-pulse entrainment.

Heat pulses act as environmental inputs regulating TOR activity, which is linked to S6 phosphorylation, protein synthesis, amino acid availability, and conidiation. The model also incorporates the proposed VTA/GTR regulatory pathway and allows manipulation of T-cycle duration, pulse length, pulse size, and the timing of the first heat pulse. In the *vta* and *gtr2* mutants in this experiment, the *vta* and *gtr2* section was removed.

Simulation of repeated heat-pulse entrainment predicted that the initiation of a new T-cycle would transiently disrupt the endogenous oscillation of TOR activity as the system adjusted to the imposed environmental rhythm. Rather than immediately synchronizing with the applied heat pulses, the model predicted that TOR activity would initially exhibit changes in both phase and amplitude before gradually re-establishing stable oscillations that became synchronized with the imposed T-cycle. This transient desynchronization followed by gradual re-entrainment is a well-established characteristic of circadian oscillators responding to a new zeitgeber, as internal clocks generally require several environmental cycles to achieve stable phase synchronization.

The representative simulation output shown in (Figure 1.17) demonstrates this predicted behavior. As illustrated, following the onset of repeated heat pulses (red), TOR activity (blue) initially deviates from its endogenous rhythmic pattern before progressively recovering stable oscillations that become aligned with the imposed T-cycle. Based on these simulations, it was hypothesized that a similar transient disruption followed by the restoration of rhythmicity would be observed experimentally in *Neurospora crassa* during heat-pulse entrainment.

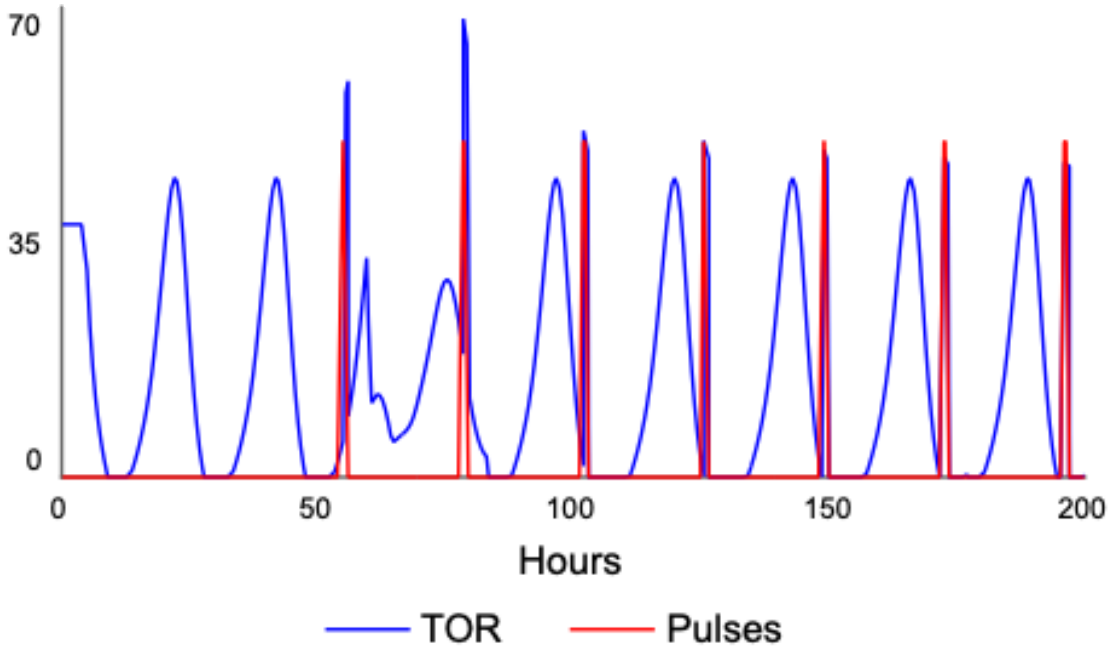


Figure 1.17 Representative output generated by the STELLA simulation showing the predicted response of TOR activity (blue) to repeated heat-pulse T-cycle entrainment (red).

The model predicts an initial disruption of the endogenous TOR rhythm immediately following the onset of heat-pulse treatment, followed by gradual re-entrainment and restoration of stable rhythmic oscillations synchronized with the imposed T-cycle.

To further investigate the proposed role of the TOR signaling pathway in regulating circadian rhythmicity, additional STELLA simulations were performed using different genetic backgrounds and heat-pulse T-cycle conditions. The objective of these simulations was to predict how alterations in key components of the proposed TOR regulatory network would influence rhythmic TOR activity prior to experimental validation. Specifically, simulations were conducted for *frq* knockout (frq^{10}), *vtafrq10*knockout ($vta^{ko}frq10$), and *gtr2frq10* knockout ($gtr2^{ko}frq10$) models under multiple T-cycle conditions.

The model is designed to simulate *frq* knockout strains that would retain rhythmic oscillations of TOR activity despite the absence of the canonical FRQ/WCC transcription–

translation feedback loop. As shown in (Figure 1.18), rhythmic TOR activity persisted under all simulated T-cycles (T19, T20, T22, and T22.5), although the timing (phase) of the oscillations shifted depending on the imposed T-cycle. These simulations demonstrate the hypothesis that an alternative oscillatory mechanism, independent of FRQ, may be capable of maintaining rhythmic TOR activity while remaining responsive to environmental entrainment.

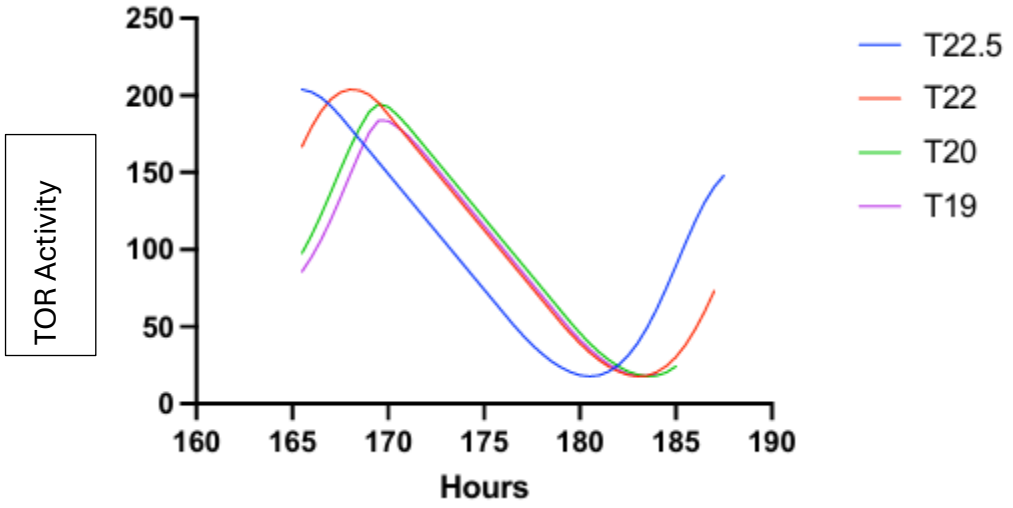


Figure 1.18 STELLA simulation predicting TOR activity in the frq knockout strain under different heat-pulse T-cycles (T19, T20, T22, and T22.5).

The model demonstrates that rhythmic TOR activity is maintained in the absence of FRQ, although the phase of the oscillations varies depending on the imposed T-cycle.

In contrast, simulations of the *vta* knockout and *gtr2* knockout strains (These mutations were simulated by removing the feedback from amino acid pools to TOR activity by deleting the VTA/GTR2 component of the model) predicted a marked disruption of rhythmic TOR activity. Rather than exhibiting sustained oscillations, TOR activity rapidly declined following the onset of the simulated heat-pulse entrainment and failed to recover rhythmic behavior across the different T-cycle conditions (Figure 1.19). These simulations assume that both VTA and GTR2 are critical components required for maintaining rhythmic TOR signaling and support the hypothesis that disruption of either protein compromises the function of the proposed FRQ-less oscillator.

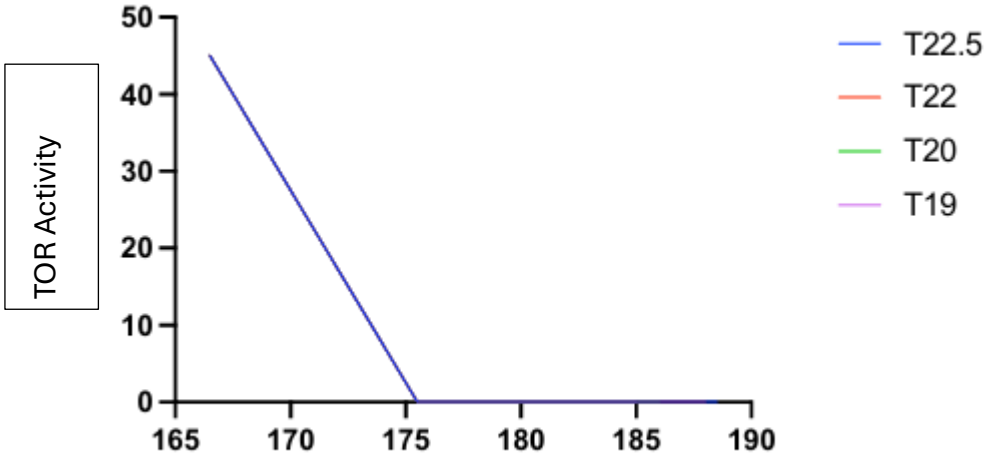


Figure 1.19 STELLA simulation predicting TOR activity in vta knockout and gtr2 knockout strains under different heat-pulse T-cycles.

The model predicts a loss of rhythmic TOR oscillations following disruption of either VTA or GTR2, indicating that these components are required for maintaining rhythmic TOR activity during heat-pulse entrainment.

Collectively, these computational predictions indicate that while FRQ-independent rhythmicity may persist under different entrainment conditions, disruption of the VTA/GTR2 signaling module is predicted to abolish rhythmic TOR activity. These observations provided the rationale for the experimental analyses presented in the following chapters, where TOR activity was examined in wild-type and mutant strains under identical heat-pulse T-cycle conditions.

1.7 Hypothesis and Objectives

This study is based on the hypothesis that circadian rhythmicity in *Neurospora crassa* is not generated exclusively by the canonical transcription–translation feedback loop (TTFL) composed of FRQ and the White-Collar Complex. Instead, the circadian system is proposed to consist of multiple autonomous yet interacting oscillatory modules, including one or more FRQ-less oscillators (FLOs) that function alongside the FRQ/WCC oscillator to produce robust rhythmic outputs. Accumulating evidence from our laboratory indicates that disruption of specific components of the TOR signaling pathway compromises FRQ-less rhythmicity, suggesting that TOR signaling may represent a core element of the FLO or act as a critical regulator of it.

The long-term goal of this work is to identify the molecular components of the FRQ-less oscillator and to clarify how this oscillator interfaces with the canonical TTFL within the broader circadian network of *Neurospora crassa*. This research aims to elucidate the relationship between cellular metabolic signaling and circadian timekeeping, with a focus on the TOR pathway as a potential link between these systems.

The immediate objectives of this thesis are to use the ribosomal protein S6, a downstream target of the TOR pathway, as a molecular readout of TOR activity and to determine whether TOR signaling exhibits circadian rhythmicity in the absence of FRQ. To address this, S6 phosphorylation dynamics are examined in circadian mutant strains under defined entrainment conditions using cyclic heat pulses with different T-cycle lengths administered in complete darkness. This experimental design allows rhythmicity to be assessed independently of light-driven transcriptional regulation.

Comparisons across the *frq10*, *Δvta*, and *Δgtr2* backgrounds were performed to evaluate the role of TOR pathway components in maintaining rhythmicity and entrainment under heat pulse conditions (Eskandari et al., 2021). In particular, rhythmicity of TOR activity was assessed in each strain by examining the periodicity and amplitude of S6 phosphorylation in different T-cycles, allowing for identification of disruptions in TOR-associated oscillatory behavior in mutant backgrounds.

2 Chapter 2: Methods

2.1 *Neurospora crassa* Strains

All *Neurospora crassa* strains used in this study were either obtained from the Fungal Genetics Stock Center (FGSC; Kansas State University, Manhattan, KS, USA) or generated in-house using established genetic crossing procedures. Each strain carries a common genetic background consisting of the *csp-1*, *ras-1*^{bd}, and *chol-1* mutations.

The *csp-1* (*conidial separation-1*) mutation confers a morphological phenotype characterized by impaired separation of conidiospores from aerial hyphae. This feature reduces the dispersal of spores and consequently minimizes the risk of cross-contamination between cultures (Akhtari et al., 2026).

The *ras-1*^{bd} mutation (formerly *bd*) is routinely incorporated into strains used for circadian studies due to its pronounced effects on rhythmic output. Specifically, this mutation results in a reduced growth rate and enhances the clarity of conidiation banding patterns, facilitating their visualization in race tube assays. Furthermore, *ras-1*^{bd} strains sustain conidiation under elevated CO_2 conditions, such as those encountered in sealed experimental systems (Belden et al., 2007).

The *chol-1* mutation disrupts phospholipid biosynthesis by impairing the methylation pathway responsible for the conversion of phosphatidylethanolamine to phosphatidylcholine. Consequently, supplementation with exogenous choline is required to support normal cellular growth. In addition to its metabolic effects, the *chol-1* mutation is associated with a lengthened circadian period and is widely employed in this laboratory to enable the characterization of FRQ-less rhythmicity under choline-dependent conditions (Lakin-Thomas & Brody, 2000).

To facilitate the detection of ribosomal protein S6, a FLAG-tagged S6 strain was previously generated in our laboratory through a targeted knock-in approach, whereby a FLAG epitope was fused to the endogenous *rps-6* locus (Colot et al., 2006; Honda & Selker, 2009). This tagged construct was subsequently introduced into all experimental strains via standard genetic crosses. (Appendix II)

2.1.1 Genotyping of Progeny

Progeny were first screened and selected based on the presence of the *bd*, *csp-1*, *chol-1*, and *frq10* mutations. For genotyping, cultures were grown in liquid medium consisting of minimal media supplemented with glucose and choline. For each progeny, two replicate cultures (2 mL each) were prepared in 12-well plates, with 2 mL of medium per well.

Spores were inoculated into the wells and incubated at room temperature under constant light (LL) conditions for 2 days to allow sufficient growth. Following incubation, fungal mats were harvested and genomic DNA was extracted.

Polymerase chain reaction (PCR) was then performed using primers specific for the s6FLAG construct to confirm the presence of the tagged allele in the selected progeny.

2.1.2 Genomic DNA Isolation

Genomic DNA was extracted from *Neurospora crassa* samples using a modified protocol adapted from (Jin et al., 2007). Frozen fungal tissues were first ground into a fine powder in liquid nitrogen using a pre-chilled mortar and pestle. The powdered samples were immediately transferred into extraction buffer (100 mM Tris-HCl, 50 mM EDTA, pH 8.0) supplemented with 1% SDS and proteinase K (20 mg/mL), and vortexed to ensure thorough mixing.

Samples were incubated at 65 °C for 1 hour to facilitate cell lysis and protein digestion. Following incubation, ammonium acetate (7.5 M) was added to precipitate proteins, and samples were placed on ice prior to centrifugation at 14,000 RCF for 3 minutes at 4 °C. The supernatant was transferred to fresh tubes, and RNase A was added to remove RNA contamination, followed by incubation at 37 °C for 1 hour.

To further purify DNA, chloroform extraction was performed. Samples were mixed with chloroform, vortexed, and centrifuged to separate phases. The aqueous (upper) phase was carefully transferred to a new tube, and DNA was precipitated by the addition of isopropanol. Following centrifugation, the resulting DNA pellet was washed with 70% ethanol, air-dried at room temperature, and resuspended in TE buffer (10 mM Tris-HCl, 1 mM EDTA, pH 8.0).

The extracted DNA samples were stored at −20 °C for downstream applications.

2.1.3 S6-FLAG PCR and Agarose Gel Electrophoresis

Genotyping of the S6FLAG construct was performed using polymerase chain reaction (PCR) followed by agarose gel electrophoresis. PCR reactions were prepared using a Q5 high-fidelity

DNA polymerase system. Each reaction contained 1× Q5 reaction buffer, 10 mM dNTPs, 10 µM forward and reverse primers, Q5 DNA polymerase (New England Biolabs, catalog number M0491S), and nuclease-free water, with a final reaction volume of 25 µL. Template DNA (0.5–500 ng) was added to each reaction, and samples were briefly centrifuged prior to amplification.

PCR amplification was carried out under the following thermocycling conditions: initial denaturation at 98 °C for 3 minutes, followed by 34 cycles of denaturation at 98 °C for 30 seconds, annealing at 68 °C for 30 seconds, and extension at 72 °C for 2 minutes. A final extension step was performed at 72 °C for 10 minutes, after which samples were held at 4 °C.

PCR products were analyzed by agarose gel electrophoresis using a 1.5% agarose gel prepared in 1× TAE buffer and stained with RedSafe (FroggaBio, catalog number 21141). Prior to loading, samples were mixed with loading dye master mix containing Ficoll and proteinase K. Samples were loaded alongside a reference lane containing standard loading dye with bromophenol blue. Electrophoresis was performed at a constant voltage until adequate separation was achieved.

DNA bands were visualized using a UV gel imaging system, and fragment sizes were compared to expected product lengths, with wild-type bands at approximately 985 bp and mutant bands at approximately 1823 bp, allowing for confirmation of successful genotyping. (Figure 2.1)

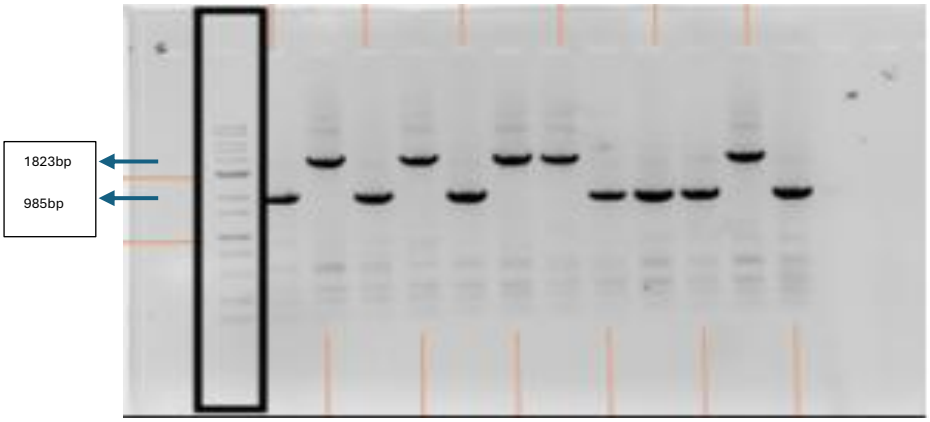


Figure 2.1 Checking the genotypes of different strains for s6FLAG by PCR.

Samples are: #259, #669, ##A20, #A21, #A97, #A60, #A57, #T49, #T55, #T21, #T36, #T75 in order.

2.2 Solid Agar Culture

To investigate TOR pathway activity, *Neurospora crassa* cultures were grown on solid agar medium prepared using standard formulations (VOGEL, 1956); (Davis & de Serres, 1970). The medium consisted of 2.5 g maltose, 10 mL of 50× Vogel's salts, 5 mL of 10 mM choline, 10 g agar, and 2.5 mL arginine (20 mg/mL), brought to a final volume of 500 mL with distilled water.

Approximately 50 mL of sterile medium was poured into 150 mm Petri plates and allowed to solidify under UV light for 4 hours. Plates were then inoculated and incubated under constant light at 30 °C for 48 hours to allow initial mycelial growth.

Following this period, agar plugs of freshly grown mycelia from the growth front were transferred to fresh solid medium and subjected to constant darkness (DD) under controlled temperature cycles for an additional 48 hours. Temperature entrainment was achieved using cyclic heat pulses (16 h or 24 h cycles), consisting of alternating temperatures between 22 °C and 37 °C, as previously described for circadian entrainment studies in *Neurospora*(Lakin-Thomas, 2006a; Merrow et al., 1999;Pregueiro et al., 2005).

To facilitate sample collection and prevent hyphal penetration into the agar, a sterile cellophane overlay was applied. (Cellophane is made of cellulose and lets the fungus absorb the nutrients through it). Cellophane sheets(Futamura USA, uncoated cellophane film, catalog 110 NP25) were cut to size, rinsed thoroughly with distilled water, and autoclaved at 121 °C for 30 minutes. The sterilized cellophane was then placed onto freshly prepared agar plates and allowed to dry under UV light for 24 hours.

Mycelial plugs from growth fronts of temperature-treated cultures were transferred onto the cellophane-covered plates under darkroom conditions and positioned near the plate edge. Cultures were then returned to the same heat pulse cycles in constant darkness.

After approximately 48 hours, when the growth front reached midway across the plate, the distal ~1 cm region of actively growing mycelium was harvested from the cellophane surface using a spatula. Samples were immediately flash-frozen in liquid nitrogen and stored at −80 °C for downstream analyses.

2.2.1 Linear Growth Rate Measurement on Solid Agar Culture

To evaluate how different heat pulse cycles (16 h and 24 h T-cycles) affect the linear growth rate and conidiation density pattern, the position of the mycelial growth front was marked on the

plates each day. Once the cultures had fully grown and reached the edge of the plate, the bottom of each plate was scanned for analysis. (Figure 2.2)

The scanned images were analyzed using ImageJ software to track the progression of growth over time. Based on the distance traveled by the growth front and the corresponding time points, the average linear growth rate was calculated. These calculations were performed using two pre-coded Excel macros, FijiTau and MacTau (Lakin-Thomas, 1998). The plot profile function in ImageJ was used to measure conidial density across the center of the plate from inoculation to the edge of the plates (Figure 2.3)

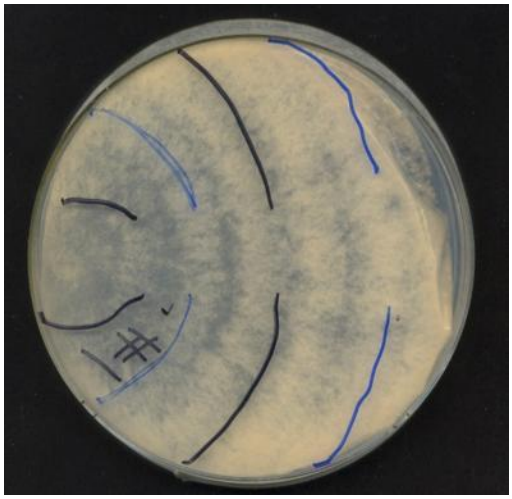


Figure 2.2 Representative plate image used for conidiation density analysis under a 16-h temperature cycle in constant darkness.

A *Neurospora crassa* plate cultured under a T16 heat-pulse cycle in constant darkness (DD) was scanned after the mycelium reached the edge of the plate. The central axis of the plate was selected in ImageJ, and the Plot Profile function was used to measure pixel intensity along the growth path from the inoculation point to the growth front. Inoculation was at the left edge of the plate. Growth fronts were marked daily in black or blue pens. Variations in pixel intensity correspond to differences in conidiation density, allowing visualization and quantification of rhythmic banding patterns entrained by the 16-h temperature cycle from 22 degrees to 37 degrees.

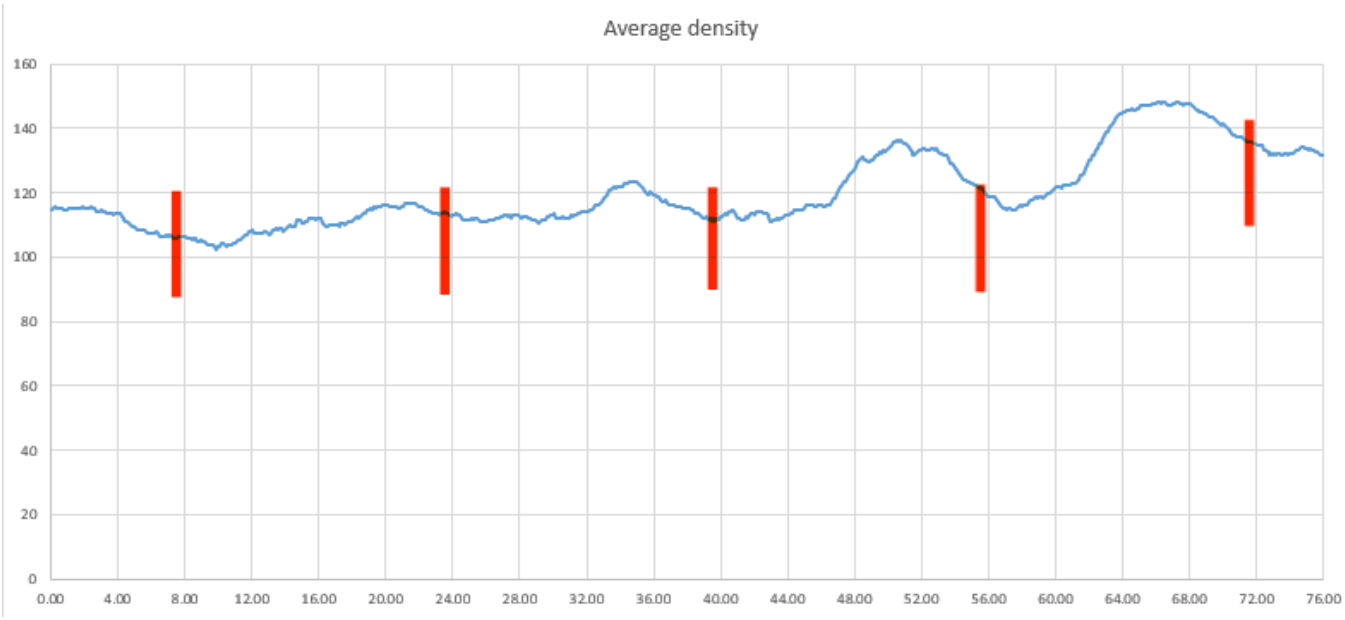


Figure 2.3 Measurement through ImageJ-based tracking of mycelial growth front over time in *frq10* under a 16 h T-cycle with temperature pulses from 22 °C to 37 °C in DD. Pulses are indicated by red bars.

2.2.2 Heat Pulse Treatment

To investigate the relationship between circadian entrainment and TOR pathway activity, a controlled heat pulse protocol was applied. Cultures were grown in Petri plates under constant darkness at a baseline temperature (~22 °C) to eliminate light-dependent entrainment and isolate temperature-driven effects (Merrow et al., 1999; Lakin-Thomas, 2006a).

Short-duration heat pulses (2 hours) were administered at elevated temperatures up to 37 °C and repeated across defined T-cycle regimes of 16 h and 24 h. These cycles were selected to assess entrainment behavior under both shorter and near-circadian environmental periods. The use of brief ,2 hour, heat pulses, rather than long-duration heat pulses of, for example 12 hours, was intended to minimize masking effects and allow for clearer observation of endogenous oscillator responses (Lakin-Thomas, 2006a).

Following the final heat pulse of each cycle, samples were harvested beginning 2 hours post-treatment, at 1-hour intervals for the first 8 hours, and subsequently at 2-hour intervals for the remainder of the cycle. (Appendix III)

Conidiation banding patterns were monitored as a readout of circadian output, while TOR pathway activity was assessed through S6 phosphorylation using the S6-FLAG tagged strains (Akhtari et al., 2026). Temporal alignment between conidiation peaks and TOR activity peaks

was analyzed to determine whether conidiation rhythms precede, coincide with, or follow TOR signaling dynamics.

2.3 Immunoblotting

2.3.1 Protein Extraction

The harvested time course samples were kept at -80°C. To extract protein from the frozen samples, they were ground with pre-cooled mortar and pestle in liquid nitrogen and the mycelia powder was transferred to 1.5 ml microfuge tubes on ice and then protein extraction buffer (PEB), (50 mM Tris pH 6.8, 2% SDS, 10% Glycerol, and 1 mM PMSF) with the ratio of 1:1 v:v (buffer: mycelia powder) was added to the powder. The tubes were vortexed for 20 seconds and then boiled for 5 minutes and then vortexed again, then were put on ice for 2 minutes. The samples were heated for 30 seconds in 80°C water and vortexed to redissolve and then were centrifuged for 5 minutes at 25°C and 12000g. The supernatant was transferred to a clean 1.5 ml tube for protein assay. To prepare dilutions for protein assay, a 1:10 (5 µl of supernatant: 45 µl of PEB) and 1:3 (20 µl of supernatant: 40 µl of PEB) were made for each sample. From these dilutions, additional 1:100 (2.5 µl of 1/10 dilution: 22.5 µl of ddH2O) and 1:30 (2.5 µl of 1/3 dilution: 22.5 µl of ddH2O) was prepared.

2.3.2 Bio-Rad DC Protein Assay

Protein concentrations were determined using the Bio-Rad DC Protein Assay following the manufacturer's protocol (catalog number 500-0007). A standard curve was prepared using bovine serum albumin (BSA) at a concentration of 0.5 mg/mL. Six standard points were generated by adding varying volumes of BSA (0, 2.5, 5, 10, 15, and 20 µL) and adjusting each to a constant final volume with ddH_2O.

Samples were diluted at 1:100 and 1:30, and 300 µL of each dilution was loaded in triplicate into a 96-well plate. Absorbance was measured at 750 nm using a plate reader. Protein concentrations were then calculated based on the BSA standard curve and expressed in mg/mL.

2.3.3 Protein Separation by SDS-PAGE

Proteins were separated using discontinuous SDS-PAGE (sodium dodecyl sulfate–polyacrylamide gel electrophoresis) on a 12.5% acrylamide gel, allowing resolution of different phosphorylation states of the *Neurospora crassa* ribosomal protein S6. To enable detection of

phosphorylated forms, the gel was supplemented with Phos-tagPhosTag (Cedarlane, Phos-tag Acrylamide AAL-107, catalog number 304-93521). Specifically, 50 µL of Phos-tag solution (3.03 mg/mL) and 50 µL of $MnCl_2$ (10 mM) were incorporated into the resolving gel during polymerization.

Phos-tag interacts specifically with phosphorylated amino acid residues, such as serine, threonine, and tyrosine, through a metal ion complex (typically Mn^{2+}), which binds to the negatively charged phosphate groups. This interaction slows the migration of phosphorylated proteins, allowing separation based on phosphorylation level.

Protein samples (10 µg) were prepared using concentrations obtained from the standard curve and diluted with PEB to a final volume of 10 µL. To each sample, 0.1 µL DTT and 0.5 µL of 0.4% bromophenol blue were added. Samples were then mixed thoroughly and heated at 95–100 °C for 2 minutes before loading onto the gel. Tris-glycine-SDS buffer (3.0 g Tris base, 14.4 g Glycine, 1.0 g SDS, 1 L water) was used as running buffer and the protein separation was performed for about 90 minutes at 200 V current.

2.3.4 Blotting

After electrophoresis, gels were washed three times in cathode buffer (25 mM Tris base, 40 mM glycine, 10% methanol, pH 9.4) supplemented with 0.5 M EDTA (pH 8.0) to remove any remaining $MnCl_2$. Each wash was performed for 15 minutes on a shaker set to approximately 25–29 rpm.

Proteins were then transferred onto a PVDF membrane (Immobilon P (Millipore, catalog number IPVH00010) using a semi-dry blotting system. The transfer process utilized three buffers: Anode buffer I (0.3 M Tris base, 10% methanol, pH 10.4), Anode buffer II (25 mM Tris base, 10% methanol, pH 10.4), and cathode buffer (25mM Tris base, 40mM glycine, 10% Methanol , pH 9.4). Transfer was carried out at ~2 mA per cm^2 of gel area for 45 minutes, with the voltage maintained between 7–8 V.

Following transfer, membranes were briefly soaked in 100% methanol for approximately 10 seconds, then placed on clean filter paper and allowed to air dry for 15–20 minutes. The membranes were subsequently stored at 4 °C until further analysis.

2.3.5 Immunodetection

Before antibody incubation, PVDF membranes were blocked in 1× blocking buffer (prepared from a 10× stock containing 10% BSA in 1× TBST(1.21 g Tris, 8.5g NaCl, 1L ddH_2O, pH 7.5, 1 mL Tween-20)) for 1 hour at room temperature with continuous gentle agitation to reduce non-specific binding.

Following blocking, membranes were incubated with the primary antibody (monoclonal Anti-FLAG M2, Sigma-Aldrich, catalog number F3165) diluted 1:10,000 in blocking buffer for 1 hour under constant agitation. Membranes were then washed three times in TBST buffer, each wash lasting 5 minutes.

The membranes were subsequently incubated with horseradish peroxidase (HRP)-conjugated secondary antibody (Bio-Rad goat anti-mouse IgG-HRP (Cedarlane, catalog number TA130004)), diluted 1:50,000 in blocking buffer, for 1 hour at room temperature. After incubation, membranes were washed four times with TBST buffer for 5 minutes each.

For signal detection, chemiluminescent substrate (Immobilon Western Chemiluminescent HRP Substrate (Millipore, catalog number WBKLS)) was applied and allowed to react for approximately 5 minutes. The emitted signal was captured using a MicroChemi imaging system equipped with a CCD camera.

The *Neurospora crassa* ribosomal protein S6 exhibited three distinct bands corresponding to different phosphorylation states: the lowest band representing the unphosphorylated form, the middle band representing the monophosphorylated form, and the upper band corresponding to the diphosphorylated form. These bands were resolved based on their apparent molecular weights, ranging from approximately 48–63 kDa (2.4.5). Phosphatase treatment resulted in the collapse of the upper two bands into the lowest band, confirming that the band shifts were due to differences in phosphorylation (Figure 2.4) (Akhtari et al., 2026).

Band intensities were quantified using ImageJ software by measuring the mean gray value within a fixed-size region for each band. Background signal was subtracted to obtain the net intensity. The total signal for S6 was calculated by summing the intensities of all three bands. Relative phosphorylation levels were determined by dividing the intensity of the upper (highly phosphorylated) band by the total S6 signal.

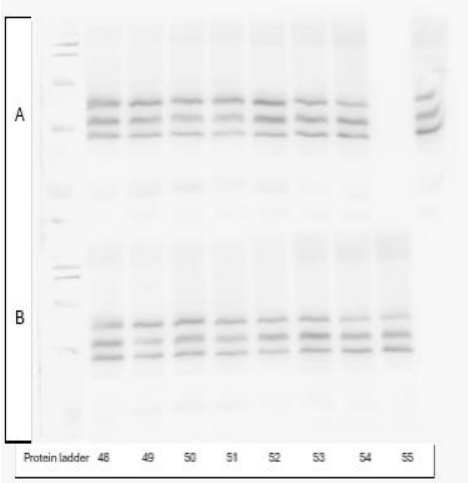


Figure 2.4 Western blot of the 24h T cycle with heat pulses from 22-37 degrees.

A) 48-55 time-points of *gtr2, frq10 S6FLAG* strain. B) 48-55 time-points of *vta, frq10 S6FLAG* strain. The fungus was grown in dark and was harvested every 1 hour. The numbers represent the hours of growth in dark.

3 Chapter 3: Results

3.1 Construction of *frq* knockout strains

3.1.1 PCR Validation of *frq* Genotypes and S6-FLAG Detection

The primary objective of this study was to investigate the rhythmicity of TOR pathway activity under different heat-pulse entrainment conditions in *Neurospora crassa*. The TOR (Target of Rapamycin) signaling pathway is a central regulator of cellular growth, metabolism, and stress responses, and its activity can be monitored through the phosphorylation of ribosomal protein S6, a downstream target of TOR signaling. Previous studies have demonstrated links between TOR signaling and both canonical and FRQ-less rhythmicity in *Neurospora*, suggesting that TOR may play a role in rhythmic processes independent of the classical transcription–translation feedback loop. Therefore, before assessing S6 phosphorylation as a readout of TOR activity, it was essential to verify that the strains used in this study carried the S6-FLAG construct required for downstream protein detection and analysis (Lakin-Thomas, 2019).

Three S6-FLAG strains were used throughout this study: *frq10 S6-FLAG*, *vtako frq10 S6-FLAG*, and *gtr2ko frq10 S6-FLAG*. The *frq10 S6-FLAG* strain served as the primary experimental strain and was used extensively in the heat-pulse entrainment experiments described in this thesis. The *vtako frq10 S6-FLAG* and *gtr2ko frq10 S6-FLAG* strains were also included in the study to further examine the relationship between TOR signaling and FRQ-less rhythmicity. PCR validation of these latter strains had been completed previously by members of the laboratory, and their genotypes had already been confirmed. Therefore, the present analysis focused on validating the primary *frq10 S6-FLAG* strain prior to initiating the experimental work.

PCR genotyping was performed on two strains, #259 (wild-type) and #668 (mutant, *csp-1; chol-1; ras-1bd frq10 S6-FLAG*), to validate the reliability of the genotype before proceeding with the heat-pulse experiments and S6 phosphorylation analyses. Using genomic DNA extracted as described in the methods, PCR amplification with S6-FLAG–specific primers produced clear and reproducible bands in both samples following agarose gel electrophoresis.

The wild-type strain exhibited a band at approximately 985 bp, while the mutant strain showed a larger band at approximately 1823 bp, consistent with the expected size difference between S6+ and S6-FLAG alleles. The presence of S6-FLAG was confirmed in #668. (Figure 3.1)

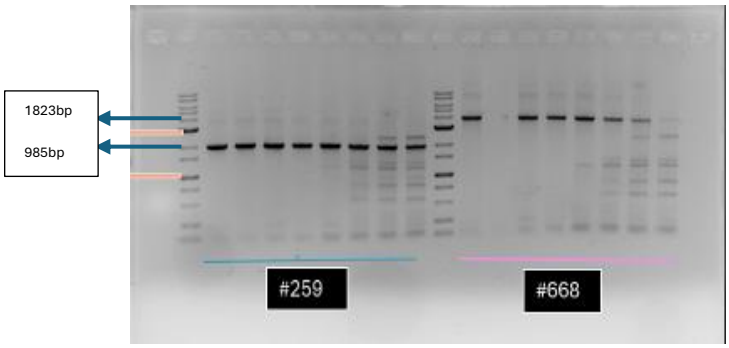


Figure 3.1 *S6-FLAG* genotyping of #259, #668 strains by PCR.

Wild type is 985 bp, mutant is 1823 bp. This figure shows a temperature gradient to find the correct annealing temperature for the primers.

3.1.2 Western Blot Analysis of S6-FLAG Expression in Selected Strains

. To further validate the presence and expression of the S6-FLAG construct, a subset of previously genotyped strains was re-examined using Western blot analysis. Seven strains were included in this experiment: six strains previously identified as S6-FLAG–positive (#668 = *csp-1; chol-1; ras-1^{bd}; frq10 S6FLAG*, #669 = *csp-1; chol-1; ras-1^{bd}; frq10 S6FLAG*, #A21 = *chol-2; ras-1^{bd}; S6FLAG*, #A57 = *csp-1; chol-1; ras-1^{bd}*; *frq7 S6FLAG*, #A60 = *csp-1; chol-1; ras-1^{bd}; frq1 S6FLAG*, #T36= *csp-1; wc-2; ras-1^{bd}; S6FLAG)* and one strain (#80 = *csp-1; chol-1; ras-1^{bd}; frq10*) used as a negative control. Cultures were grown under controlled conditions, including initial growth in constant light (LL) at 30 °C, followed by transfer to cellophane plates and subsequent incubation in constant darkness (DD) at 22 °C prior to harvesting.

Although strain #668 (*frq10 S6-FLAG*) was the primary strain required for the subsequent experiments described in this thesis, the inclusion of additional S6-FLAG strains allowed for a broader validation of S6-FLAG expression across multiple genetic backgrounds. Furthermore, comparison with the non-tagged control strain (#80) provided confirmation of the specificity of the FLAG signal. Since several of these strains were also being utilized in parallel projects within the laboratory, their inclusion in the Western blot analysis provided an opportunity to simultaneously verify S6-FLAG expression and confirm their suitability for future experimental applications.

Protein extracts were prepared from harvested samples and analyzed by Western blot to detect S6-FLAG expression. Consistent with PCR-based genotyping results, all six previously identified strains showed detectable S6-FLAG signal, confirming successful expression of the tagged protein. In contrast, the control strain (#80) did not exhibit any detectable S6-FLAG signal. These results further support the accuracy of the initial PCR-based identification and confirm that the selected strains express the S6-FLAG construct at the protein level. (Figure 3.2)

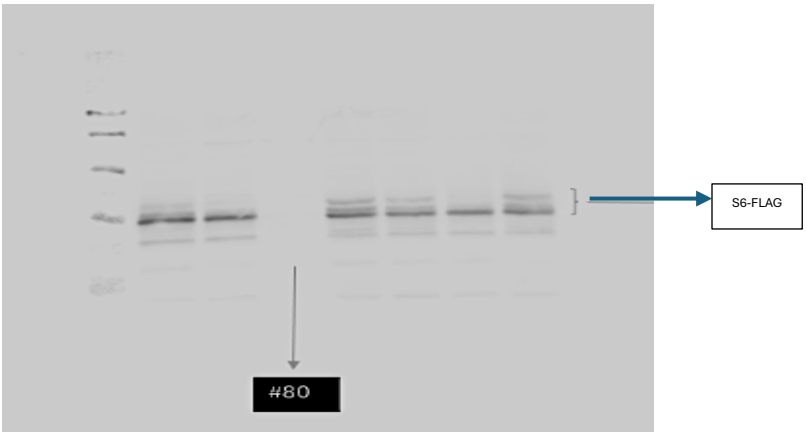


Figure 3.2 western blotting of *S6-FLAG* to see phosphorylation state (S6-P) of different strains.

#668, #669, #80,#A21, #A57, #A60, #T36 strains in order.

3.2 Analysis of Conidiation Timing and TOR Activity Under T-Cycle Entrainment in *frq10*, *vta*, *gtr2* Strains

3.2.1 Analysis of Rhythmic Growth Patterns in *frq10 S6-FLAG* Under Heat Pulse Conditions

Following validation of S6-FLAG expression, subsequent experiments focused on the *frq10 S6-FLAG* strain (#668) to examine its rhythmic growth response under heat pulse conditions. The objective of this analysis was to assess differences in growth density patterns and identify distinct peaks in response to varying temperature cycles, which could inform the selection of optimal time points for downstream analysis of TOR activity.

Cultures were initially grown under constant light conditions and subsequently transferred to constant darkness under different temperature cycle (T-cycle) conditions, including 16-hour and 24-hour cycles with maximum temperatures of 32 °C and 37 °C. Growth patterns were

monitored over multiple days, and plates were scanned after 4 days to quantify average growth density. (Figure 3.3)

To quantify growth dynamics, linear growth rates were measured by tracking the daily progression of the mycelial growth front on solid agar plates. Growth fronts were marked daily, and the marking times were recorded. Scanned plate images were analyzed using ImageJ software, and growth distances over time were used to calculate average linear growth rates. Calculations were performed using FijiTau and MacTau macros, allowing for standardized comparison across different T-cycle conditions.

Analysis of the scanned images revealed condition-dependent differences in rhythmic growth patterns. A density profile across the plate from the point of inoculation to the plate edge was generated using the plot profile function in ImageJ.(Figure 3.4, 3.5, 3.6, 3.7) Notably, the T16 cycle at 37 °C produced more distinct and reproducible peaks in growth density compared to other conditions, indicating a clear rhythmic response to heat pulse treatment under this condition. Based on these observations, the T16 37 °C condition was selected for the first subsequent experiments. After that for the following experiment I used the T24 cycle at 37 degrees as well.

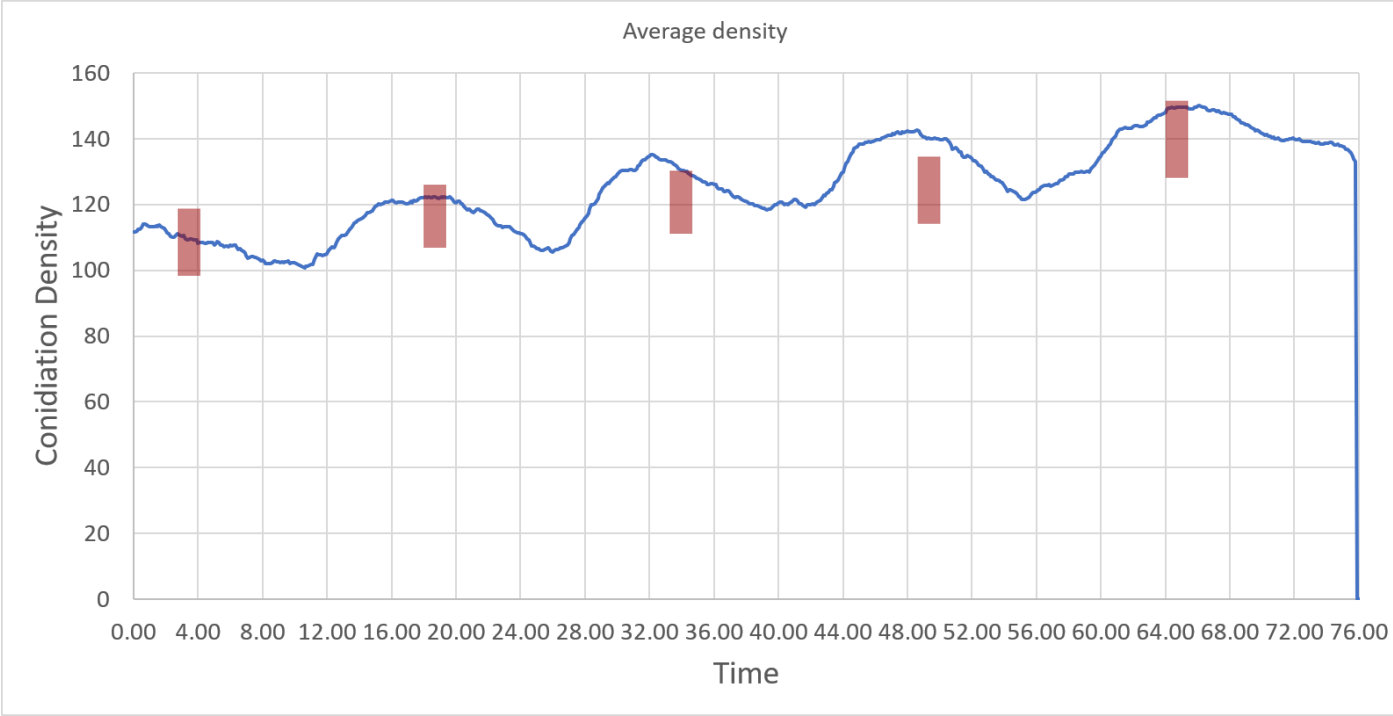


Figure 3.4 Average conidiation density over time in *frq10 S6-FLAG* under a 16-h T-cycle with temperature shifts from 22°C to 32°C in constant darkness (DD), based on three experiments.

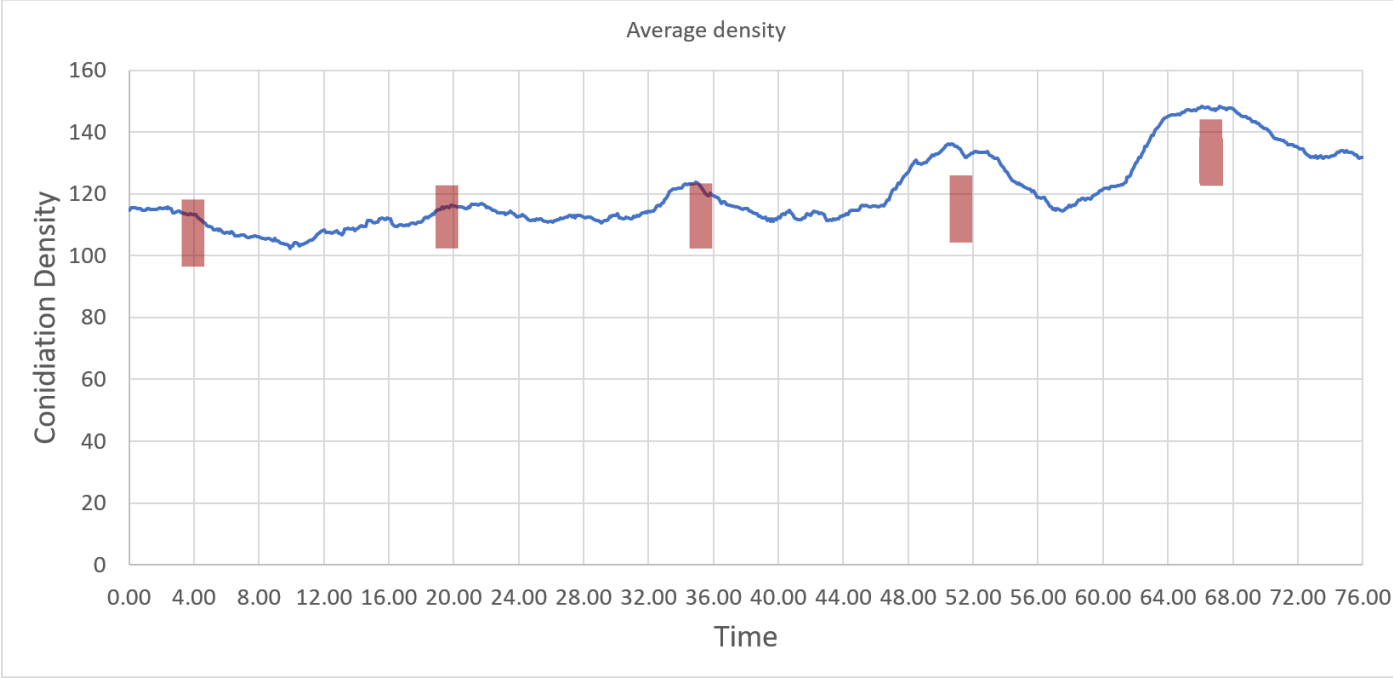


Figure 3.5 Average conidiation density over time in *frq10 S6-FLAG* under a 16-h T-cycle with temperature shifts from 22°C to 37°C in constant darkness (DD), based on three experiments.

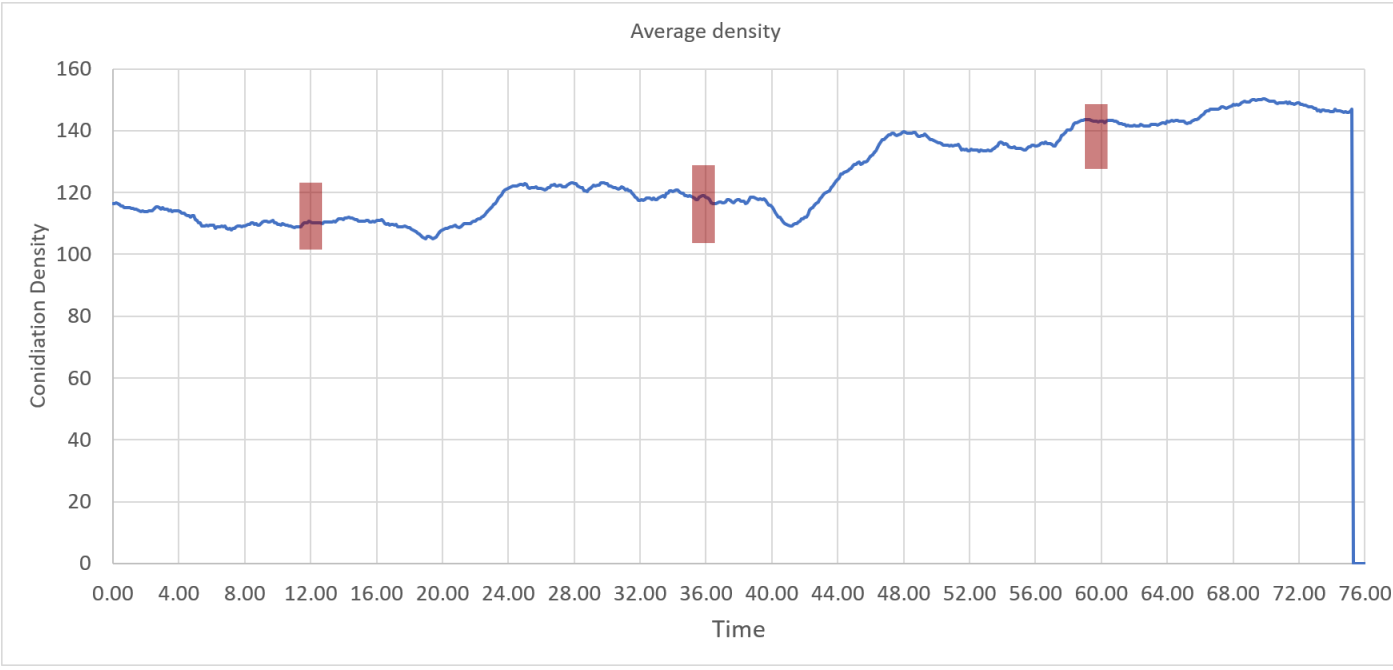


Figure 3.6 Average conidiation density over time in *frq10 S6-FLAG* under a 24-h T-cycle with temperature shifts from 22°C to 32°C in constant darkness (DD), based on three experiments.

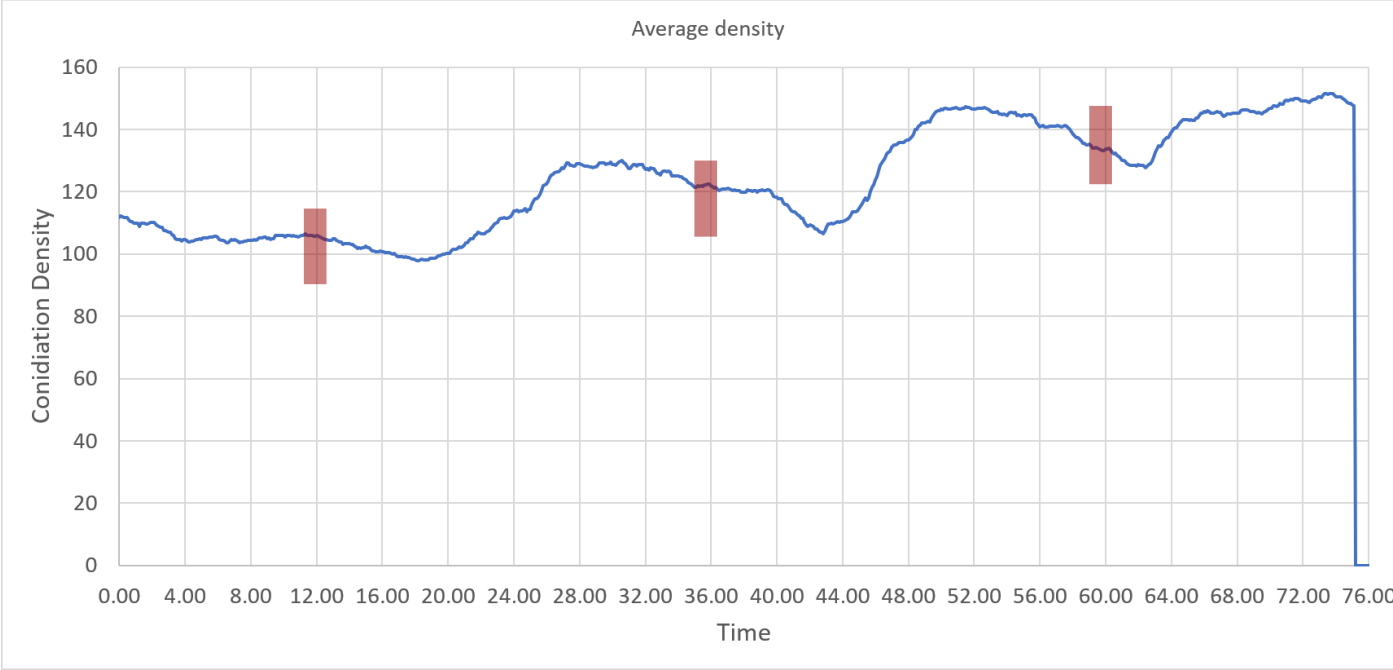


Figure 3.7 Average conidiation density over time in *frq10 S6-FLAG* under a 24-h T-cycle with temperature shifts from 22°C to 37°C in constant darkness (DD), based on three experiments.

3.2.2 TOR Activity in *frq10* Strain Under Heat Pulse Entrainment

Previous time-course analyses conducted in our laboratory demonstrated that ribosomal protein S6 phosphorylation exhibits clear rhythmicity in the wildtype (*chol-1*; *csp-1*; ras^{bd}) strain under constant darkness (Figure 3.8), with an approximate period of 22 hours. In contrast, in the frq-null background (*csp-1*; *rasbd*; *chol-1*; *frq10*), S6 phosphorylation was not consistently rhythmic. While individual trials occasionally suggested oscillatory patterns, these rhythms were not synchronized across replicates, resulting in an overall loss of clear rhythmicity at the population level. These findings suggested that, under free-running conditions, coordinated TOR pathway rhythmicity is disrupted in the absence of a functional *frq* gene. (Figure 3.9)

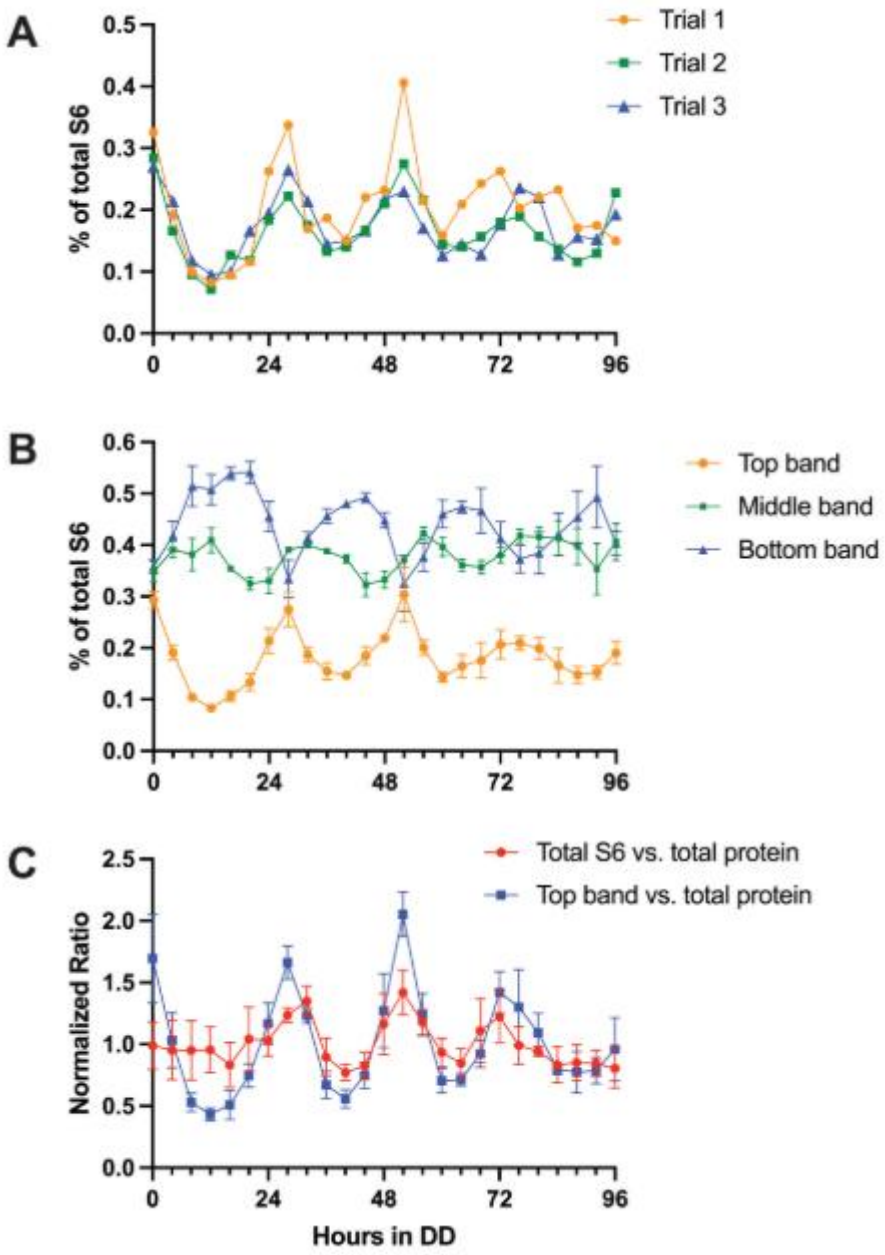


Figure 3.8 S6 phosphorylation rhythm of the "wild-type" strain from 0 to 96 h in DD.

The "wild-type" strain carries the *ras*^{bd}, *csp-1* and *chol-1* mutations and the FLAG-tagged S6 gene. a and b): The anti-FLAG immunodetection data are plotted as the fraction of each band relative to total S6. (a) Results of three independent experiments for the top band only. (b) Mean ± SEM of three biological replicates for all three bands. (c) S6 protein relative to total protein. S6 protein immunodetection band intensities are calculated relative to total protein in that lane on the gel, assayed by the intensity of colloidal gold staining. For b and c, error bars indicate SEM for *N* = 3 biological replicates. For c only, each time-course is normalized to its own mean. (Adapted from Akhtari, 2026)

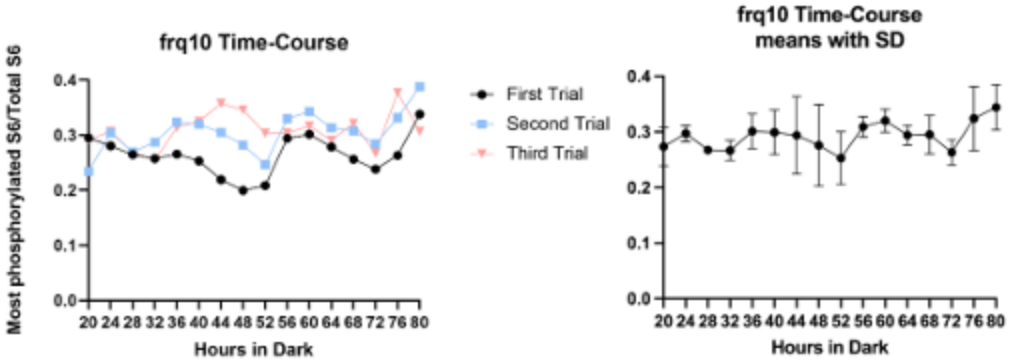


Figure 3.9 Time-course experiment for the *frq10* strain.

All 3 biologically separate trials are plotted on the graph on the left. The average of all trials with standard deviation are plotted on the right graph. (Adapted from Akhtari, 2023)

To investigate whether external entrainment cues could reveal or restore rhythmic TOR activity in a *frq*-deficient background, heat pulse treatments were performed on the *frq10 S6-FLAG* strain under both T16 and T24 cycles with heat pulses ranging from 22 to 37°C (Figure 3.5, 3.7). Cultures were grown under controlled heat pulse conditions, and samples were collected for 16 hours after the last heat pulse, in order to capture immediate post-entrainment dynamics. Each experimental condition included 3 to 4 biological replicates to ensure reproducibility.

Analysis of samples collected under the T16 cycle (Figure 3.10) revealed a distinct and reproducible peak in S6 phosphorylation, corresponding to TOR pathway activation. (Figure 3.11) Notably, this peak consistently occurred prior to the conidiation peak, (Figure 3.12) indicating a temporal separation between TOR signaling activity and overt developmental output. This phase relationship suggests that TOR activity may act upstream of, or independently regulate, processes associated with conidiation rhythms. Importantly, the presence of a defined S6 phosphorylation peak in the *frq10* background indicates that TOR signaling can exhibit temporally organized behavior even in the absence of the canonical circadian regulator *frq*.

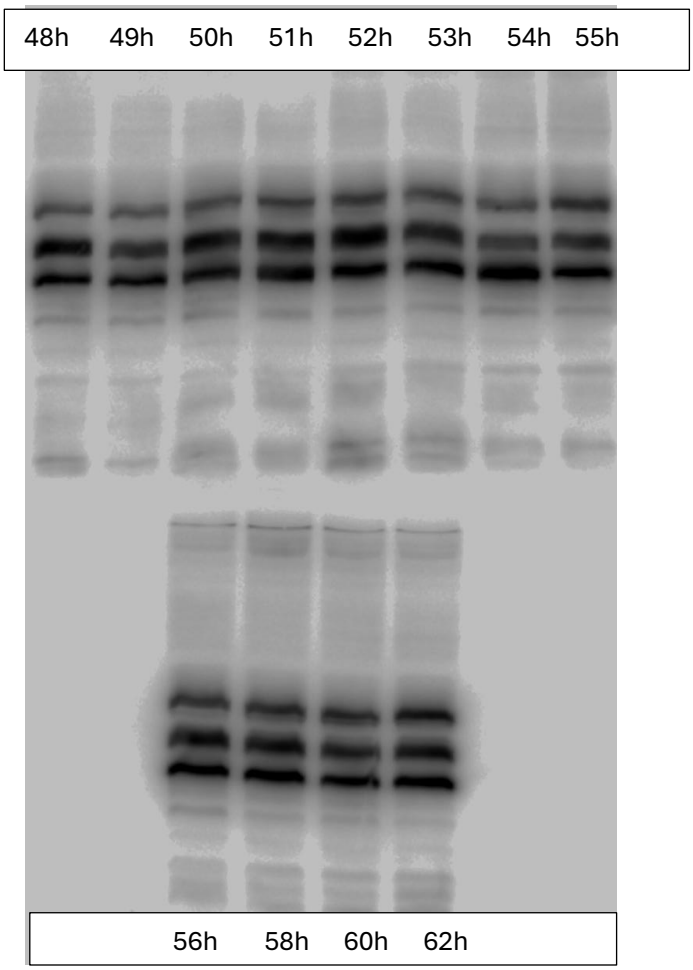


Figure 3.10 Western blot analysis of S6-FLAG expression following T16 heat-pulse entrainment in constant darkness (DD) using the *frq10 S6-FLAG* strain.

The numbers are the hours in DD.

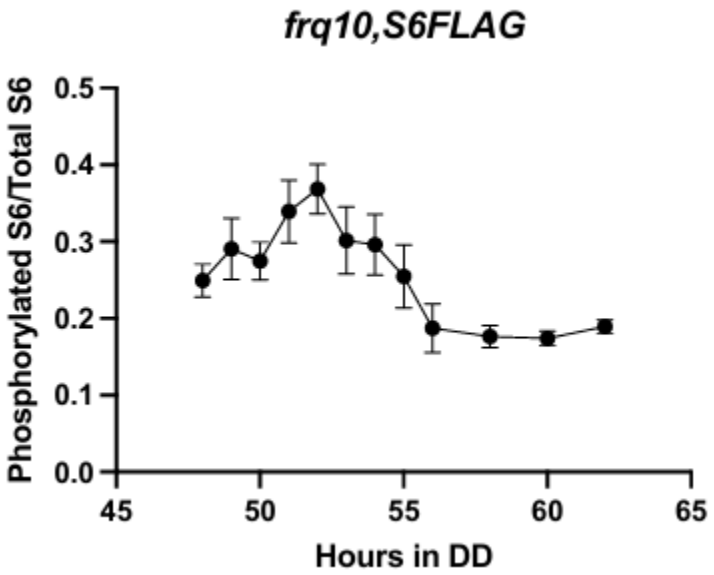


Figure 3.11 Average of S6 Phosphorylation of *frq10 S6 FLAG* strain in DD with T cycle 16 and heat pulses from 22 to 37 degrees.

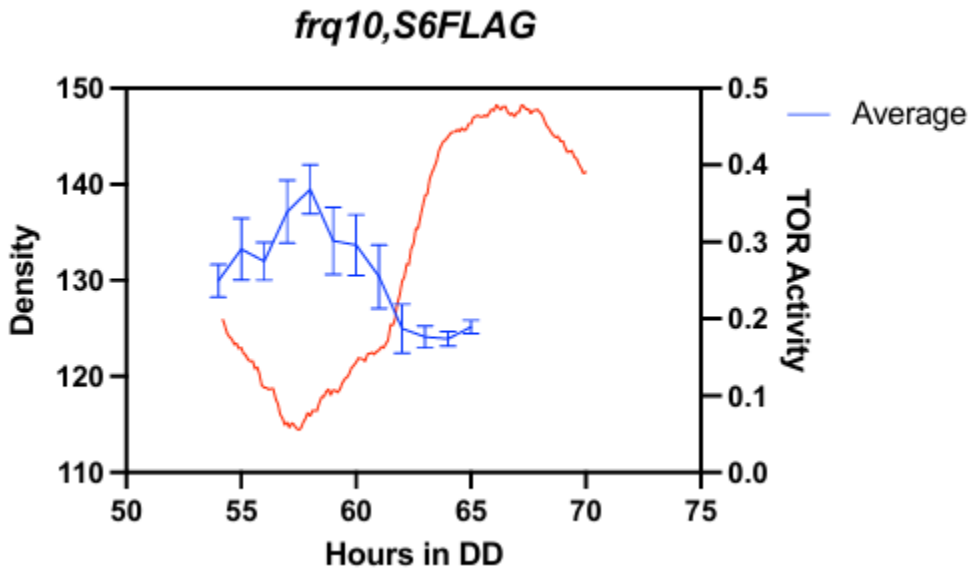


Figure 3.12 Peak of TOR activity occurred before the conidiation peak of the strain in DD with T cycle 16 and heat pulses from 22 to 37 degrees.

Crucially, the observed S6 phosphorylation peak did not occur immediately following the heat pulse, indicating that this pattern cannot be explained solely as a direct or transient response to temperature stimulation. Instead, the delayed timing of the peak supports the presence of an underlying temporally regulated mechanism, rather than a simple stimulus-driven effect.

Furthermore, comparison with previously characterized wildtype data revealed a striking similarity in the timing of peak S6 phosphorylation. (Figure 3.13) Suggesting that the temporal regulation of TOR activity is preserved across genotypes under entrained conditions.

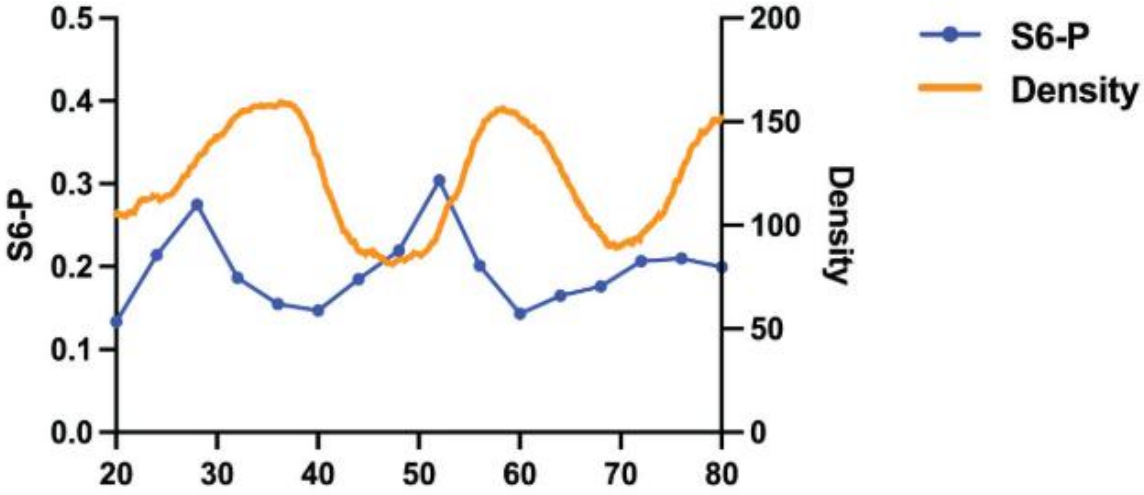


Figure 3.13 Conidiation density compared to S6P timecourses.

Thick curves: Mean density of conidiation from scans of five replicate race tube cultures. Thin lines with plot symbols: S6P rhythm (top band as percent of total S6). (Adapted from Akhtari, 2026)

In contrast, a peak was not observed under the T24 cycle. (Figure 3.14, 3.15, 3.16) As identical timing schedules for growth in constant light (LL), transfer to constant darkness (DD), and sample harvesting were applied for both T16 and T24 conditions, for future T24 experiments, it may be necessary to adjust the harvesting time to better capture the peak of TOR activity. A change in TOR expression pattern with a change in T-cycle is predicted if TOR activity is being regulated by an oscillator. (Figure 1.18)

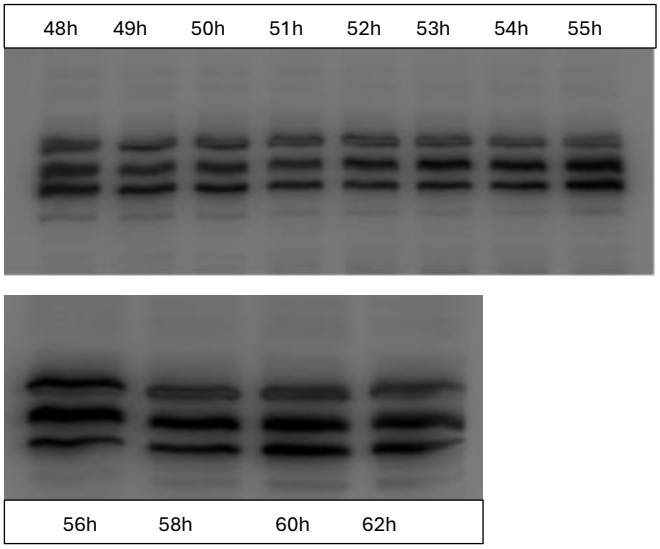


Figure 3.14 Western blot analysis of S6-FLAG expression following T24 heat-pulse entrainment in constant darkness (DD) using the *frq10 S6-FLAG* strain.

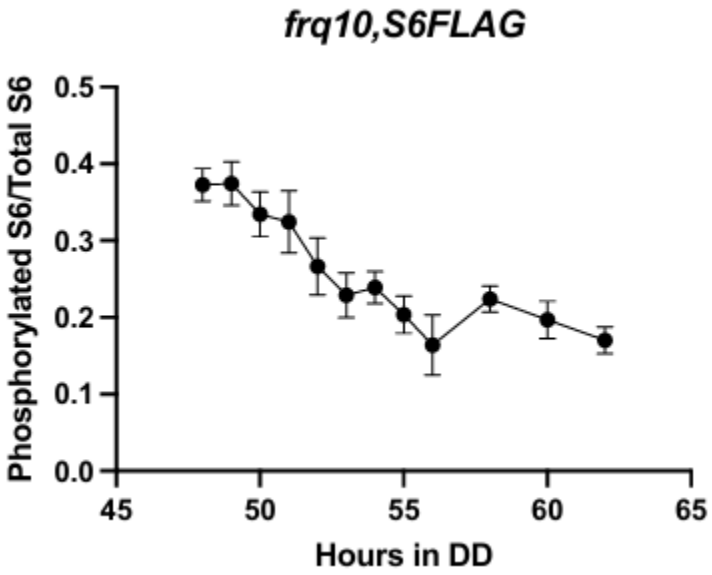


Figure 3.15 Average of S6 Phosphorylation of *frq10 S6 FLAG* strain in DD with T cycle 24 and heat pulses from 22 to 37 degrees.

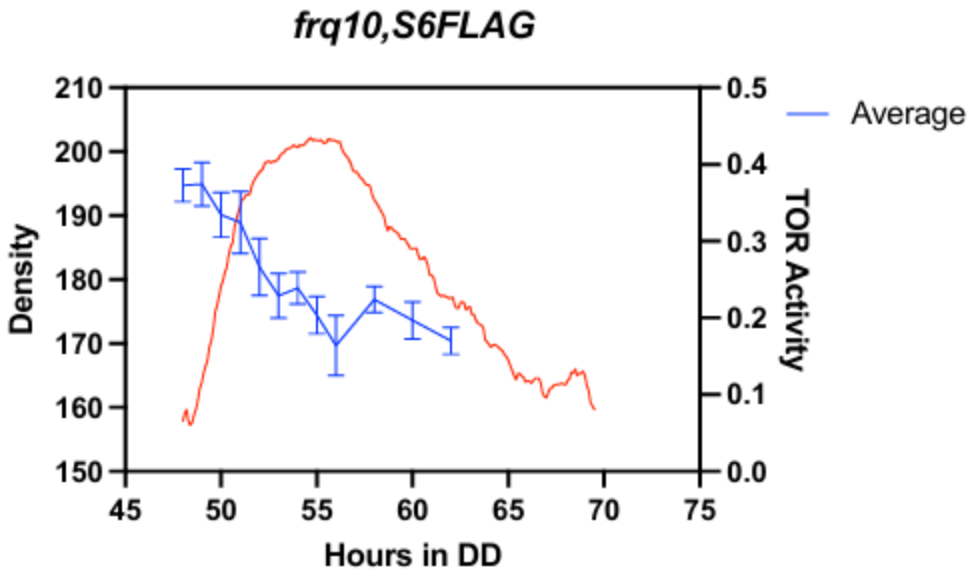


Figure 3.16 Peak of TOR activity occurred before the conidiation peak of the strain in DD with T cycle 24 and heat pulses from 22 to 37 degrees.

Taken together, these results contrast with prior observations under constant darkness, where *frq10* strains lacked synchronized rhythmicity, and instead demonstrate that heat pulse entrainment can induce coordinated and reproducible TOR activity patterns. This suggests that TOR signaling may operate through a FRQ-independent mechanism that remains responsive to external environmental cues, thereby revealing an underlying rhythmic potential that is otherwise masked in free-running conditions.

3.2.3 Role of VTA in Maintaining TOR Rhythmicity Under Heat Pulse Entrainment

Previous time-course analyses conducted in our laboratory demonstrated that S6 phosphorylation in the *vta*^{ko} *S6-FLAG* strain exhibits clear rhythmicity under constant darkness, with an approximate period of 28 hours. However, this rhythmic pattern was observed to dampen over successive cycles, with a noticeable reduction in amplitude by the third cycle. These findings indicate that, although rhythmic TOR activity is present in the absence of VTA, its stability and persistence over time are compromised. Importantly, these experiments were performed in a background where the *frq* gene remained intact. (Figure 3.17)

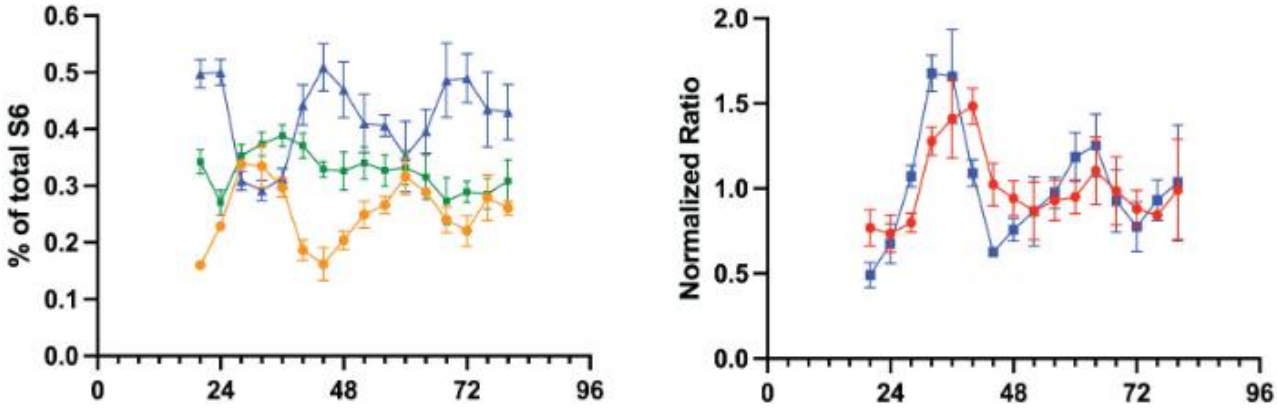


Figure 3.17 S6 phosphorylation rhythm of VTA mutant strain from 20 to 80 h in DD.

Error bars indicate SEM for *N* = 3 biological replicates. Left: The anti-FLAG immunodetection data are plotted as the fraction of each band relative to total S6. Right: S6 protein relative to total protein. S6 protein immunodetection band intensities are calculated relative to total protein on the gel, assayed by colloidal gold staining. For the right only, each replicate time-course is normalized to its own mean. (Adapted from Akhtari, 2026)

To further investigate the combined role of VTA and FRQ in regulating TOR signaling, heat pulse entrainment experiments were performed using a *vta^{ko} frq10 S6-FLAG* strain. The experimental design mirrored that used for the frq10 S6-FLAG strain, with cultures subjected to T16 and T24 heat pulse cycles ranging from 22°C to 37°C, with each heat pulse lasting 2 hours. Samples were harvested right after the treatment to assess S6 phosphorylation dynamics under entrained conditions. (Figure 3.18,3.21)

In contrast to the rhythmic patterns observed in *vta^{ko}* strains with an intact FRQ background, analysis of the *vta^{ko} frq10* strain revealed a complete absence of detectable rhythmicity in S6 phosphorylation under both T16 and T24 cycles. Instead of exhibiting oscillatory behavior, S6 phosphorylation levels showed a predominantly steady decline over time. I expected to see a peak of TOR activity before the conidiation peak like the wild-type strain if the vta mutant is rhythmic.This lack of rhythmic pattern suggests a disruption in the temporal regulation of TOR signaling when both VTA and FRQ are absent. (Figure 3.19,3.22)

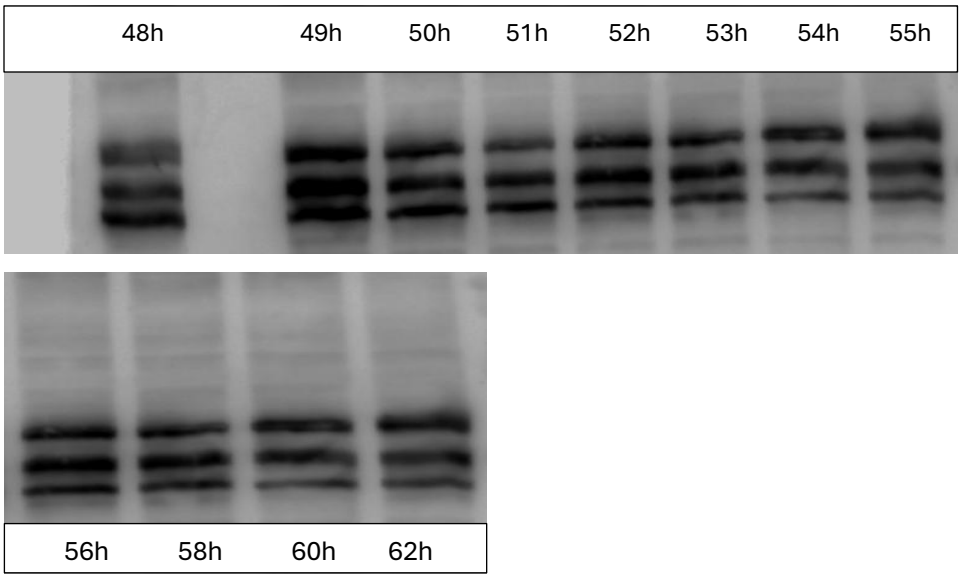


Figure 3.18 Western blot analysis of S6-FLAG expression following T16 heat-pulse entrainment in constant darkness (DD) using the *vta ^{ko} frq10 S6-FLAG* strain.

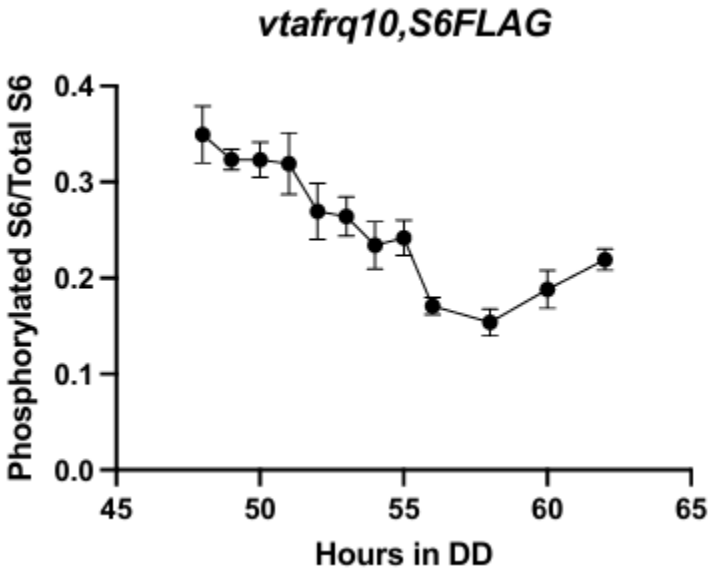


Figure 3.19 Average of S6 Phosphorylation of *vta frq10 S6 FLAG* strain in DD with T cycle 16 and heat pulses from 22 to 37 degrees.

Three replicate experiments were averaged with SEM.

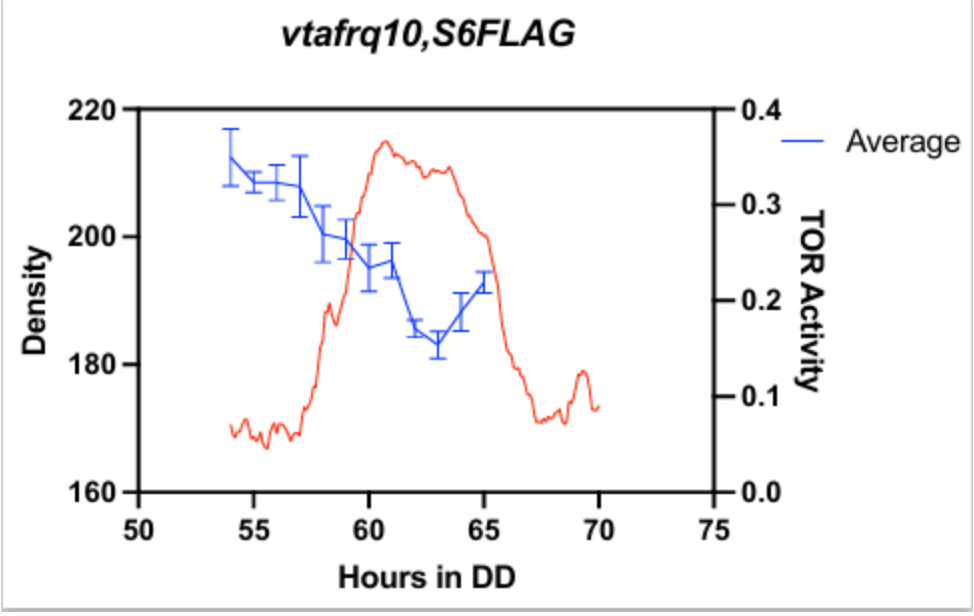


Figure 3.20 TOR activity in *frq10 vtako S6 FLAG* strain and the conidiation peak of the strain in DD with T cycle 16 and heat pulses from 22 to 37 degrees.

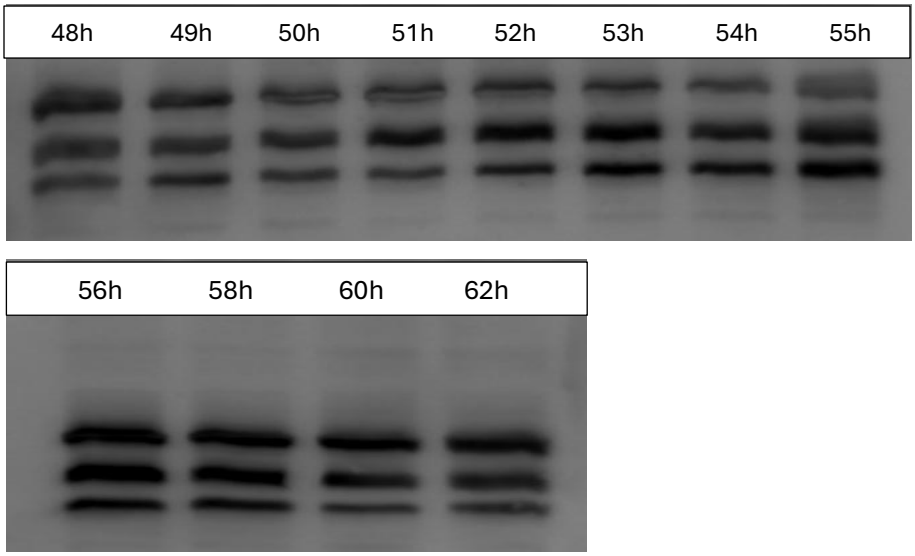


Figure 3.21 Western blot analysis of S6-FLAG expression following T24 heat-pulse entrainment in constant darkness (DD) using the *vta ^{ko} frq10 S6-FLAG* strain.

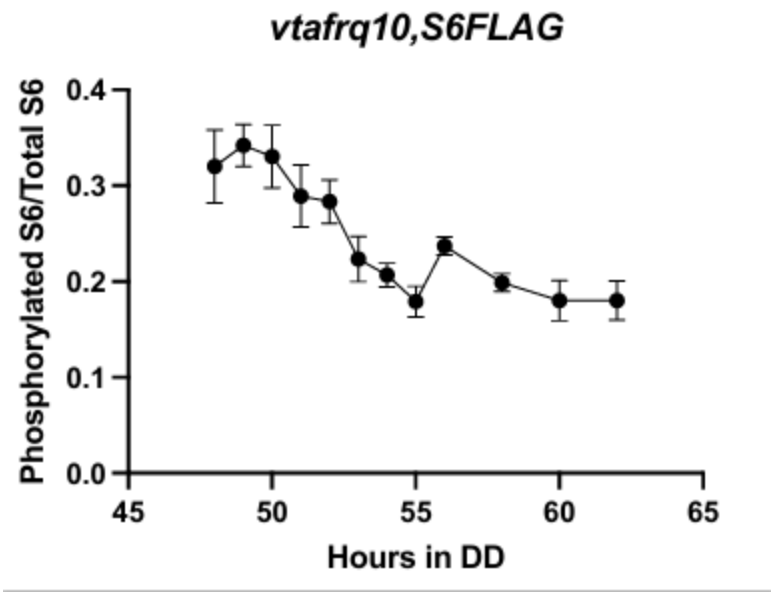


Figure 3.22 Average of S6 Phosphorylation of *vta frq10 S6 FLAG* strain in DD with T cycle 24 and heat pulses from 22 to 37 degrees.

Three replicate experiments were averaged with SEM.

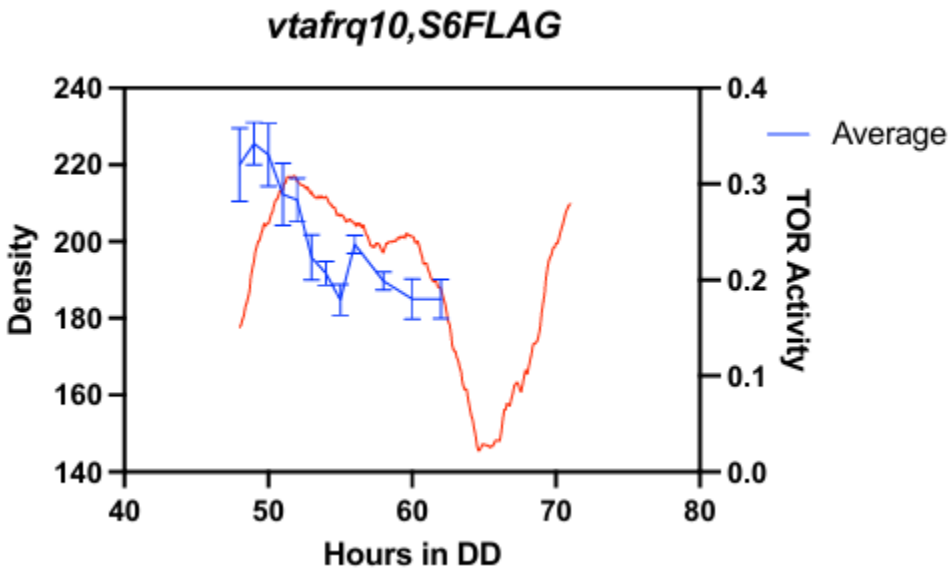


Figure 3.23 TOR activity in *frq10 vtako S6 FLAG* strain and the conidiation peak of the strain in DD with T cycle 24 and heat pulses from 22 to 37 degrees.

Notably, the experimental conditions in this study were consistent with those used in the *frq10 S6-FLAG* heat pulse experiments, where rhythmic TOR activity was observed despite the absence of *frq*. Therefore, the key variable distinguishing these conditions is the additional

knockout of VTA, an upstream component of the TOR pathway. The complete loss of rhythmicity in the *vta^{ko} frq10* strain suggests that VTA plays a critical role in maintaining or enabling rhythmic TOR signaling under entrained conditions. (Figure 3.20,3.23)

3.2.4 Role of GTR2 in Maintaining TOR Rhythmicity Under Heat Pulse Entrainment

Previous time-course analyses conducted in our laboratory demonstrated that S6 phosphorylation in the *gtr2^{ko} S6-FLAG* strain (*csp-1*; *ras^{bd}*; *chol-1*; *gtr2*) exhibits clear rhythmicity under constant darkness, with an approximate period of 28 hours. However, similar to other TOR pathway perturbations, this rhythmic pattern was observed to dampen over successive cycles, with a reduction in amplitude occurring after the second peak. These findings indicate that, while rhythmic TOR activity can be maintained in the absence of GTR2, its stability is compromised. Importantly, these experiments were performed in a background where the *frq* gene remained intact. (Figure 3.24)

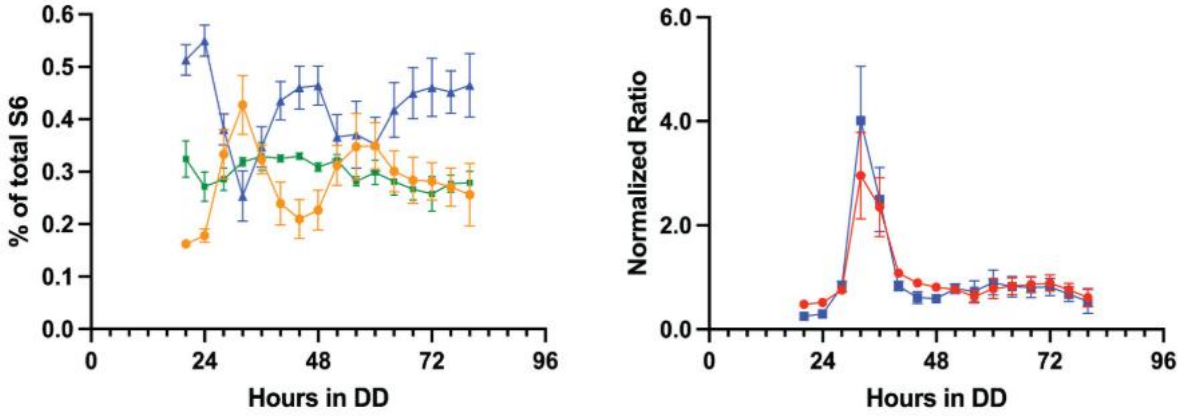


Figure 3.24 S6 phosphorylation rhythm of GTR2 mutant strain from 20 to 80 h in DD.

Error bars indicate SEM for *N* = 3 biological replicates. Left: The anti-FLAG immunodetection data are plotted as the fraction of each band relative to total S6. Right: S6 protein relative to total protein. S6 protein immunodetection band intensities are calculated relative to total protein on the gel, assayed by colloidal gold staining. For the right only, each replicate time-course is normalized to its own mean. (Adapted from Akhtari, 2026)

To assess the combined contribution of GTR2 and FRQ to TOR signaling dynamics, heat pulse entrainment experiments were performed using a *gtr2^{ko} frq10 S6-FLAG* strain. The experimental design was consistent with that used for previous strains.

Analysis of the *gtr2^{ko} frq10* strain revealed a complete absence of detectable rhythmicity in S6 phosphorylation under both T16 and T24 cycles. Similar to observations in the *vtako frq10 strain,* S6 phosphorylation levels (Figure 3.25,3.28) did not exhibit oscillatory behavior and

instead showed a largely steady decline over time. This pattern indicates a disruption in the temporal regulation of TOR signaling when both GTR2 and FRQ are absent. (Figure 3.26,3.29)

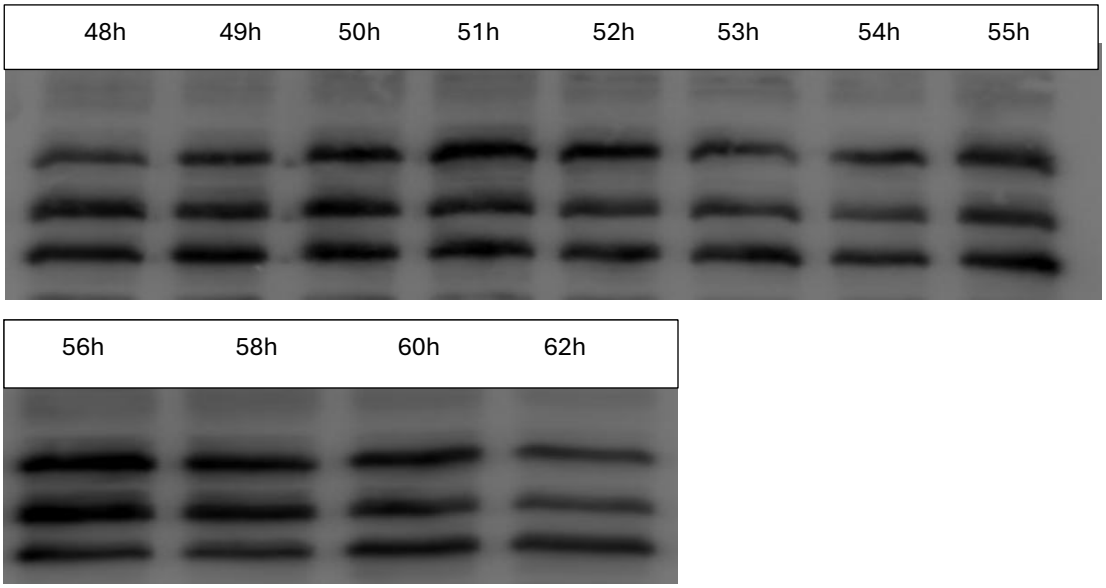


Figure 3.25 Western blot analysis of S6-FLAG expression following T16 heat-pulse entrainment in constant darkness (DD) using the *gtr2 ^{ko} frq10 S6-FLAG* strain.

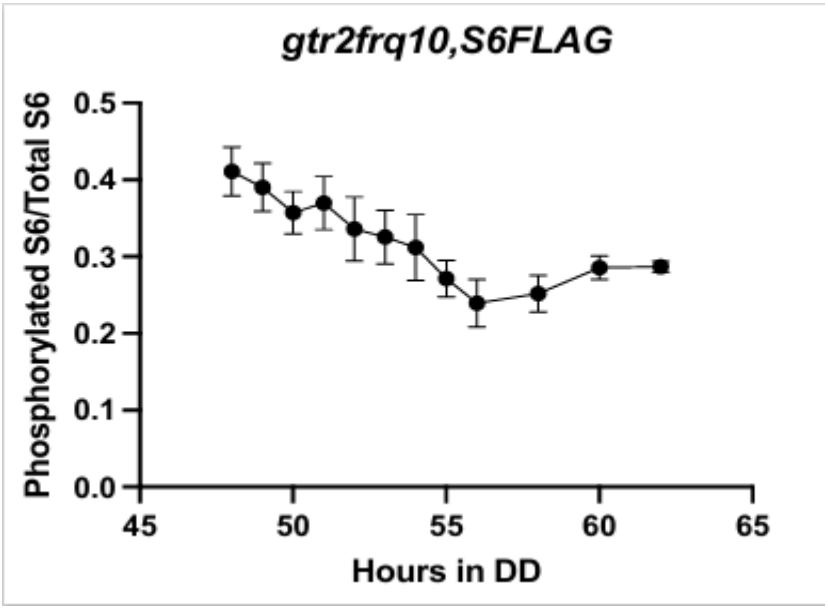


Figure 3.26 Average of S6 Phosphorylation of *gtr2 frq10 S6 FLAG* strain in DD with T cycle 16 and heat pulses from 22 to 37 degrees.

Three replicate experiments were averaged with SEM.

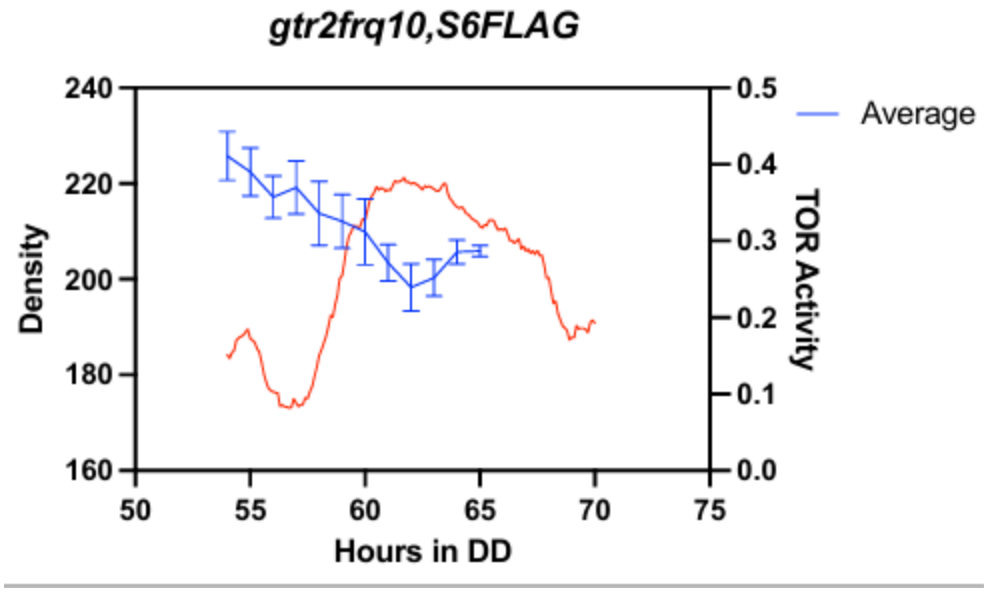


Figure 3.27 TOR activity in *frq10 gtr2ko S6 FLAG* strain and the conidiation peak of the strain in DD with T cycle 16 and heat pulses from 22 to 37 degrees.

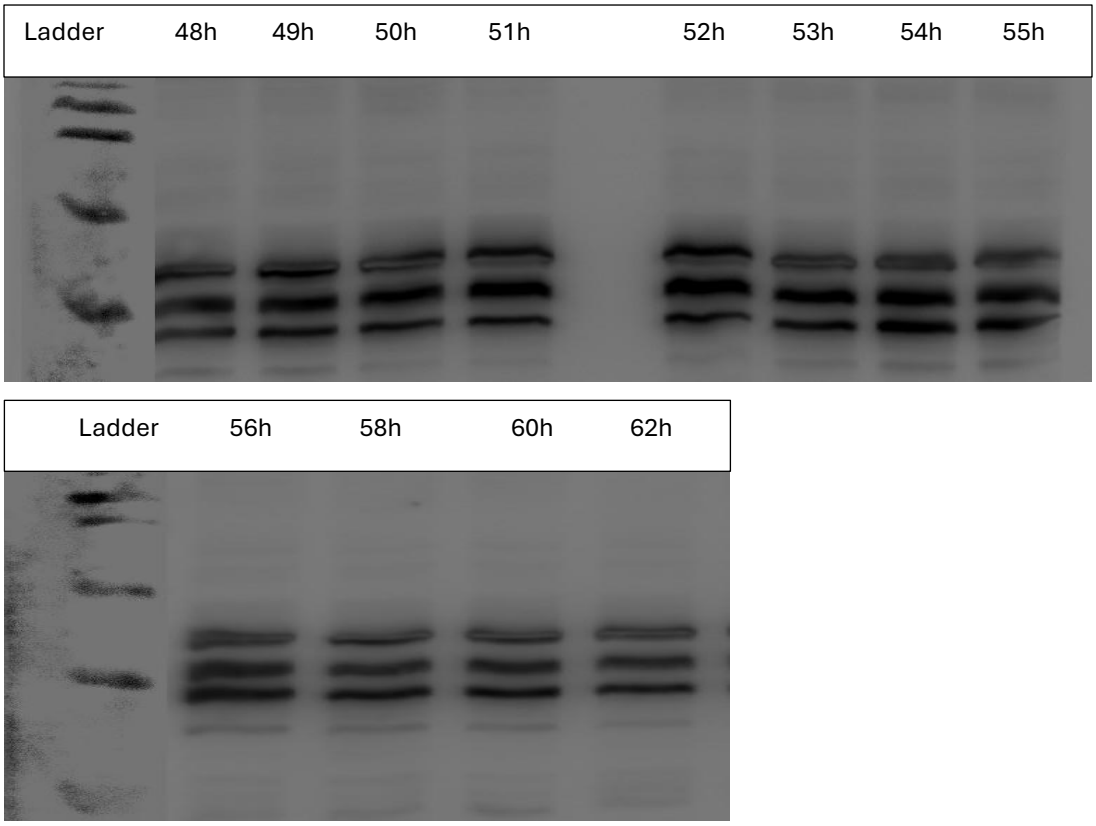


Figure 3.28 Western blot analysis of S6-FLAG expression following T24 heat-pulse entrainment in constant darkness (DD) using the *gtr2 ^{ko} frq10 S6-FLAG* strain.

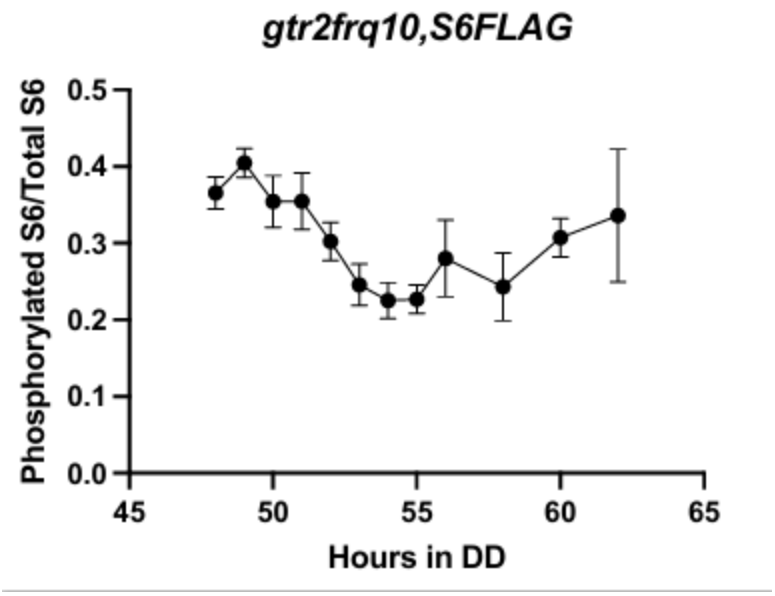


Figure 3.29 Average of S6 Phosphorylation of *gtr2 frq10 S6 FLAG* strain in DD with T cycle 24 and heat pulses from 22 to 37 degrees.

Three replicate experiments were averaged with SEM.

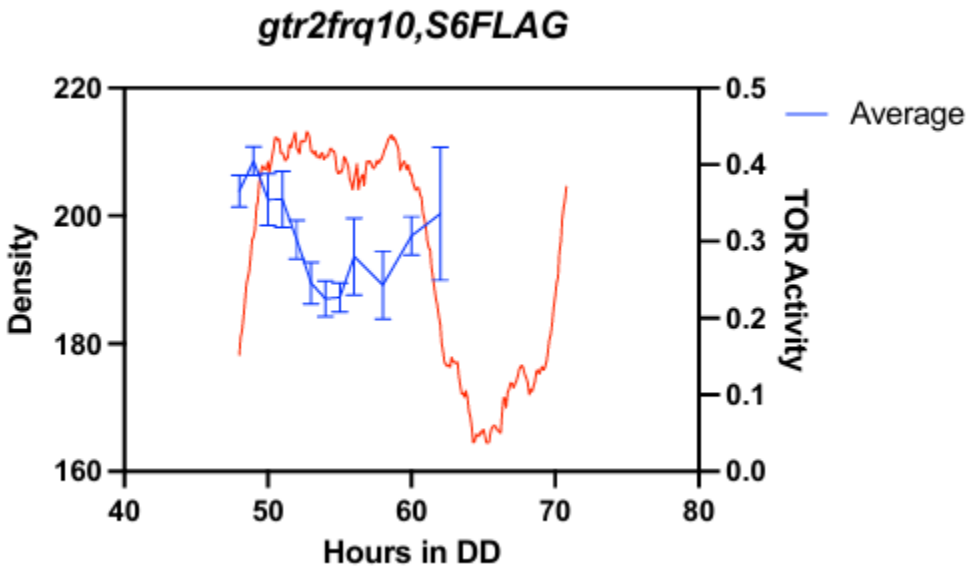


Figure 3.30 TOR activity in *frq10 gtr2ko S6 FLAG* strain and the conidiation peak of the strain in DD with T cycle 24 and heat pulses from 22 to 37 degrees.

Notably, this loss of rhythmicity contrasts with previous findings in both *gtr2ko* and *vtako* single knockout strains, where rhythmic S6 phosphorylation was still detectable despite damping over time. Furthermore, under identical heat pulse conditions, the *frq10 S6-FLAG* strain retained rhythmic TOR activity, indicating that FRQ is not strictly required for rhythmicity under

entrained conditions. Therefore, the critical difference in the present experiment is the simultaneous disruption of *frq* and GTR2, an upstream regulator of TOR signaling. (Figure 3.27,3.30)

Taken together, these findings demonstrate that while TOR signaling can maintain FRQ-independent rhythmicity under heat pulse entrainment, this capability is dependent on the integrity of upstream regulatory components such as GTR2. The complete loss of rhythmicity in the *gtr2*^{ko} *frq10* strain suggests that GTR2 plays a crucial role in enabling or sustaining temporally organized TOR activity, and that disruption of upstream signaling inputs abolishes the rhythmic potential of the pathway.

4 Chapter 4: Discussion

Circadian rhythms in *Neurospora crassa* have traditionally been explained by the transcriptional-translational feedback loop (TTFL), in which FRQ serves as the central component of the molecular clock. However, numerous studies have demonstrated that rhythmic physiological processes can persist in the absence of FRQ, supporting the existence of an alternative timing mechanism known as the FRQ-less oscillator (FLO). Although the molecular basis of FLO remains largely unknown, previous work has suggested that it is capable of generating rhythmic outputs independently of the canonical TTFL.

Published studies from our laboratory further support the existence of this alternative oscillator. Under heat pulse entrainment, the *frq10* strain exhibited phase shifts in conidiation peaks in response to different T-cycle lengths, demonstrating that conidiation remained entrainable despite the absence of FRQ. In contrast, both vta^{ko} and $gtr2^{ko}$ mutant strains failed to adjust the timing of their conidiation peaks across different T-cycles, indicating a loss of rhythmic entrainment.(Eskandari et al., 2021) These findings suggest that while the canonical FRQ clock is not essential for entrained conidiation rhythms, components of the TOR pathway may be required for the function or output of the proposed FRQ-less oscillator.

The present study aimed to determine whether rhythmic TOR activity, assessed by ribosomal protein S6 phosphorylation, is also regulated by this FRQ-independent timing mechanism. Previous time-course experiments performed under constant darkness demonstrated that S6 phosphorylation in the *frq10* strain lacked reproducible rhythmicity because biological replicates were not synchronized.(Akhtari, 2023) In contrast, rhythmic S6 phosphorylation was maintained in the wild-type, vta^{ko}, and $gtr2^{ko}$ strains, although rhythms in the TOR pathway mutants gradually dampened over successive cycles (Figure 4.1). These observations suggested that rhythmic TOR activity can be maintained despite disruption of individual TOR pathway components, provided that the canonical FRQ oscillator remains intact.

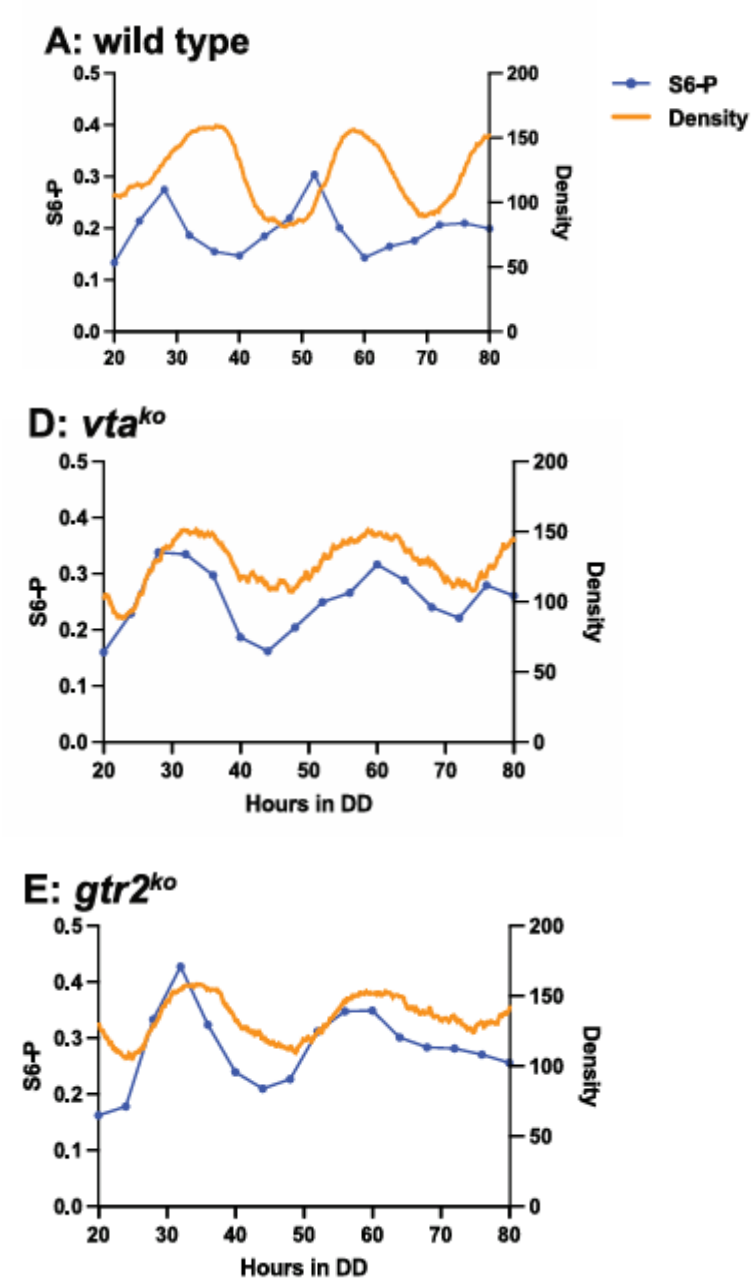


Figure 4.1 Conidiation density compared to s6P timecourses.

Thick curves: Mean density of conidiation from scans of five replicate race tube cultures. Thin lines with plot symbols: s6P rhythm (top band as percent of total s6). (Adapted from Akhtari, 2026)

In the present study, heat pulse entrainment revealed a distinct and reproducible rhythm of S6 phosphorylation in the *frq10 S6-FLAG* strain under the T16 cycle. The phosphorylation peak consistently occurred before the peak of conidiation and closely resembled the temporal relationship previously observed in the wild-type strain. Importantly, the S6 phosphorylation

peak did not occur immediately following the heat pulse, indicating that the observed oscillation is unlikely to represent a simple acute response to temperature stimulation. Instead, the delayed timing of TOR activation suggests regulation by an underlying biological oscillator that is synchronized by environmental temperature cycles rather than being directly driven by each individual heat pulse.

Together with previously published conidiation data, these findings provide evidence that rhythmic TOR activity is regulated by the same FRQ-independent timing mechanism responsible for entrainment of conidiation rhythms. The observation that both conidiation and S6 phosphorylation exhibit coordinated temporal organization in the *frq10* strain suggests that rhythmic TOR activity may represent a downstream physiological output of the proposed FLO. This provides a potential molecular connection between the FRQ-less oscillator and cellular growth regulation in *Neurospora crassa*. Another possibility investigated in this study, which was the primary focus of this master's thesis, was that the TOR pathway functions as the FLO oscillator. The results of these experiments provide the strongest evidence to date supporting this possibility, suggesting that TOR is the most likely candidate for the oscillator underlying FLO conditions.

Unlike the T16 experiments, reproducible rhythmic S6 phosphorylation was not observed under the T24 entrainment cycle, even in the *frq10* strain. A possible explanation is that the timing of culture transfers between constant light (LL) and constant darkness (DD), as well as the harvesting schedule, was identical to that used for the T16 experiments. Because cultures exposed to a longer entrainment cycle may require additional time to establish stable phase relationships before sampling, the experimental design may not have provided sufficient time for complete entrainment under T24 conditions. The average conidiation pattern shown in Figure 3.7 suggests that the sample was stably entrained. Future studies should therefore optimize transfer and harvesting schedules for individual T-cycle lengths to reveal reproducible rhythmic TOR activity under T24 entrainment. The effect of changes in sample harvesting time across different T-cycles is demonstrated by the results obtained from the Stella simulation model (Figure 1.18). The model predicts that the peak timing in the T22.5 cycle differs from that observed in shorter-period T-cycles, such as T19.

The double knockout experiments further clarify the molecular requirements for FRQ-independent rhythmic TOR activity. Although rhythmic S6 phosphorylation was maintained in

the *frq10* strain under T16 entrainment, rhythmicity was completely abolished when either VTA or GTR2 was additionally deleted. Neither the *vta*^{ko} *frq10* nor the *gtr2*^{ko} *frq10* strain exhibited detectable oscillations in S6 phosphorylation under either T16 or T24 conditions. Instead, S6 phosphorylation gradually declined throughout the experiment, indicating a complete disruption of temporal organization.

Comparison with previous laboratory studies further strengthens this conclusion. Both *vta*^{ko} and *gtr2*^{ko} single knockout strains retained rhythmic S6 phosphorylation, although the rhythms gradually dampened under constant darkness. Similarly, the present study demonstrates that deletion of FRQ alone does not abolish rhythmic S6 phosphorylation under T16 entrainment. However, simultaneous deletion of FRQ together with either VTA or GTR2 completely eliminated rhythmic TOR activity. These observations indicate that although rhythmic TOR activity can be maintained independently of the canonical FRQ oscillator, it requires an intact TOR pathway. Upstream regulators, such as VTA and GTR2, therefore appear to be essential for maintaining rhythmic TOR activity in the absence of FRQ. These regulators may be essential for providing the feedback required to generate oscillatory TOR activity.

Overall, the findings of this study support a model in which the FRQ-less oscillator regulates rhythmic TOR activity independently of the canonical FRQ transcriptional-translational feedback loop. The feedback mechanisms within the TOR pathway may generate a FRQ-less oscillator. Environmental heat pulse cycles act as entrainment cues that synchronize this alternative oscillator, allowing rhythmic TOR activity to become detectable. However, the rhythmic pattern observed cannot be explained solely as a direct response to heat pulses, since TOR activation consistently precedes conidiation. Furthermore, the complete loss of rhythmic S6 phosphorylation following deletion of either VTA or GTR2 demonstrates that the integrity of the TOR pathway is required for this FRQ-independent rhythmic regulation. Together, these findings establish a previously unrecognized functional relationship between the proposed FRQ-less oscillator and the TOR pathway, providing new insight into how metabolic signaling pathways may participate in circadian regulation independently of the canonical FRQ clock in *Neurospora crassa*.

5 Future Work

Although a clear rhythm of TOR activity was observed in the *frq10* strains under the T16 heat pulse cycle, a similar rhythmic pattern was not detected under the T24 cycle. One possible explanation is that the sampling strategy used in this study was based on the same transfer and harvesting schedule for both T16 and T24 treatments. Different entrainment periods may require different durations for sample transfer, acclimation, and harvesting in order to accurately capture the phase of TOR activity. Therefore, future experiments should optimize these time intervals for each individual T-cycle rather than applying a common sampling schedule. In addition to the T16 and T24 cycles, other entrainment periods, such as T20 and T28, should also be examined to determine whether TOR activity shifts its phase according to the entrainment period, as would be expected for a FRQ-less oscillator. Another direction for future work is to identify improved growth conditions for the samples based on the free-running experiment (Figure 3.9) and to repeat the experiments using the VTA and GTR2 mutant strains. Together, these experiments would provide a more comprehensive evaluation of the role of TOR as a potential FRQ-independent oscillator and further clarify its contribution to circadian rhythmicity in *Neurospora crassa*.

6 References

Adams, S., Manfield, I., Stockley, P., & Carré, I. A. (2015). Revised Morning Loops of the Arabidopsis Circadian Clock Based on Analyses of Direct Regulatory Interactions. *PLoS ONE*, *10*(12). https://doi.org/10.1371/journal.pone.0143943

Akhtari, G. (2023). THE relationship between TOR activity and the circadian clock of *Neurospora crassa* [Master's]. York University.

Akhtari, G., Falahat Chian, M., Sooklal, E. M., & Lakin-Thomas, P. (2026). Rhythmicity of TOR (Target of Rapamycin) Activity Supports Circadian Function in *Neurospora crassa*. *Journal of Biological Rhythms*, *41*(2). https://doi.org/10.1177/07487304251393577

Albert, V., & Hall, M. N. (2015). mTOR signaling in cellular and organismal energetics. In *Current Opinion in Cell Biology* (Vol. 33, Number 1). https://doi.org/10.1016/j.ceb.2014.12.001

Allada, R., & Chung, B. Y. (2009). Circadian organization of behavior and physiology in *Drosophila*. In *Annual Review of Physiology* (Vol. 72). https://doi.org/10.1146/annurev-physiol-021909-135815

Aramayo, R., & Selker, E. U. (2013). *Neurospora crassa*, a model system for epigenetics research. *Cold Spring Harbor Perspectives in Biology*, *5*(10). https://doi.org/10.1101/cshperspect.a017921

Aronson, B. D., Johnson, K. A., & Dunlap, J. C. (1994). Circadian clock locus frequency: Protein encoded by a single open reading frame defines period length and temperature compensation. *Proceedings of the National Academy of Sciences of the United States of America*, *91*(16). https://doi.org/10.1073/pnas.91.16.7683

Baker, C. L., Loros, J. J., & Dunlap, J. C. (2012). The circadian clock of *Neurospora crassa*. In *FEMS Microbiology Reviews* (Vol. 36, Number 1). https://doi.org/10.1111/j.1574-6976.2011.00288.x

Bass, J., & Takahashi, J. S. (2010). Circadian integration of metabolism and energetics. In *Science* (Vol. 330, Number 6009). https://doi.org/10.1126/science.1195027

Belden, W. J., Larrondo, L. F., Froehlich, A. C., Shi, M., Chen, C. H., Loros, J. J., & Dunlap, J. C. (2007). The band mutation in *Neurospora crassa* is a dominant allele of ras-1 implicating RAS signaling in circadian output. *Genes and Development*, *21*(12). https://doi.org/10.1101/gad.1551707

Bell-Pedersen, D., Cassone, V. M., Earnest, D. J., Golden, S. S., Hardin, P. E., Thomas, T. L., & Zoran, M. J. (2005). Circadian rhythms from multiple oscillators: Lessons from diverse organisms. In *Nature Reviews Genetics* (Vol. 6, Number 7). https://doi.org/10.1038/nrg1633

Ben-Sahra, I., & Manning, B. D. (2017). mTORC1 signaling and the metabolic control of cell growth. In *Current Opinion in Cell Biology* (Vol. 45). https://doi.org/10.1016/j.ceb.2017.02.012

Bhadra, U., Thakkar, N., Das, P., & Pal Bhadra, M. (2017). Evolution of circadian rhythms: from bacteria to human. In *Sleep Medicine* (Vol. 35). https://doi.org/10.1016/j.sleep.2017.04.008

Borkovich, K. A., Alex, L. A., Yarden, O., Freitag, M., Turner, G. E., Read, N. D., Seiler, S., Bell-Pedersen, D., Paietta, J., Plesofsky, N., Plamann, M., Goodrich-Tanrikulu, M., Schulte, U., Mannhaupt, G., Nargang, F. E., Radford, A., Selitrennikoff, C., Galagan, J. E., Dunlap, J. C., … Pratt, R. (2004). Lessons from the Genome Sequence of *Neurospora crassa*: Tracing the Path from Genomic Blueprint to Multicellular Organism. *Microbiology and Molecular Biology Reviews*, *68*(1). https://doi.org/10.1128/mmbr.68.1.1-108.2004

Brunner, M., & Káldi, K. (2008). Interlocked feedback loops of the circadian clock of *Neurospora crassa.* In *Molecular Microbiology* (Vol. 68, Number 2). https://doi.org/10.1111/j.1365-2958.2008.06148.x

Buhr, E. D., & Takahashi, J. S. (2013). Molecular components of the mammalian circadian clock. *Handbook of Experimental Pharmacology*, *217*. https://doi.org/10.1007/978-3-642-25950-0_1

Burkart, G. M., & Brandizzi, F. (2021). A Tour of TOR Complex Signaling in Plants. In *Trends in Biochemical Sciences* (Vol. 46, Number 5). https://doi.org/10.1016/j.tibs.2020.11.004

Cao, P., Kim, S. J., Xing, A., Schenck, C. A., Liu, L., Jiang, N., Wang, J., Last, R. L., & Brandizzi, F. (2019). Homeostasis of branched-chain amino acids is critical for the activity of TOR signaling in Arabidopsis. *ELife*, *8*. https://doi.org/10.7554/eLife.50747

Cha, J., Zhou, M., & Liu, Y. (2015). Mechanism of the Neurospora circadian clock, a FREQUENCY-centric view. *Biochemistry*, *54*(2). https://doi.org/10.1021/bi5005624

Chatterjee, A., Tanoue, S., Houl, J. H., & Hardin, P. E. (2010). Regulation of Gustatory Physiology and Appetitive Behavior by the *Drosophila* Circadian Clock. *Current Biology*, *20*(4). https://doi.org/10.1016/j.cub.2009.12.055

Chi-Castañeda, D., & Ortega, A. (2016). Clock Genes in Glia Cells. *ASN Neuro*, *8*(5). https://doi.org/10.1177/1759091416670766

Cohen, S. E., & Golden, S. S. (2015). Circadian Rhythms in Cyanobacteria. *Microbiology and Molecular Biology Reviews*, *79*(4). https://doi.org/10.1128/mmbr.00036-15

Colot, H. V., Park, G., Turner, G. E., Ringelberg, C., Crew, C. M., Litvinkova, L., Weiss, R. L., Borkovich, K. A., & Dunlap, J. C. (2006). A high-throughput gene knockout procedure for Neurospora reveals functions for multiple transcription factors. *Proceedings of the National*

Academy of Sciences of the United States of America, *103*(27). https://doi.org/10.1073/pnas.0601456103

Condon, K. J., & Sabatini, D. M. (2019). Nutrient regulation of mTORC1 at a glance. *Journal of Cell Science*, *132*(21). https://doi.org/10.1242/JCS.222570

Creux, N., & Harmer, S. (2019). Circadian rhythms in plants. *Cold Spring Harbor Perspectives in Biology*, *11*(9). https://doi.org/10.1101/cshperspect.a034611

Davis, R. H., & de Serres, F. J. (1970). Genetic and Microbiological Research Techniques for *Neurospora crassa*. *Methods in Enzymology*, *17*. https://doi.org/10.1016/0076-6879(71)17168-6

Davis, R. H., & Perkins, D. D. (2002). Neurospora: A model of model microbes. In *Nature Reviews Genetics* (Vol. 3, Number 5). https://doi.org/10.1038/nrg797

de Barros Dantas, L. L., Eldridge, B. M., Dorling, J., Dekeya, R., Lynch, D. A., & Dodd, A. N. (2023). Circadian regulation of metabolism across photosynthetic organisms. In *Plant Journal* (Vol. 116, Number 3). https://doi.org/10.1111/tpj.16405

Di Como, C. J., & Arndt, K. T. (1996). Nutrients, via the Tor proteins, stimulate the association of Tap42 with type 2A phosphatases. *Genes and Development*, *10*(15). https://doi.org/10.1101/gad.10.15.1904

Ditty, J. L., Williams, S. B., & Golden, S. S. (2003). A Cyanobacterial Circadian Timing Mechanism. In *Annual Review of Genetics* (Vol. 37). https://doi.org/10.1146/annurev.genet.37.110801.142716

Dodd, A. N., Salathia, N., Hall, A., Kévei, E., Tóth, R., Nagy, F., Hibberd, J. M., Millar, A. J., & Webb, A. A. R. (2005). Cell biology: Plant circadian clocks increase photosynthesis, growth, survival, and competitive advantage. *Science*, *309*(5734). https://doi.org/10.1126/science.1115581

Dokládal, L., Stumpe, M., Hu, Z., Jaquenoud, M., Dengjel, J., & De Virgilio, C. (2021). Phosphoproteomic responses of TORC1 target kinases reveal discrete and convergent mechanisms that orchestrate the quiescence program in yeast. *Cell Reports*, *37*(13). https://doi.org/10.1016/j.celrep.2021.110149

Dong, W., Tang, X., Yu, Y., Nilsen, R., Kim, R., Griffith, J., Arnold, J., & Schüttler, H. B. (2008). System biology of the Clock in *Neurospora crassa*. *PLoS ONE*, *3*(8). https://doi.org/10.1371/journal.pone.0003105

Dunlap, J. C. (1999). Molecular bases for circadian clocks. In *Cell* (Vol. 96, Number 2). https://doi.org/10.1016/S0092-8674(00)80566-8

Dunlap, J. C., & Loros, J. J. (2005). Analysis of circadian rhythms in Neurospora: Overview of assays and genetic and molecular biological manipulation. *Methods in Enzymology*, *393*. https://doi.org/10.1016/S0076-6879(05)93001-2

Dunlap, J. C., & Loros, J. J. (2017). Making Time: Conservation of Biological Clocks from Fungi to Animals. *Microbiology Spectrum*, *5*(3). https://doi.org/10.1128/microbiolspec.funk-0039-2016

Eltschinger, S., & Loewith, R. (2016). TOR Complexes and the Maintenance of Cellular Homeostasis. In *Trends in Cell Biology* (Vol. 26, Number 2). https://doi.org/10.1016/j.tcb.2015.10.003

Eskandari, R., Ratnayake, L., & Lakin-Thomas, P. L. (2021). Shared Components of the FRQ-Less Oscillator and TOR Pathway Maintain Rhythmicity in Neurospora. *Journal of Biological Rhythms*, *36*(4). https://doi.org/10.1177/0748730421999948

Fagiani, F., Di Marino, D., Romagnoli, A., Travelli, C., Voltan, D., Mannelli, L. D. C., Racchi, M., Govoni, S., & Lanni, C. (2022). Molecular regulations of circadian rhythm and implications for physiology and diseases. In *Signal Transduction and Targeted Therapy* (Vol. 7, Number 1). https://doi.org/10.1038/s41392-022-00899-y

Finger, A. M., & Kramer, A. (2021). Mammalian circadian systems: Organization and modern life challenges. In *Acta Physiologica* (Vol. 231, Number 3). https://doi.org/10.1111/apha.13548

Foster, R. G., & Kreitzman, L. (2009). Seasons of life: The biological rhythms that enable living things to thrive and survive. In *Seasons of Life: The Biological Rhythms that Enable Living Things to Thrive and Survive*. https://doi.org/10.5860/choice.47-1401

Fu, L., Wang, P., & Xiong, Y. (2020). Target of rapamycin signaling in plant stress responses1[open]. *Plant Physiology*, *182*(4). https://doi.org/10.1104/PP.19.01214

Galagan, J. E., Calvo, S. E., Borkovich, K. A., Selker, E. U., Read, N. O., Jaffe, D., FitzHugh, W., Ma, L. J., Smirnov, S., Purcell, S., Rehman, B., Elkins, T., Engels, R., Wang, S., Nielsen, C. B., Butler, J., Endrizzi, M., Qui, D., Ianakiev, P., … Birren, B. (2003). The genome sequence of the filamentous fungus *Neurospora crassa*. *Nature*, *422*(6934). https://doi.org/10.1038/nature01554

Giebultowicz, J. (2004). Chronobiology: Biological Timekeeping. *Integrative and Comparative Biology*, *44*(3). https://doi.org/10.1093/icb/44.3.266

González, A., & Hall, M. N. (2017). Nutrient sensing and TOR signaling in yeast and mammals. *The EMBO Journal*, *36*(4). https://doi.org/10.15252/embj.201696010

Hardin, P. E. (2004). Transcription regulation within the circadian clock: The E-box and beyond. In *Journal of Biological Rhythms* (Vol. 19, Number 5). https://doi.org/10.1177/0748730404268052

Hardin, P. E. (2005). The circadian timekeeping system of *Drosophila.* In *Current Biology* (Vol. 15, Number 17). https://doi.org/10.1016/j.cub.2005.08.019

Harmer, S. L. (2009). The circadian system in higher plants. *Annual Review of Plant Biology*, *60*. https://doi.org/10.1146/annurev.arplant.043008.092054

Harmer, S. L., Hogenesch, J. B., Straume, M., Chang, H. S., Han, B., Zhu, T., Wang, X., Kreps, J. A., & Kay, S. A. (2000). Orchestrated transcription of key pathways in Arabidopsis by the circadian clock. *Science*, *290*(5499). https://doi.org/10.1126/science.290.5499.2110

Hickey, P. C., Jacobson, D. J., Read, N. D., & Louise Glass, N. (2002). Live-cell imaging of vegetative hyphal fusion in *Neurospora crassa*. *Fungal Genetics and Biology*, *37*(1). https://doi.org/10.1016/S1087-1845(02)00035-X

Hidalgo, S., & Chiu, J. C. (2024). Integration of photoperiodic and temperature cues by the circadian clock to regulate insect seasonal adaptations. In *Journal of Comparative Physiology A: Neuroethology, Sensory, Neural, and Behavioral Physiology* (Vol. 210, Number 4). https://doi.org/10.1007/s00359-023-01667-1

Honda, S., & Selker, E. U. (2009). Tools for fungal proteomics: Multifunctional neurospora vectors for gene replacement, protein expression and protein purification. *Genetics*, *182*(1). https://doi.org/10.1534/genetics.108.098707

Honma, S. (2018). The mammalian circadian system: a hierarchical multi-oscillator structure for generating circadian rhythm. In *Journal of Physiological Sciences* (Vol. 68, Number 3). https://doi.org/10.1007/s12576-018-0597-5

Hsu, P. Y., & Harmer, S. L. (2014). Wheels within wheels: The plant circadian system. In *Trends in Plant Science* (Vol. 19, Number 4). https://doi.org/10.1016/j.tplants.2013.11.007

Huang, R. C. (2018). The discoveries of molecular mechanisms for the circadian rhythm: The 2017 Nobel Prize in Physiology or Medicine. In *Biomedical Journal* (Vol. 41, Number 1). https://doi.org/10.1016/j.bj.2018.02.003

Jin, Y., Allan, S., Baber, L., Bhattarai, E. K., Lamb, T. M., & Versaw, W. K. (2007). Rapid genetic mapping in *Neurospora crassa*. *Fungal Genetics and Biology*, *44*(6). https://doi.org/10.1016/j.fgb.2006.09.002

Johnson, C. H., Stewart, P. L., & Egli, M. (2011). The cyanobacterial circadian system: From biophysics to bioevolution. *Annual Review of Biophysics*, *40*(1). https://doi.org/10.1146/annurev-biophys-042910-155317

Karpowicz, P., Zhang, Y., Hogenesch, J. B., Emery, P., & Perrimon, N. (2013). The Circadian Clock Gates the Intestinal Stem Cell Regenerative State. *Cell Reports*, *3*(4). https://doi.org/10.1016/j.celrep.2013.03.016

Kim, E. Y., Ko, H. W., Yu, W., Hardin, P. E., & Edery, I. (2007). A DOUBLETIME Kinase Binding Domain on the *Drosophila* PERIOD Protein Is Essential for Its Hyperphosphorylation, Transcriptional Repression, and Circadian Clock Function . *Molecular and Cellular Biology*, *27*(13). https://doi.org/10.1128/mcb.02339-06

Kim, Y. I., Dong, G., Carruthers, C. W., Golden, S. S., & LiWang, A. (2008). The day/night switch in KaiC, a central oscillator component of the circadian clock of cyanobacteria. *Proceedings of the National Academy of Sciences of the United States of America*, *105*(35). https://doi.org/10.1073/pnas.0800526105

Ko, C. H., & Takahashi, J. S. (2006). Molecular components of the mammalian circadian clock. In *Human Molecular Genetics* (Vol. 15, Number SUPPL. 2). https://doi.org/10.1093/hmg/ddl207

Lakin-Thomas, P. (2019). Circadian rhythms, metabolic oscillators, and the target of rapamycin (TOR) pathway: the Neurospora connection. In *Current Genetics* (Vol. 65, Number 2). https://doi.org/10.1007/s00294-018-0897-6

Lakin-Thomas, P. (2023). The Case for the Target of Rapamycin Pathway as a Candidate Circadian Oscillator. In *International Journal of Molecular Sciences* (Vol. 24, Number 17). https://doi.org/10.3390/ijms241713307

Lakin-Thomas, P. L. (1998). Choline Depletion, frq Mutations, and Temperature Compensation of the Circadian Rhythm in *Neurospora crassa*. *Journal of Biological Rhythms*, *13*(4). https://doi.org/10.1177/074873098129000101

Lakin-Thomas, P. L. (2006a). Circadian clock genes frequency and white collar-1 are not essential for entrainment to temperature cycles in *Neurospora crassa*. *Proceedings of the National Academy of Sciences of the United States of America*, *103*(12). https://doi.org/10.1073/pnas.0510404103

Lakin-Thomas, P. L. (2006b). Transcriptional feedback oscillators: Maybe, maybe not... In *Journal of Biological Rhythms* (Vol. 21, Number 2). https://doi.org/10.1177/0748730405286102

Lakin-Thomas, P. L., Bell-Pedersen, D., & Brody, S. (2011). The genetics of circadian rhythms in Neurospora. In *Advances in Genetics* (Vol. 74). https://doi.org/10.1016/B978-0-12-387690-4.00003-9

Lakin-Thomas, P. L., & Brody, S. (2000). Circadian rhythms in *Neurospora crassa*: Lipid deficiencies restore robust rhythmicity to null frequency and white-collar mutants.

Proceedings of the National Academy of Sciences of the United States of America, *97*(1). https://doi.org/10.1073/pnas.97.1.256

Lakin-Thomas, P. L., & Brody, S. (2004). Circadian rhythms in microorganisms: New complexities. In *Annual Review of Microbiology* (Vol. 58). https://doi.org/10.1146/annurev.micro.58.030603.123744

Laplante, M., & Sabatini, D. M. (2012). MTOR signaling in growth control and disease. In *Cell* (Vol. 149, Number 2). https://doi.org/10.1016/j.cell.2012.03.017

Liu, Y., & Bell-Pedersen, D. (2006). Circadian rhythms in *Neurospora crassa* and other filamentous fungi. In *Eukaryotic Cell* (Vol. 5, Number 8). https://doi.org/10.1128/EC.00133-06

Liu, Y., Hu, J., Duan, X., Ding, W., Xu, M., & Xiong, Y. (2025). Target of Rapamycin (TOR): A Master Regulator in Plant Growth, Development, and Stress Responses. In *Annual Review of Plant Biology* (Vol. 76, Number 1). https://doi.org/10.1146/annurev-arplant-083123-050311

Loewith, R., & Hall, M. N. (2011). Target of rapamycin (TOR) in nutrient signaling and growth control. In *Genetics* (Vol. 189, Number 4). https://doi.org/10.1534/genetics.111.133363

Loros, J. J., & Dunlap, J. C. (1991). *Neurospora crassa* clock-controlled genes are regulated at the level of transcription. *Molecular and Cellular Biology*, *11*(1). https://doi.org/10.1128/mcb.11.1.558

Ma, D., Przybylski, D., Abruzzi, K. C., Schlichting, M., Li, Q., Long, X., & Rosbash, M. (2021). A transcriptomic taxonomy of *Drosophila* circadian neurons around the clock. *ELife*, *10*. https://doi.org/10.7554/eLife.63056

Ma, L., Chen, Z., Erdjument-Bromage, H., Tempst, P., & Pandolfi, P. P. (2005). Phosphorylation and functional inactivation of TSC2 by Erk: Implications for tuberous sclerosis and cancer pathogenesis. *Cell*, *121*(2). https://doi.org/10.1016/j.cell.2005.02.031

Mao, W., Ge, X., Chen, Q., & Li, J. Da. (2025). Epigenetic Mechanisms in the Transcriptional Regulation of Circadian Rhythm in Mammals. In *Biology* (Vol. 14, Number 1). https://doi.org/10.3390/biology14010042

Markson, J. S., Piechura, J. R., Puszynska, A. M., & O'Shea, E. K. (2013). XCircadian control of global gene expression by the cyanobacterial master regulator RpaA. *Cell*, *155*(6). https://doi.org/10.1016/j.cell.2013.11.005

McClung, C. R. (2019). The plant circadian oscillator. In *Biology* (Vol. 8, Number 1). https://doi.org/10.3390/biology8010014

McClung, C. R., Salomé, P. A., & Michael, T. P. (2002). The Arabidopsis Circadian System. *The Arabidopsis Book*, *1*. https://doi.org/10.1199/tab.0044

Menet, J. S., Rodriguez, J., Abruzzi, K. C., & Rosbash, M. (2012). Nascent-Seq reveals novel features of mouse circadian transcriptional regulation. *ELife*, *2012*(1). https://doi.org/10.7554/eLife.00011

Merrow, M., Brunner, M., & Roenneberg, T. (1999). Assignment of circadian function for the Neurospora clock gene frequency. *Nature*, *399*(6736). https://doi.org/10.1038/21190

Montenegro-Montero, A., Canessa, P., & Larrondo, L. F. (2015). Around the Fungal Clock: Recent Advances in the Molecular Study of Circadian Clocks in Neurospora and Other Fungi. *Advances in Genetics*, *92*. https://doi.org/10.1016/bs.adgen.2015.09.003

Morris, C. J., Purvis, T. E., Hu, K., & Scheer, F. A. J. L. (2016). Circadian misalignment increases cardiovascular disease risk factors in humans. *Proceedings of the National Academy of Sciences of the United States of America*, *113*(10). https://doi.org/10.1073/pnas.1516953113

Musiek, E. S., & Holtzman, D. M. (2016). Mechanisms linking circadian clocks, sleep, and neurodegeneration. In *Science* (Vol. 354, Number 6315). https://doi.org/10.1126/science.aah4968

O-Neill, J. S., & Reddy, A. B. (2011). Circadian clocks in human red blood cells. *Nature*, *469*(7331). https://doi.org/10.1038/nature09702

Panda, S., Hogenesch, J. B., & Kay, S. A. (2002). Circadian rhythms from flies to human. In *Nature* (Vol. 417, Number 6886). https://doi.org/10.1038/417329a

Panter, P. E., Muranaka, T., Cuitun-Coronado, D., Graham, C. A., Yochikawa, A., Kudoh, H., & Dodd, A. N. (2019). Circadian Regulation of the Plant Transcriptome Under Natural Conditions. In *Frontiers in Genetics* (Vol. 10). https://doi.org/10.3389/fgene.2019.01239

Panwar, V., Singh, A., Bhatt, M., Tonk, R. K., Azizov, S., Raza, A. S., Sengupta, S., Kumar, D., & Garg, M. (2023). Multifaceted role of mTOR (mammalian target of rapamycin) signaling pathway in human health and disease. In *Signal Transduction and Targeted Therapy* (Vol. 8, Number 1). https://doi.org/10.1038/s41392-023-01608-z

Partch, C. L., Green, C. B., & Takahashi, J. S. (2014). Molecular architecture of the mammalian circadian clock. In *Trends in Cell Biology* (Vol. 24, Number 2). https://doi.org/10.1016/j.tcb.2013.07.002

Patke, A., Young, M. W., & Axelrod, S. (2020). Molecular mechanisms and physiological importance of circadian rhythms. In *Nature Reviews Molecular Cell Biology* (Vol. 21, Number 2). https://doi.org/10.1038/s41580-019-0179-2

Pifer, G. C., Ferrara, N. C., & Kwapis, J. L. (2024). Long-lasting effects of disturbing the circadian rhythm or sleep in adolescence. In *Brain Research Bulletin* (Vol. 213). https://doi.org/10.1016/j.brainresbull.2024.110978

Pittendrigh, C. S. (1993). Temporal organization: Reflections of a Darwinian clock-watcher. In *Annual Review of Physiology* (Vol. 55). https://doi.org/10.1146/annurev.ph.55.030193.000313

Pregueiro, A. M., Price-Lloyd, N., Bell-Pedersen, D., Heintzen, C., Loros, J. J., & Dunlap, J. C. (2005). Assignment of an essential role for the Neurospora frequency gene in circadian entrainment to temperature cycles. *Proceedings of the National Academy of Sciences of the United States of America*, *102*(6). https://doi.org/10.1073/pnas.0406506102

Rabanal-Ruiz, Y., & Korolchuk, V. I. (2018). mTORC1 and nutrient homeostasis: The central role of the lysosome. In *International Journal of Molecular Sciences* (Vol. 19, Number 3). https://doi.org/10.3390/ijms19030818

Ratnayake, L., Adhvaryu, K. K., Kafes, E., Motavaze, K., & Lakin-Thomas, P. (2018). A component of the TOR (Target Of Rapamycin) nutrient-sensing pathway plays a role in circadian rhythmicity in *Neurospora crassa*. *PLoS Genetics*, *14*(6). https://doi.org/10.1371/journal.pgen.1007457

Reinke, H., & Asher, G. (2019). Crosstalk between metabolism and circadian clocks. In *Nature Reviews Molecular Cell Biology* (Vol. 20, Number 4). https://doi.org/10.1038/s41580-018-0096-9

Robinson, I., & Reddy, A. B. (2014). Molecular mechanisms of the circadian clockwork in mammals. In *FEBS Letters* (Vol. 588, Number 15). https://doi.org/10.1016/j.febslet.2014.06.005

Roche, C. M., Loros, J. J., McCluskey, K., & Louise Glass, N. (2014). *Neurospora crassa*: Looking back and looking forward at a model microbe. In *American Journal of Botany* (Vol. 101, Number 12). https://doi.org/10.3732/ajb.1400377

Roelants, F. M., Leskoske, K. L., Marshall, M. N. M., Locke, M. N., & Thorner, J. (2017). The TORC2-dependent signaling network in the yeast Saccharomyces cerevisiae. In *Biomolecules* (Vol. 7, Number 3). https://doi.org/10.3390/biom7030066

Roenneberg, T., & Merrow, M. (2005). Circadian clocks - The fall and rise of physiology. In *Nature Reviews Molecular Cell Biology* (Vol. 6, Number 12). https://doi.org/10.1038/nrm1766

Roenneberg, T., & Merrow, M. (2016). The circadian clock and human health. In *Current Biology* (Vol. 26, Number 10). https://doi.org/10.1016/j.cub.2016.04.011

Roux, P. P., & Topisirovic, I. (2012). Regulation of mRNA translation by signaling pathways. *Cold Spring Harbor Perspectives in Biology*, *4*(11). https://doi.org/10.1101/cshperspect.a012252

Ruvinsky, I., & Meyuhas, O. (2006). Ribosomal protein S6 phosphorylation: from protein synthesis to cell size. In *Trends in Biochemical Sciences* (Vol. 31, Number 6). https://doi.org/10.1016/j.tibs.2006.04.003

Saini, C., Brown, S. A., & Dibner, C. (2015). Human peripheral clocks: Applications for studying circadian phenotypes in physiology and pathophysiology. *Frontiers in Neurology*, *6*(MAY). https://doi.org/10.3389/fneur.2015.00095

Saini, R., Jaskolski, M., & Davis, S. J. (2019). Circadian oscillator proteins across the kingdoms of life: Structural aspects. In *BMC Biology* (Vol. 17, Number 1). https://doi.org/10.1186/s12915-018-0623-3

Sancak, Y., Bar-Peled, L., Zoncu, R., Markhard, A. L., Nada, S., & Sabatini, D. M. (2010). Ragulator-rag complex targets mTORC1 to the lysosomal surface and is necessary for its activation by amino acids. *Cell*, *141*(2). https://doi.org/10.1016/j.cell.2010.02.024

Sanchez, S. E., & Kay, S. A. (2016). The plant circadian clock: From a simple timekeeper to a complex developmental manager. *Cold Spring Harbor Perspectives in Biology*, *8*(12). https://doi.org/10.1101/cshperspect.a027748

Saxton, R. A., & Sabatini, D. M. (2017). mTOR Signaling in Growth, Metabolism, and Disease. In *Cell* (Vol. 168, Number 6). https://doi.org/10.1016/j.cell.2017.02.004

Schafmeier, T., Haase, A., Káldi, K., Scholz, J., Fuchs, M., & Brunner, M. (2005). Transcriptional feedback of Neurospora circadian clock gene by phosphorylation-dependent inactivation of its transcription factor. *Cell*, *122*(2). https://doi.org/10.1016/j.cell.2005.05.032

Scheer, F. A. J. L., Hilton, M. F., Mantzoros, C. S., & Shea, S. A. (2009). Adverse metabolic and cardiovascular consequences of circadian misalignment. *Proceedings of the National Academy of Sciences of the United States of America*, *106*(11). https://doi.org/10.1073/pnas.0808180106

Shen, L., Su, Z., Yang, K., Wu, C., Becker, T., Bell-Pedersen, D., Zhang, J., & Sachs, M. S. (2021). Structure of the translating Neurospora ribosome arrested by cycloheximide. *Proceedings of the National Academy of Sciences of the United States of America*, *118*(48). https://doi.org/10.1073/pnas.2111862118

Shertz, C. A., Bastidas, R. J., Li, W., Heitman, J., & Cardenas, M. E. (2010). Conservation, duplication, and loss of the Tor signaling pathway in the fungal kingdom. *BMC Genomics*, *11*(1). https://doi.org/10.1186/1471-2164-11-510

Shi, L., Wu, Y., & Sheen, J. (2018). TOR signaling in plants: conservation and innovation. In Development *(Cambridge, England)* (Vol. 145, Number 13). https://doi.org/10.1242/dev.160887

Shimobayashi, M., & Hall, M. N. (2014). Making new contacts: The mTOR network in metabolism and signalling crosstalk. *Nature Reviews Molecular Cell Biology*, *15*(3). https://doi.org/10.1038/nrm3757

Shukla, N., Neal, M. L., Farré, J. C., Mast, F. D., Sarkar, R., Truong, L., Simon, T., Miller, L. R., Aitchison, J. D., & Subramani, S. (2025). TOR and heat shock response pathways regulate peroxisome biogenesis during proteotoxic stress. *Nature Communications* , *16*(1). https://doi.org/10.1038/s41467-025-65776-y

Swan, J. A., Golden, S. S., LiWang, A., & Partch, C. L. (2018). Structure, function, and mechanism of the core circadian clock in cyanobacteria. In *Journal of Biological Chemistry* (Vol. 293, Number 14). https://doi.org/10.1074/jbc.TM117.001433

Takahashi, J. S. (2017). Transcriptional architecture of the mammalian circadian clock. In *Nature Reviews Genetics* (Vol. 18, Number 3). https://doi.org/10.1038/nrg.2016.150

Tataroglu, O., & Emery, P. (2015). The molecular ticks of the *Drosophila* circadian clock. In *Current Opinion in Insect Science* (Vol. 7). https://doi.org/10.1016/j.cois.2015.01.002

Tatebe, H., & Shiozaki, K. (2017). Evolutionary conservation of the components in the tor signaling pathways. In *Biomolecules* (Vol. 7, Number 4). https://doi.org/10.3390/biom7040077

Tomita, J., Nakajima, M., Kondo, T., & Iwasaki, H. (2005). No transcription-translation feedback in circadian rhythm of KaiC phosphorylation. *Science*, *307*(5707). https://doi.org/10.1126/science.1102540

Tseng, R., Goularte, N. F., Chavan, A., Luu, J., Cohen, S. E., Chang, Y. G., Heisler, J., Li, S., Michael, A. K., Tripathi, S., Golden, S. S., LiWang, A., & Partch, C. L. (2017). Structural basis of the day-night transition in a bacterial circadian clock. *Science*, *355*(6330). https://doi.org/10.1126/science.aag2516

Urban, J., Soulard, A., Huber, A., Lippman, S., Mukhopadhyay, D., Deloche, O., Wanke, V., Anrather, D., Ammerer, G., Riezman, H., Broach, J. R., De Virgilio, C., Hall, M. N., & Loewith, R. (2007). Sch9 Is a Major Target of TORC1 in Saccharomyces cerevisiae. *Molecular Cell*, *26*(5). https://doi.org/10.1016/j.molcel.2007.04.020

VOGEL, H. J. (1956). A convenient growth medium for *Neurospora crassa*. *Genetic Bulletin*, *13*.

Walker, W. H., Walton, J. C., DeVries, A. C., & Nelson, R. J. (2020). Circadian rhythm disruption and mental health. In *Translational Psychiatry* (Vol. 10, Number 1). https://doi.org/10.1038/s41398-020-0694-0

Wright, K. P., Drake, A. L., Frey, D. J., Fleshner, M., Desouza, C. A., Gronfier, C., & Czeisler, C. A. (2015). Influence of sleep deprivation and circadian misalignment on cortisol, inflammatory markers, and cytokine balance. *Brain, Behavior, and Immunity*, *47*. https://doi.org/10.1016/j.bbi.2015.01.004

Wu, Y., Shi, L., Li, L., Fu, L., Liu, Y., Xiong, Y., & Sheen, J. (2019). Integration of nutrient, energy, light, and hormone signalling via TOR in plants. In *Journal of Experimental Botany* (Vol. 70, Number 8). https://doi.org/10.1093/jxb/erz028

Wullschleger, S., Loewith, R., & Hall, M. N. (2006). TOR signaling in growth and metabolism. In *Cell* (Vol. 124, Number 3). https://doi.org/10.1016/j.cell.2006.01.016

Yan, G., Shen, X., & Jiang, Y. (2006). Rapamycin activates Tap42-associated phosphatases by abrogating their association with Tor complex 1. *EMBO Journal*, *25*(15). https://doi.org/10.1038/sj.emboj.7601239

Young, M. W., & Kay, S. A. (2001). Time zones: A comparative genetics of circadian clocks. *Nature Reviews Genetics*, *2*(9). https://doi.org/10.1038/35088576

7 Appendices

7.1 Appendix I. STELLA Model Equations and Simulation Parameters

Complete list of equations, variables, parameter values, and simulation settings used to construct the STELLA model for predicting TOR rhythmicity during heat-pulse entrainment in *Neurospora crassa.* The settings were used to generate the predicted oscillatory patterns presented in Chapter 1.6

Total	Count	Including Array Elements
Variables	13	13
Stocks	1	1
Flows	2	2
Converters	10	10
Constants	6	6
Equations	6	6
Graphicals	0	0

	Equation	Properties	Units	Documentation	Annotation
Top-Level Model:					
"S6-P"(t)	"S6-P"(t - dt) + (TOR - Phosphatases) * dt	INIT "S6-P" = 24			NON-NEGATIVE
Phosphatases	15				UNIFLOW
TOR	"VTA/GTR" + Pulses				UNIFLOW
Amino_Acid_Pool	77 - Protein_Synthesis			Original equation has 60. Making it 77 increases value of Amino Acid Pool above zero (but only if Protein Synthesis denominator is 40 instead of 37).	
Conidiation	Protein_Synthesis				

First_pulse_time	30		Hours	Give pulse times at 25, 30, 35, 37 to see phase shifts with T=500 for one pulse only.	
				Pulse time at 1 for entrainment with T cycles.	
Lag_Time	4.6				
Protein_Synthesis	100 * DELAY("S6-P", Lag_Time)/(37 + (DELAY("S6-P", Lag_Time)))			Original equation has 40 in denominator. Changing to 37 makes it return faster.	
Pulse_length	2		Hours	Use pulse length 1	
Pulse_size	55			Use 50 for pulse size or 0 for no pulse.	
Pulses	STEP(Pulse_size, First_pulse_time, Pulse_length, T_cycle)				

T cycle	22.5			T=22, pulse size 50 entrains well T=19 entrains, 18 does not At 19, S6-P peak is later than the pulse. T=22.5 entrains, S6-P peak is right after pulse. T=23 does not entrain. Use T= 500 for only one pulse.	
"VTA/GTR"	Amino Acid Pool				

Run Specs	
Start Time	0
Stop Time	200
DT	1/100
Fractional DT	True
Save Interval	0.01
Sim Duration	1.5
Time Units	Hours
Pause Interval	0
Integration Method	RK4
Track flow quantities	True
Keep all variable results	True
Run By	Run
Calculate loop dominance information	False

7.2 Appendix II

List of the *Neurospora crassa* strains used in this study. All strains carry the FLAG-tagged S6 gene.

Strain	Genotype	Lab Stock Number
frq^{10}	*csp-1*; S6::FLAG; *chol-1, ras-1*^{bd}*; frq*^{10}	668
Δ*vta*	*csp-1*; S6::FLAG; *chol-1, ras-1*^{bd}*; vta*; *frq*^{10}	694
Δ*gtr2*	*csp-1*; S6::FLAG; *gtr2*; *chol-1, ras-1*^{bd}; *frq*^{10}	769

7.3 Appendix III

A. Sampling schedule for the first 8 h of the T16 temperature-cycle experiment. Cultures were maintained in constant light (LL) for 48 h before transfer to constant darkness (DD). Samples were entrained under a 16-h temperature cycle (T16) consisting of temperature pulses between 22°C and 37°C. Harvesting was performed at 1-h intervals during the first 8 h of the cycle.

Sample	Hours in DD	Hours in LL	Total Growth Time (h)	Harvest Time
A	160	48	208	10:00 AM
B	161	48	209	11:00 AM
C	162	48	210	12:00 PM
D	163	48	211	1:00 PM
E	164	48	212	2:00 PM
F	165	48	213	3:00 PM
G	166	48	214	4:00 PM
H	167	48	215	5:00 PM

B. Sampling schedule for the first 8 h of the T24 temperature-cycle experiment. Cultures were maintained in constant light (LL) for 48 h before transfer to constant darkness (DD). Samples were entrained under a 24-h temperature cycle (T24) consisting of temperature pulses between 22°C and 37°C. Harvesting was performed at 1-h intervals during the first 8 h of the cycle.

Sample	Hours in DD	Hours in LL	Total Growth Time (h)	Harvest Time
A	136	48	184	10:00 AM
B	137	48	185	11:00 AM
C	138	48	186	12:00 PM
D	139	48	187	1:00 PM
E	140	48	188	2:00 PM
F	141	48	189	3:00 PM
G	142	48	190	4:00 PM
H	143	48	191	5:00 PM

C. Sampling schedule for the second 8 h of the T16 temperature-cycle experiment.
Cultures were maintained in constant light (LL) for 48 h before transfer to constant darkness (DD). Samples were entrained under a 16-h temperature cycle (T16) consisting of temperature pulses between 22°C and 37°C. Harvesting was performed at 2-h intervals during the second 8 h of the cycle.

Sample	Hours in DD	Hours in LL	Total Growth Time (h)	Harvest Time
A	168	48	216	6:00 PM
B	170	48	218	8:00 PM
C	172	48	220	10:00 PM
D	174	48	222	12:00 AM

D. Sampling schedule for the second 8 h of the T24 temperature-cycle experiment.
Cultures were maintained in constant light (LL) for 48 h before transfer to constant darkness (DD). Samples were entrained under a 24-h temperature cycle (T24) consisting of temperature pulses between 22°C and 37°C. Harvesting was performed at 2-h intervals during the second 8 h of the cycle.

Sample	Hours in DD	Hours in LL	Total Growth Time (h)	Harvest Time
A	144	48	192	6:00 PM
B	146	48	194	8:00 PM
C	148	48	196	10:00 PM
D	150	48	198	12:00 AM